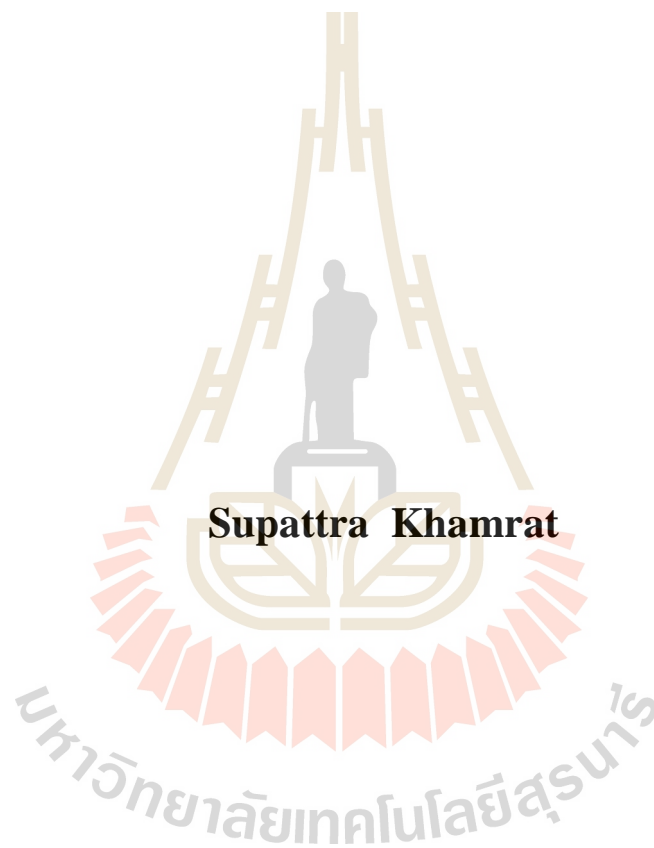


**MECHANICAL AND HYDRAULIC PERFORMANCE OF
CONSOLIDATED CRUSHED SALT FOR BACKFILLING
IN SALT AND POTASH MINES**



**A Thesis Submitted in Partial Fulfillment of the Requirements for the
Degree of Doctor of Philosophy of Engineering in Geotechnology**

Suranaree University of Technology

Academic Year 2016

ศักยภาพเชิงกลศาสตร์และพลศาสตร์ของเกลื่อหินบดอัดสำหรับเป็น
วัสดุถมกลับในเมืองเกลื่อและเมืองโพแทช



นางสาวสุภัทรา คำราช

วิทยานิพนธ์นี้เป็นส่วนหนึ่งของการศึกษาตามหลักสูตรปริญญาวิศวกรรมศาสตรดุษฎีบัณฑิต
สาขาวิชาเทคโนโลยีธรณี
มหาวิทยาลัยเทคโนโลยีสุรนารี
ปีการศึกษา 2559

**MECHANICAL AND HYDRAULIC PERFORMANCE OF
CONSOLIDATED CRUSHED SALT FOR BACKFILLING
IN SALT AND POTASH MINES**

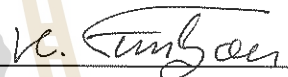
Suranaree University of Technology has approved this thesis submitted in partial fulfillment of the requirements for the Degree of Doctor of Philosophy.

Thesis Examining Committee



(Assoc. Prof. Dr. Pornkasem Jongpradist)

Chairperson



(Prof. Dr. Kittitep Fuenkajorn)

Member (Thesis Advisor)



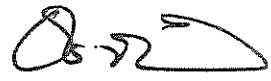
(Asst. Dr. Decho Phueakphum)

Member



(Dr. Prachya Tepnarong)

Member



(Dr. Anisong Chitnarin)

Member



(Assoc. Prof. Flt. Lt. Dr. Kontorn Chamniprasart)



(Prof. Dr. Sukit Limpijumnong)

Vice Rector for Academic Affairs
and Innovation

Dean of Institute of Engineering

สุภัทรา คำราช : ศักยภาพเชิงกลศาสตร์และชลศาสตร์ของเกลือหินบดอัดสำหรับเป็นวัสดุ
ถมกลับในเหมืองเกลือและเหมืองโพแทช (MECHANICAL AND HYDRAULIC
PERFORMANCE OF CONSOLIDATED CRUSHED SALT FOR BACKFILLING IN
SALT AND POTASH MINES) อาจารย์ที่ปรึกษา : ศาสตราจารย์ ดร.กิตติเทพ เพ็องขจร,
94 หน้า.

วัตถุประสงค์ของการศึกษาคือ เพื่อศึกษาผลกระทบของความเค็มกรดและระยะเวลาต่อ
คุณสมบัติเชิงกลศาสตร์ของเกลือหินบดด้วยวิธีการทดสอบการอัดตัวในห้องปฏิบัติการ ตัวอย่าง
เกลือหินบดมีขนาดคละกันระหว่าง 0.075 ถึง 4.75 มิลลิเมตร โดยนำเกลือหินบดผสมกับน้ำเกลือ
อิ่มตัว 5 เปอร์เซ็นต์โดยน้ำหนัก ทำการทดสอบภายใต้ความเค็มกรด 2.5 ถึง 10 เมกะปาสกาล ผลการ
ทดสอบระบุว่าความหนาแน่น กำลังกด และความยืดหยุ่นของเกลือหินบดหลังจากอัดตัวเป็น
ระยะเวลา 30 ถึง 180 วัน มีค่าเพิ่มขึ้นตามความเค็มกรดและระยะเวลาของการอัดตัว ประสิทธิภาพ
ของเกลือหินบดที่ใช้ถมกลับในช่องเหมืองเกลือและช่องเหมืองโพแทชได้ถูกประเมิน โดยใช้
แบบจำลองทางคอมพิวเตอร์ ผลการวิเคราะห์ระบุว่าเกลือหินบดมีประสิทธิภาพในการลดการทรุด
ตัวของผิวดินมากขึ้นเมื่อทำการถมกลับในช่องเหมืองที่มีความสูงมาก โดยเฉพาะอย่างยิ่งในเหมือง
โพแทชเนื่องจากเหมืองโพแทชมีการเปลี่ยนแปลงรูปร่างของเสาค้ำยันมากกว่าในเหมืองเกลือ ผล
การทดสอบในห้องปฏิบัติการได้ถูกนำมาสร้างความสัมพันธ์เชิงคณิตศาสตร์กับค่าพลังงาน
ความเครียดเฉลี่ยระหว่างการอัดตัว สมการดังกล่าวสามารถนำมาใช้คาดคะเนคุณสมบัติของเกลือ
หินบดที่ถมกลับในหลุมเจาะสำรวจภายใต้การผันแปรความเค็มรอบหลุมเจาะ ผลระบุว่าปัจจัย
สำคัญที่มีผลต่อความหนาแน่น กำลังกด และความยืดหยุ่นของเกลือหินบดในระยะยาว คือ ความลึก
ของหลุมเจาะสำรวจ และระยะเวลาที่เกลือหินบดถูกถมกลับหลังจากการขุดเจาะ

สาขาวิชา เทคโนโลยีธรณี
ปีการศึกษา 2559

ลายมือชื่อนักศึกษา สุภัทรา คำราช
ลายมือชื่ออาจารย์ที่ปรึกษา ดร. กิตติเทพ เพ็องขจร

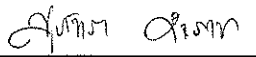
SUPATTRA KHAMRAT : MECHANICAL AND HYDRAULIC
PERFORMANCE OF CONSOLIDATED CRUSHED SALT FOR
BACKFILLING IN SALT AND POTASH MINES. THESIS ADVISOR :
PROF. KITTITEP FUENKAJORN, Ph.D., P.E., 94 PP.

STRAIN ENERGY/STRENGTH/ELASTICITY/BACKFILL/RECRYSTALLIZATION

Consolidation tests have been performed to determine the mechanical properties of crushed salt as affected by applied stresses and consolidation period. The crushed salt with particle sizes ranging from 0.075 to 4.76 mm mixed with 5% saturated brine are consolidated under axial stresses ranging from 2.5 to 10 MPa. The densities, uniaxial compressive strengths and elastic moduli measured after consolidation for 30 to 180 days increase with the applied stresses and duration. The effectiveness of the crushed salt backfill is assessed by performing numerical simulations of the openings in salt and potash mines. The results indicate that the effectiveness for subsidence reduction increases as the pillar height increases, particularly for the potash pillars that yield plastic deformation greater than that of the salt pillars. The crushed salt properties are calculated as a function of mean strain energy required during consolidation. The relations can be used to predict the crushed salt properties installed in exploratory boreholes under various external pressures. The opening depth and the time at which the crushed salt backfill is installed are significant factors controlling its long-term density, strength and elasticity.

School of Geotechnology

Academic Year 2016

Student's Signature 

Advisor's Signature 

ACKNOWLEDGMENTS

I wish to acknowledge the funding supported by Suranaree University of Technology (SUT).

I would like to express my sincere thanks to Prof. Dr. Kittitep Fuenkajorn for his valuable guidance and efficient supervision. I appreciate his strong support, encouragement, suggestions and comments during the research period. My heartiness thanks to Assoc. Prof. Dr. Pornkasem Jongpradist, Assist. Dr. Decho Phueakphum, Dr. Prachya Tepnarong and Dr. Anisong Chitnarin for their constructive advice, valuable suggestions and comments on my research works as thesis committee members. Grateful thanks are given to all staffs of Geomechanics Research Unit, Institute of Engineering who supported my work.

Finally, I would like to thank beloved parents for their love, support and encouragement.

Supattra Khamrat

TABLE OF CONTENTS

	Page
ABSTRACT (THAI)	I
ABSTRACT (ENGLISH).....	II
ACKNOWLEDGEMENTS	III
TABLE OF CONTENTS.....	IV
LIST OF TABLES	IX
LIST OF FIGURES	XI
SYMBOLS AND ABBREVIATIONS.....	XVII
CHAPTER	
I INTRODUCTION.....	1
1.1 Background and rationale	1
1.2 Research objectives.....	3
1.3 Scope and limitations	4
1.4 Research methodology	4
1.4.1 Literature review	5
1.4.2 Crushed salt preparation and instrumentation.....	6
1.4.3 Laboratory testing	6
1.4.4 Modelling of subsidence reduction by crushed salt backfill in mine openings.....	7
1.4.5 Derivation of empirical equations.....	7

TABLE OF CONTENTS (Continued)

	Page
1.4.6 Analytical solution of crushed salt properties after emplacement in borehole	7
1.4.7 Discussions, conclusion and thesis writing.....	7
1.5 Thesis contents	8
II LITERATURE REVIEW	9
2.1 Introduction	9
2.2 Physical properties of crushed salt consolidation	9
2.3 Hydraulic properties of crushed salt consolidation	10
2.4 Mechanical properties of consolidated crushed salt	11
2.5 Constitutive models of crushed salt consolidation.....	16
2.6 Healing mechanisms	22
2.7 Effect of particle size	23
2.8 Conclusion of review	26
III CRUSHED SALT PREPARATION AND INSTRUMENTATION	27
3.1 Introduction	27
3.2 Crushed salt sample	27
3.3 Saturated brine	31
3.4 Fabrication of test cylinder	31
3.5 Suitable brine content.....	31

TABLE OF CONTENTS (Continued)

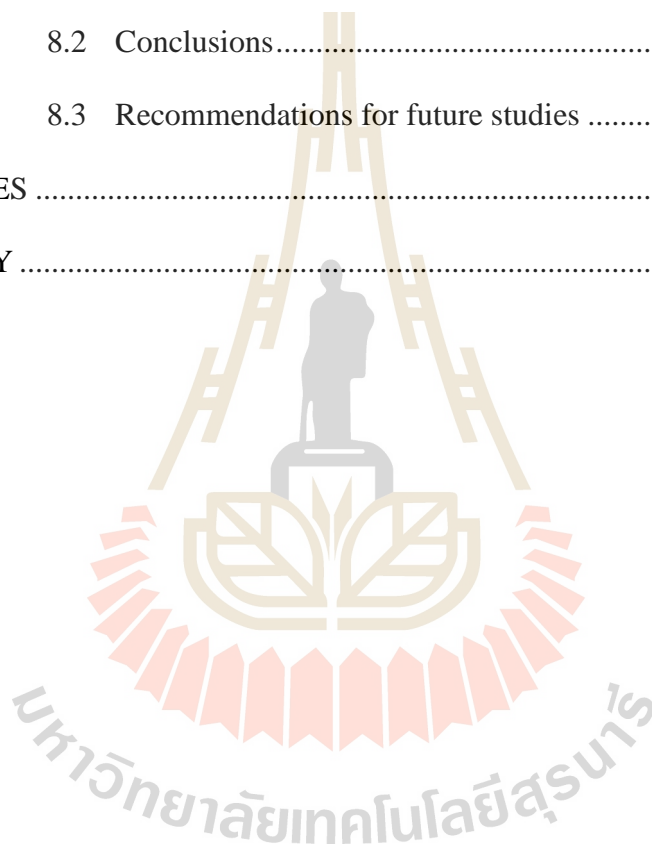
	Page
IV LABORATORY TESTING	34
4.1 Introduction	34
4.2 Consolidation test	34
4.2.1 Test method	34
4.2.2 Consolidation test results	34
4.2.3 Deformation mechanisms	36
4.2.4 Strain energy density principle	37
4.3 Permeability test	39
4.4 Uniaxial compression tests	41
4.4.1 Test method	41
4.4.2 Uniaxial compression test results	43
4.4.3 Predications	46
4.4.4 Octahedral shear stresses and shear strains	49
4.5 Direct shear test	50
4.5.1 Test method	50
4.5.2 Direct shear test results	52
V MODELLING OF SUBSIDENCE REDUCTION BY CRUSHED SALT BACKFILL IN MINE OPENINGS	54
5.1 Introduction	54
5.2 Boundary conditions	54

TABLE OF CONTENTS (Continued)

	Page
5.3 Mechanical properties	55
5.4 Boundary conditions	58
5.5 Numerical results	59
5.5.1 Surface subsidence.....	59
5.5.2 Roof and pillar deformations	64
5.5.3 Factor of safety of pre-consolidated crushed salt	66
VI DERIVATION OF EMPIRICAL EQUATIONS.....	71
6.1 Introduction.....	71
6.2 Crushed salt properties as a function of mean strain energy density.....	71
6.2.1 Crushed salt density	72
6.2.2 Crushed salt porosity.....	72
6.2.3 Crushed salt strength.....	73
6.2.4 Crushed salt elastic modulus.....	73
VII ANALYTICAL SOLUTION OF CRUSHED SALT PROPERTIES AFTER EMPLACEMENT IN BOREHOLE... 77	
7.1 Introduction.....	77
7.2 Circular opening in salt mass subjected to uniform external pressure	77
7.3 Prediction of crushed salt properties after emplacement	82

TABLE OF CONTENTS (Continued)

	Page
VIII DISCUSSIONS AND CONCLUSIONS	89
8.1 Discussions	89
8.2 Conclusions.....	91
8.3 Recommendations for future studies	94
REFERENCES	95
BIOGRAPHY	104



LIST OF TABLES

Table	Page
2.1	Permeability tests data of densified crushed salt (Wang et al., 1994).....11
2.2	Test data of densification and mechanical properties of crushed rock salt (Miao et al., 1995).....12
2.3	Test data of densification and mechanical properties (Wang et al., 1994).....15
3.1	Chemical compositions of crushed salt obtained by XRF analysis.....28
3.2	Particle shape classification of crushed salt based on Powers (1982).....29
3.3	Particle shape classification of crushed salt based on Krumbein and Sloss (1963).....30
4.1	Physical properties of crushed salt after consolidation.....36
4.2	Mean stresses and strains and mean strain energy densities applied to crushed salt during consolidation.....39
4.3	Crushed salt consolidation specimens prepared for uniaxial compression tests.....44
4.4	Mechanical properties of crushed salt after consolidation.....47
5.1	Parameters used in numerical simulations (Sriapai et al., 2012; Crosby, 2007; Luangthip et al., 2016).....56
5.2	Creep properties of pure salt and potash used in FLAC simulations (Wilalak and Fuenkajorn, 2016; Luangthip et al., 2016).....57

LIST OF TABLES (Continued)

Table		Page
5.3	Stresses, strains, octahedral shear stresses and factors of safety of crushed salt backfill.....	70
7.1	Mechanical and rheological parameters of the rock salt and potash (Wilalak and Fuenkajorn, 2016; Luangthip et al., 2016).....	80



LIST OF FIGURES

Figure	Page
1.1 Research methodology.....	5
2.1 Relationship between inelastic strain in z-direction and densification time for crushed rock salt with water content of 3.17% densified under 15 MPa for 97.0 Days (Miao et al., 1995).....	12
2.2 Gradations of crushed salt samples (Wang et al., 1994).....	14
2.3 Unconfined compressive strength of intact and crushed salt as a function of porosity (Kelsall et al., 1984).....	15
2.4 Permeability in a crushed-salt shaft seal component (Callahan et al., 1996)...	17
2.5 Crushed salt fractional density history in a shaft (Callahan and Hansen, 2002).....	19
2.6 Calculated vertical and horizontal closure rates in the test stope (Van Sambeek, 1992).....	20
2.7 Calculated backfill density history for the test stope (Van Sambeek, 1992)...	21
2.8 Calculated vertical and horizontal backfill stresses in the center of the test stope (Van Sambeek, 1992).....	21
2.9 Influence of creep consolidation characteristics on consolidation rate (Kelsall et al., 1984).....	22

LIST OF FIGURES (Continued)

Figure	Page
2.10 Packing of 900 particles where a, c and e are frictionless and b, d and f are frictional ($\mu = 0.5$) (Guises et al., 2009).....	25
3.1 Grain size distribution of crushed salt	28
3.2 Examples of salt grains for different size ranges using Power (1982) method.....	29
3.3 Examples of salt grains for different size ranges fitting with circle outline using Krumbein and Sloss (1963) method.....	30
3.4 Laboratory arrangement for consolidation testing.....	32
3.5 Axial strains as a function of time for different axial stresses and brine contents.....	33
4.1 Laboratory arrangement for consolidation testing.....	35
4.2 Axial strain (ϵ_{ax}) and density (ρ) as a function of consolidation period (t) for different consolidation stresses (σ_{cons}).....	35
4.3 Conceptual mechanism of crushed salt deformation.....	38
4.4 Mean strain energy densities (W_m) as a function of consolidation period (t) for different consolidation stresses (σ_{cons}).....	40
4.5 Laboratory arrangement for permeability testing.....	41
4.6 Intrinsic permeability (k) as a function of consolidation period (t) and for different consolidation stresses (σ_{cons}).....	42

LIST OF FIGURES (Continued)

Figure	Page
4.7 Uniaxial compression test.....	42
4.8 Density of crushed salt specimens after consolidation.....	45
4.9 Stress-strain curves obtained from uniaxial compression testing of crushed salt specimens after consolidation.....	46
4.10 Post-test specimens of uniaxial compression testing.....	47
4.11 Uniaxial compressive strength (a), elastic modulus (b) and Poisson's ratio (c) as a function of consolidation period (t) for different consolidation stresses (σ_{cons}).....	48
4.12 Predicted uniaxial compressive strength (a), elastic modulus (b) and Poisson's ratio (c) as a function of consolidation period (t) for different consolidation stresses (σ_{cons}).....	50
4.13 Octahedral shear stress-strain curves of crushed salt after consolidation under different consolidation stresses and periods.....	51
4.14 Direct shear test results of rock salt; (a) shear stress (τ) as a function of shear displacement (d_s); (b) shear strength (τ_p) as a function of normal stress (σ_n).....	53
4.15 Direct shear test results of crushed salt; (a) shear stress (τ) as a function of shear displacement (d_s); (b) shear strength (τ_p) as a function of normal stress (σ_n).....	53

LIST OF FIGURES (Continued)

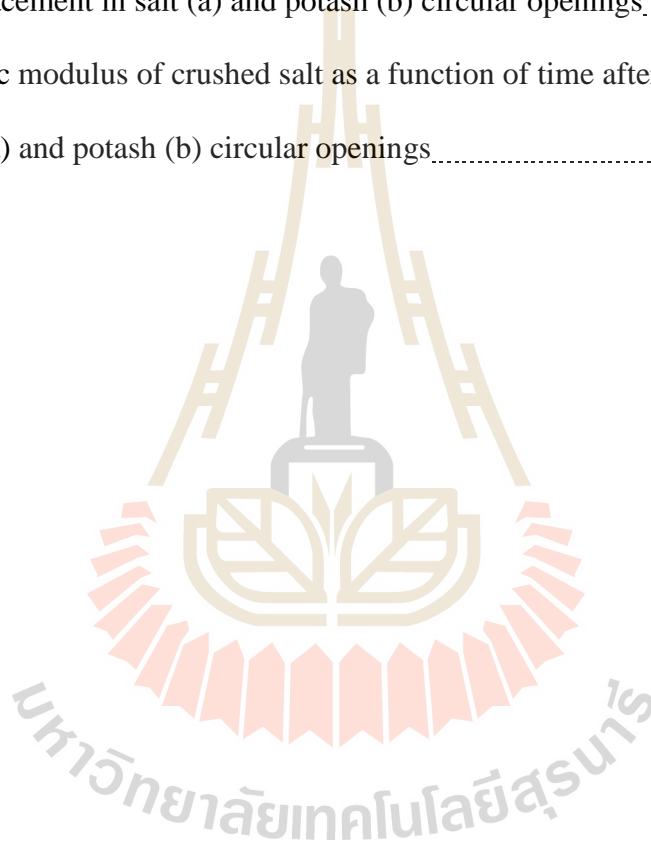
Figure	Page
5.1	Geologic sequences used in simulations for salt mine.....55
5.2	Geologic sequences used in simulations for potash mine.....56
5.3	Example of finite difference mesh developed for FLAC simulation of salt mine opening.....58
5.4	Example of finite difference mesh developed for FLAC simulation of potash mine opening.....59
5.5	Example of comparison surface subsidence between mine opening with and without backfilled after 2 years excavation under various backfill properties in salt (a, b) and potash (c, d) mines.....60
5.6	Surface subsidence under various consolidation stresses (σ_{cons}) of backfill material after consolidation for 15 days in salt (a) and potash (b) openings...61
5.7	Surface subsidence as a function of time for salt (a) and potash (b) openings with different time of crushed salt backfill.....62
5.8	Surface subsidence in salt (a, b, c) and potash (d, e, f) openings with different pillar heights and depths.....62
5.9	Surface subsidence rate in salt (a) and potash (b) openings with different pillar heights and depths.....63
5.10	Roof deformation in salt (a, b, c) and potash (d, e, f) opening.....64
5.11	Floor deformation in salt (a, b, c) and potash (d, e, f) opening.....65
5.12	Vertical room closure in salt (a, b, c) and potash (d, e, f) opening.....66

LIST OF FIGURES (Continued)

Figure	Page
5.13 Pillar deformation in salt (a, b, c) and potash (d, e, f) opening.....	67
5.14 Pillar yielding in salt (a, b, c) and potash (d, e, f) opening.....	68
5.15 Shear stresses induced in salt and potash openings.....	69
6.1 Density as a function of mean strain energy density.....	75
6.2 Porosity as a function of mean strain energy density.....	75
6.3 Uniaxial compressive strength as a function of mean strain energy density....	76
6.4 Elastic modulus (d) as a function of mean strain energy density.....	76
7.1 Mean strain energy density (W_m) released from closure of circular openings excavated in rock salt under different uniform external pressure (P_o).....	81
7.2 Mean strain energy density (W_m) released from closure of circular openings excavated in potash under different uniform external pressure (P_o).....	81
7.3 Remaining mean strain energy density (ΔW_m) as a function of time after backfill emplacement in salt circular hole.....	84
7.4 Remaining mean strain energy density (ΔW_m) as a function of time after backfill emplacement in potash circular hole.....	84
7.5 Density of crushed salt as a function of time after emplacement in salt (a) and potash (b) circular openings.....	85
7.6 Porosity of crushed salt as a function of time after emplacement in salt (a) and potash (b) circular openings.....	86

LIST OF FIGURES (Continued)

Figure		Page
7.7	Uniaxial compressive strength of crushed salt as a function of time after emplacement in salt (a) and potash (b) circular openings.....	87
7.8	Elastic modulus of crushed salt as a function of time after emplacement in salt (a) and potash (b) circular openings.....	88



SYMBOLS AND ABBREVIATIONS

S.G.B.	=	Specific gravity of the saturated brine
ρ_{Brine}	=	Density of saturated brine
$\rho_{\text{H}_2\text{O}}$	=	Density of water
ρ_{cons}	=	Density of crushed salt consolidation
ρ	=	Density
ρ_{initial}	=	Initial density before applying the mean strain energy
$\Delta\rho_{\text{cons}}$	=	Reduction of bulk density due to the strain energy and consolidation period
n	=	Porosity
n_{initial}	=	Initial crushed salt porosity
Δn_{cons}	=	Porosity reduction
σ_{cons}	=	Consolidation stress
σ_1	=	Major principal stress
σ_2	=	Intermediate principal stress
σ_3	=	Minor principal stress
$\sigma_{1,\text{backfill}}$	=	Major principal stress of backfill in the mine opening
$\sigma_{2,\text{backfill}}$	=	Intermediate principal stress of backfill in the mine opening
$\sigma_{3,\text{backfill}}$	=	Minor principal stress of backfill in the mine opening
σ_m	=	Mean stress
σ_c	=	Compressive strength

SYMBOLS AND ABBREVIATIONS (Continued)

$\Delta\sigma_{c,cons}$	=	Strength increase due to consolidation and
$\Delta\sigma_{c,rec}$	=	Strength increase by recrystallization
σ_r	=	Radial stress
σ_θ	=	Tangential stress
σ_z	=	Axial stress
σ_t	=	Tension
ϵ_{cons}	=	Axial strain of crushed salt consolidation
ϵ_1	=	Major principal strain
ϵ_2	=	Intermediate principal strain
ϵ_3	=	Minor principal strain
ϵ_r	=	Radial strain
ϵ_θ	=	Tangential strain
ϵ_z	=	Axial strain
ϵ_m	=	Mean strain
K'	=	Permeability coefficient
Δh	=	Head difference of permeability test
ΔP	=	Difference pressure at the initial point and end point of permeability test
γ_f	=	Unit weight of fluid
Q	=	Flow rate
A	=	Cross-section area of flow

SYMBOLS AND ABBREVIATIONS (Continued)

$\Delta h/L$	=	Hydraulic head gradient
k	=	Intrinsic permeability
μ	=	Dynamic viscosity of nitrogen gas
E	=	Elastic modulus
ν	=	Poisson's ratio
K	=	Bulk modulus
G	=	Shear modulus
ΔE_{cons}	=	Increase of elastic modulus due to consolidation and
ΔE_{rec}	=	Increase of elastic modulus by recrystallization
E_1	=	Elastic modulus
E_2	=	Spring constant in visco-elastic phase
η_1	=	Visco-plastic coefficient in steady-state phase
η_2	=	Visco-elastic coefficient in transient phase
τ_{oct}	=	Octahedral shear stress
$\tau_{\text{oct,backfill}}$	=	Induced octahedral shear stress obtained from numerical model
γ_{oct}	=	Octahedral shear strain
τ	=	Shear stress
τ_p	=	Peak shear strength
d_s	=	Shear displacement
σ_n	=	Normal stress
c	=	Cohesion

SYMBOLS AND ABBREVIATIONS (Continued)

c_p	=	Peak cohesion
ϕ	=	Internal friction angle
ϕ_p	=	Peak friction angle
W_m	=	Mean strain energy
$W_{m,s}$	=	Released strain energy density from borehole
$W_{m,l}$	=	Energy lost due to creep closure before backfill is installed
$\Delta W_{m,s}$	=	Strain energy left for the consolidation is needed
a	=	Opening radius
r	=	Radial distance from the opening center
ϵ_r^e	=	Elastic radial strain
ϵ_r^c	=	Time-dependent radial strain controlling the creep closure of the opening
S_r	=	Radial stress deviation
σ^*	=	Equivalent (effective) stress
P_o	=	Uniform external pressure
$C\%$	=	Carnallite content
D	=	Opening depths
FS	=	Factor of safety
t	=	Time
Δt	=	Duration for consolidation
t_B	=	Time at which the crushed salt backfill is installed

SYMBOLS AND ABBREVIATIONS (Continued)

κ'	=	Material constants of the potential creep law
β'	=	Material constants of the potential creep law
γ'	=	Material constants of the potential creep law
α	=	Empirical constant for equation (4.7)
β	=	Empirical constant for equation (4.7)
χ	=	Empirical constant for equation (4.7)
δ	=	Empirical constant for equation (4.8)
η	=	Empirical constant for equation (4.8)
φ	=	Empirical constant for equation (4.8)
κ	=	Empirical constant for equation (4.9)
λ	=	Empirical constant for equation (4.9)
ι	=	Empirical constant for equation (4.9)

CHAPTER I

INTRODUCTION

1.1 Background and rationale

Rock salt in the Maha Sarakham formation in the northeast of Thailand is separated into two basins: the Sakon Nakhon basin and the Khorat basin. Both contain three distinct salt units: the Upper, Middle and Lower members. Rock salt and potash has become ones of the prominent ores associated with Maha Sarakham salt. In the Sakon Nakhon basin, Asia Pacific Potash Corporation (APPC) has carried out an extensive exploration program, and drawn a detailed mine plan for extracting sylvite from the upper portion of the Lower Salt member (Crosby, 2005). It has been estimated that the inferred reserves of sylvite are about 302×10^9 t for the Udon South deposit and 665×10^9 t for the Udon North deposit. In the Khorat basin, Asean Potash Mining Company (APMC) has also conducted extensive studies and developed exploratory inclined shafts to investigate the feasibility of extracting carnallite from the Lower Salt member.

Common problems involving in salt and potash mining are the impacts of ground surface subsidence due to the deformation of support pillars and opening roofs. The subsidence may damage engineering structures (buildings, roads, railways and pipelines), and natural resources (farmlands, reservoir and groundwater). For salt and potash mines, the salt tailings or salt waste piles on ground surface may cause hazardous dust and may lead to salinity of surrounding farmlands and surface water.

One of the solutions is to return the salt tailings to the mined out openings underground. Therefore, the effectiveness of the pre-consolidated crushed salt for the subsidence reduction in salt and potash mines should be assessed.

In addition, the excavations and penetrations of the formation can have a detrimental impact on the environment. Open shafts and boreholes may become preferential flow path for the surface water and groundwater above to reach the mine horizon. They may allow premature and unnecessary depressurization of the formation, and may result in wasting of natural resources. Within the excavation areas these boreholes will be subjected to large ground movement due to the subsidence of overburden. As a result rigid seal, such as cementitious material, may not be a suitable candidate for sealing boreholes in these areas (Daemen and Fuenkajorn, 1996). Salt and potash mines have used the salt tailing as sealing material due to its availability, low cost and physical, chemical and mechanical compatibility with the host rock (Holcomb and Hannum, 1982; Hansen, 1997). The understanding of the consolidation behavior of crushed salt is thus the primary concern for the long-term assessment of the performance of the seal.

A variety of constitutive models have been developed to predict the behavior of crushed salt consolidation in mine openings. They are derived from test results and can be presented in several forms of mathematical functions. Some that are notably mentioned include viscoelasticity (Munson and DeVries, 1991), elastic viscoplasticity (Van Sambeek, 1992), hot-pressing (Zeuch et al., 1985), pressure solution (Spiers and Brzesowsky, 1993), healing mechanics (Wang et al., 1994; Miao et al., 1995) and empirical models (Sjaardema and Krieg, 1987). These models are complex and may not be suitable for the mining industry. They are specifically derived for the nuclear

waste repository sealing. Most models are focused on the complex influence of temperature, moisture, density, creep and healing mechanisms on the properties of crushed salt under repository environments. The results may be inappropriate for the relatively shallow salt mines where the closure rate of the openings to be sealed are low (Hansen et al., 1993). Even though the effects of consolidation on the physical and hydraulic behavior of crushed salt have been recognized and studied, experimental determination of the mechanical properties of crushed salt after consolidation has rarely been investigated. The long-term mechanical properties of the consolidated crushed salt after emplacement have never been assessed or predicted.

1.2 Research objectives

The objective of this study is to determine the effectiveness of the crushed salt after backfilling in mine opening. The effectiveness of the crushed salt backfill is assessed by performing numerical simulations. The subsidence magnitudes under a variety of crushed salt properties and emplacement periods are used as an indicator of the subsidence reduction effectiveness. The mechanical properties of crushed salt seal emplaced in boreholes are predicted. The mechanical properties of the specimens are determined as a function of the applied mean strain energy densities during consolidation. The crushed salt properties are predicted for different borehole depths and installation periods.

1.3 Scope and limitations

1. Laboratory testing is conducted on crushed salt specimens prepared from the Maha Sarakham formation. The grain sizes of crushed salt ranging from 0.075 to 4.75 mm.
2. Consolidation tests are performed by applying constant axial stresses to the crushed salt samples installed in the 54 mm diameter steel cylinders with length 200 mm.
3. Basic characterization tests are performed including consolidation test, permeability test, uniaxial compression test and direct shear test. The test procedures are following the relevant ASTM standard practices.
4. Crushed salt specimens are consolidated for 30, 90 and 180 days with applied constant axial stresses of 2.5, 5, 7.5 and 10 MPa.
5. Uniaxial compression tests are performed with constant loading rate at 0.1 MPa/s.
6. Gas flow permeability tests are performed on crushed salt during consolidation.
7. All tests are conducted under ambient temperature.
8. Up to 12 samples are tested.
9. FLAC program is used in the simulations.

1.4 Research methodology

The research methodology shown in Figure 1.1 comprises 8 steps; including 1) literature review, 2) crushed salt preparation and instrumentation, 3) laboratory testing, 4) modelling of subsidence reduction by crushed salt backfill in mine opening,

5) derivation of empirical equations, 6) analytical solution of crushed salt properties after emplacement in borehole, 7) discussions and conclusions and 8) thesis writing and presentation.

1.4.1 Literature review

Literature review is carried out to study the previous researches on consolidation testing, physical, mechanical and hydraulic properties and computer simulations of crushed salt. The sources of information are from text books, journals, technical reports and conference papers. A summary of the literature review is given in chapter two.

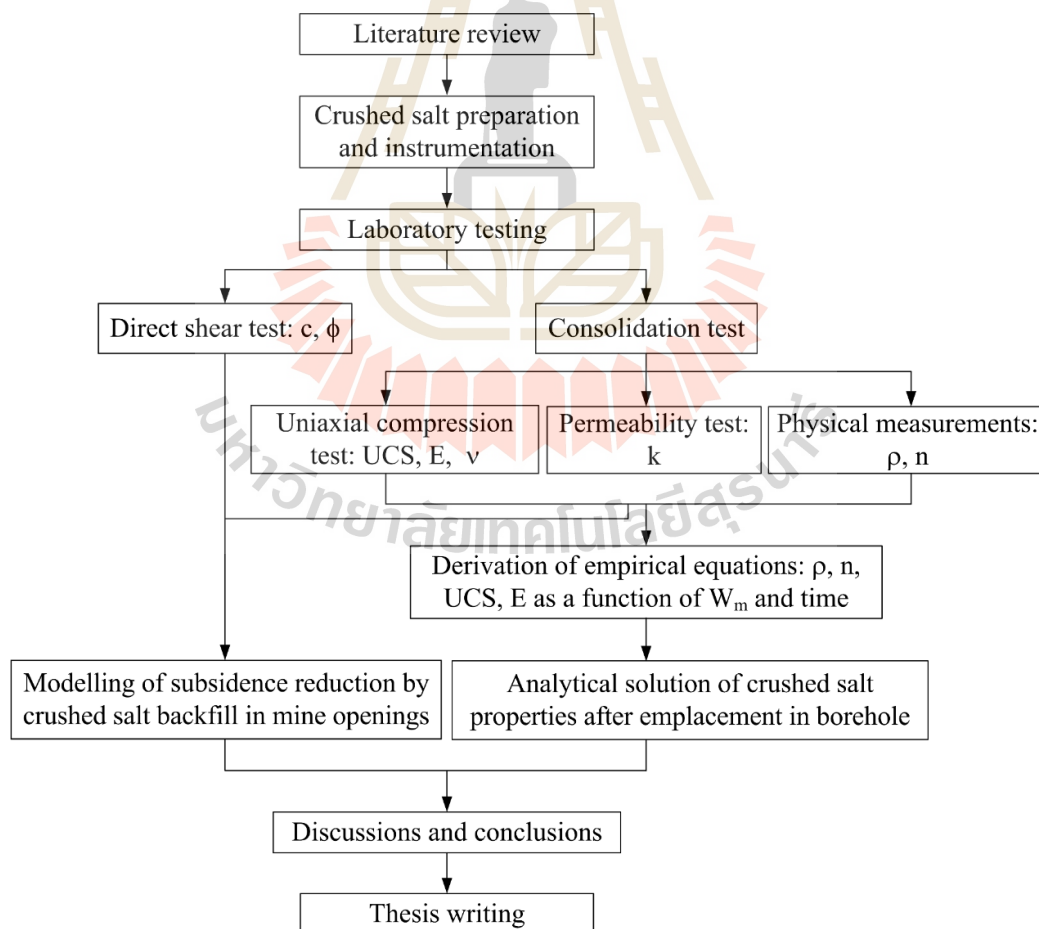


Figure 1.1 Research methodology.

1.4.2 Crushed salt preparation and instrumentation

Crushed salt used in this study is prepared from the Middle member of the Maha Sarakham Formation in the Khorat basin, northeastern Thailand. The crushed salts has grain size ranging from 0.075 to 4.75 mm for the consolidation tests. Saturated brine is prepared by mixing pure salt with distilled water in plastic tank.

The cylindrical steel tube with 54 mm internal diameter, 64 mm outside diameter and 200 mm height is used as consolidation tube. Two load platens having 53 mm diameter with 100 mm length are to applied axial load to the crushed salt specimens. Two o-rings are installed around each load platen. There is a 10 mm diameter hole at the center of the top and bottom load platens for use as inlet of N₂ to specimen for permeability testing and drained hole of water from specimen.

1.4.3 Laboratory testing

The consolidation tests are performed by applying constant axial stresses from a hydraulic load pump to the crushed salt samples installed in the 54 mm diameter steel cylinders. The constant axial stresses are 2.5, 5, 7.5 and 10 MPa. All tests were conducted under ambient temperature. The axial displacements are continuously measured as a function of time by dial gages to calculate the changes of axial strain, density, and void ratio. The nitrogen gas flow testing is performed to determine intrinsic permeability of crushed salt consolidation that changes over time. The flow rates under constant head are continuously monitored every 6 hours. The compressive strength of the consolidated crushed salts samples is determined by axially loading the crushed salt cylinder (after removing from the steel tube) with a nominal diameter of 54 mm and L/D ranging from 2 to 2.2. Uniaxial compressive strength measurements are made after 30, 90 and 180 days of consolidation.

1.4.4 Modelling of subsidence reduction by crushed salt backfill in mine openings

The finite difference code (FLAC; Itasca 1992) is used to calculate the creep deformation of room and pillar before and after the crushed salt backfill has been installed. The subsidence magnitudes under a variety of crushed salt properties and emplacement periods are used as an indicator of the subsidence reduction effectiveness.

1.4.5 Derivation of empirical equations

The crushed salt properties are used to develop a set of empirical equations as a function of mean strain energy and consolidation period by SPSS statistical software. The relations are used to predict the crushed salt properties installed in shafts and boreholes under various external pressures and installation periods.

1.4.6 Analytical solution of crushed salt properties after emplacement in borehole

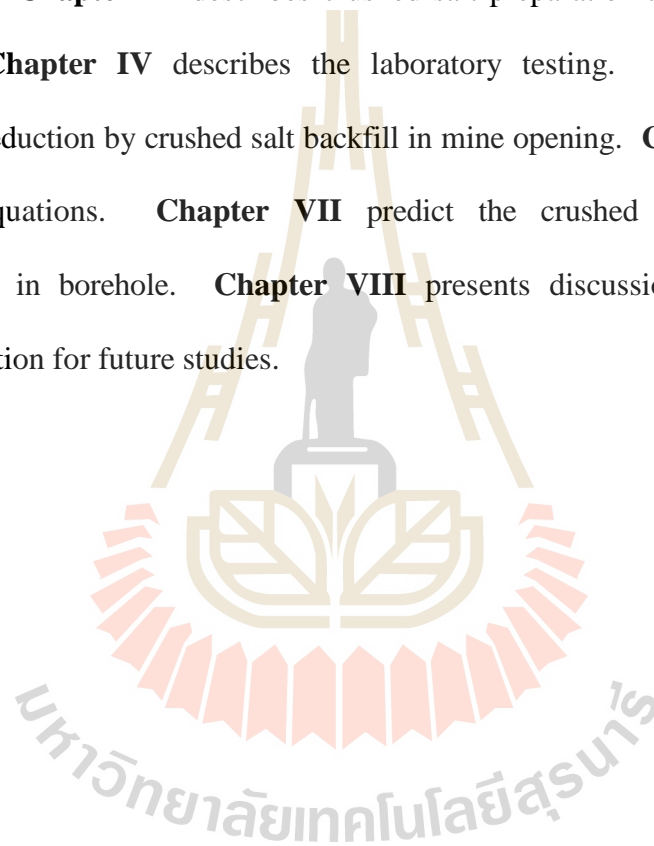
The mean strain energy released by creep closure of circular openings (shaft or borehole) in infinite salt mass subjected to uniform external pressure (in-situ stress) is determined and used to predict the changes of the crushed salt properties after emplacement.

1.4.7 Discussions, conclusion and thesis writing

All study activities, methods, and results are documented and compiled in the thesis.

1.5 Thesis contents

This research thesis is divided into eight chapters. The first chapter includes background and rationale, research objectives, scope and limitations and research methodology. **Chapter II** presents results of the literature review to improve an understanding of the physical, hydraulic and mechanical properties of consolidated crushed salt. **Chapter III** describes crushed salt preparation and fabrication of test cylinder. **Chapter IV** describes the laboratory testing. **Chapter V** presents subsidence reduction by crushed salt backfill in mine opening. **Chapter VI** derive the empirical equations. **Chapter VII** predict the crushed salt properties after emplacement in borehole. **Chapter VIII** presents discussions, conclusions and recommendation for future studies.



CHAPTER II

LITERATURE REVIEW

2.1 Introduction

Relevant topics and previous research results are reviewed to improve an understanding the physical, hydraulic and mechanical properties of crushed salt consolidation. These include the effects of moisture, duration, consolidation stresses, initial density, and particle size on the density, porosity, permeability, compressive strengths and elastic parameters of crushed salt. The constitutive models are used to describe the behavior of crushed salt consolidation are also investigated. Initial review results are summarized below.

2.2 Physical properties of crushed salt consolidation

The consolidation is effective only when moisture is available on grain contacts (IT Corporation, 1987). As a consequence, dry crushed salt shows the lowest consolidation, suggesting that mechanical deformation was not an important mechanism in consolidation. Wang et al. (1992) conduct several series of densification tests on crushed rock salt with water contents varying from 0.12% to 4.72%. The compaction of crushed salt increase with increasing brine content until the optimum brine content is reached, and decreases with further brine content increases. Case et al. (1987) conclude from their experimental work that the volumetric creep strain rate increases with time and does not reach steady state values even after 1 to 2 months of load application. The initial porosity decrease with

increasing density (Case and Kelsall, 1987; Loken and Statham, 1997; Hansen and Mellegard, 2002; Salzer et al., 2007). The relationship between void ratio and time are found to be exponential equations (Olivella and Gens, 2002). Pfeifle et al. (1987) concludes that the variables time and moisture content have the greatest influence on creep consolidation.

2.3 Hydraulic properties of crushed salt consolidation

Brodsky et al. (1995) conduct the hydrostatic and triaxial compression tests of crushed salt with brine content of 2.5% to 3% by weight. The results indicate that the permeability decreases approximately 2.1 orders of magnitude as fractional density increases from 0.9 to 0.99. The crushed salt is sufficiently impermeable as the intact rock salt at fractional densities close to 0.95. Similar permeability results have been obtained by Butcher (1991) and Holcomb and Shields (1987).

Wang et al. (1994) conduct the permeability tests of crushed salt specimens (maximum particle size of 4.76 mm) with a water content of 3% by weight. The specimens are densified under a pressure of 15 MPa. The permeability of the specimen are measured at densification times of 60, 1776, 2805 and 6095 minutes, respectively. The gas pressure are increased manually from 25 psi to 800 psi under a constraint pressure of 15 MPa during the permeability tests. Permeability are calculated and summarized in Table 2.1. It is shown that the permeability decreased as the densification time increased. No flow rate was read for the permeability test specimen densified for eight days since the measurement approached the limit of our permeability test apparatus. The results indicated that reliable data cannot be obtained unless the gas pressure reaches at least 700 psi.

Table 2.1 Permeability tests data of densified crushed salt (Wang et al., 1994).

Permeability (darcy)	Densification time (minute)	Fractional density
1.1×10^{-1}	60	0.78
2.9×10^{-4}	1776	0.85
1.2×10^{-5}	2805	0.86
2.3×10^{-7}	6095	0.88

2.4 Mechanical properties of consolidated crushed salt

The uniaxial compressive strength and Young's modulus of crushed rock salt also increase with densification time (Wang et al., 1994; Miao et al., 1995) and decreases with porosity (Kelsall et al., 1984).

Miao et al. (1995) state that the increase of Young's modulus is one of the main features of healing processes in which void space is reduced and the bonding force between particles is enhanced because of the diffusion and recrystallization that occur on the grain boundaries. Besides Young's modulus, strength, and vertical inelastic strain of densified crushed rock salt also increase with respect to densification time, as shown in Figure 2.1 and Table 2.2.

Pfeifle et al. (1987) performs the hydrostatic compression creep tests of crushed salt specimen from Avery Island dome salt. The experiments are performed to assess the influence of the following four variables on the consolidation and unconfined strength of crushed salt: grain size distribution, temperature, time, and moisture content. The levels of each variable investigated are grain size distribution, uniform-graded and well-graded (coefficient of uniformity of 1 and 8); temperature 25 °C and 100 °C; time, 3.5×10^3 s and 950×10^3 s (approximately 60 minutes and 11 days, respectively);

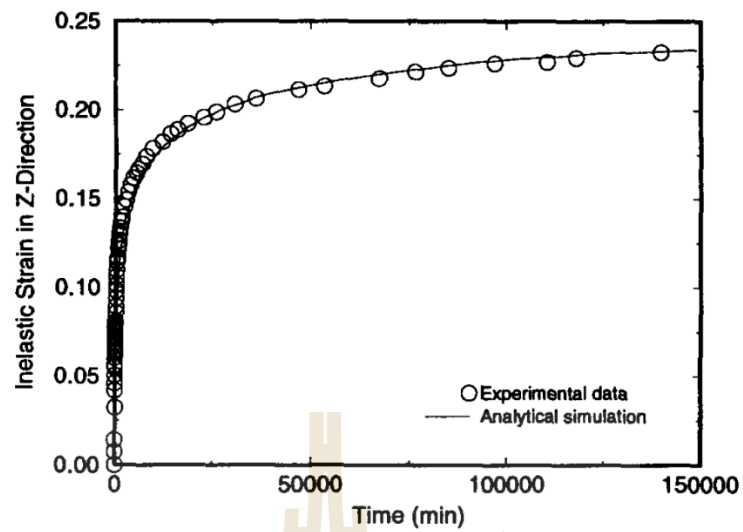


Figure 2.1 Relationship between inelastic strain in z-direction and densification time for crushed rock salt with water content of 3.17% densified under 15 MPa for 97.0 Days (Miao et al., 1995).

Table 2.2 Test data of densification and mechanical properties of crushed rock salt (Miao et al., 1995).

	Specimen Nos.					
	1	2	3	4	5	6
Consolidation duration (min)	1	4,030	7,030	14,700	21,300	140,000
Initial height of specimen (mm)	122	122	122	122	117	122
Instantaneous height of specimen (mm)	106	106	107	105	104	106
Final height of specimen (mm)	103	88.7	87.1	85.1	83.3	81.3
Weight of specimen (grams)	341	344	346	340	337	341
Water content (by weight) (%)	2.97	3.01	3.23	2.60	2.93	3.17
Average prepeak unloading-reloading Young's modulus (MPa)	2,741	5,960	7,430	7,630	8,380	9,640
Unconfined compression strength (MPa)	0.61	17.0	23.7	25.5	27.1	28.4

and moisture content, dry and wet (85 percent relative humidity for 24 hours). The hydrostatic creep stress is 10 MPa. The unconfined compression tests are performed at an axial strain rate of $1 \times 10^{-5} \text{ s}^{-1}$. Results show that the variables time and moisture content have the greatest influence on creep consolidation, while grain size distribution and, to a somewhat lesser degree, temperature have the greatest influence on total consolidation. Time and moisture content and the confounded two-factor interactions between either grain size distribution and time or temperature and moisture content have the greatest influence on unconfined strength.

Pfeifle (1991) conducts uniaxial compression tests on three densified crushed rock salt specimens with water contents of 5.24%, 5.30% and 9.97% by weight, respectively, densified for up to 167 days. The results indicated that the uniaxial compressive strength varied from 0.5 to 8.1 MPa. The results are used to relate mechanical properties with water content but not densification of time and applied stresses. Consequently, it should be confirmed that the mechanical properties of consolidated crushed salt are changed with densification times in long term.

Wang et al. (1994) study the densification processes and mechanical properties of crushed salt. The crushed salt sample used in experimental are sieved and remixed into three gradation types A, B and C with maximum particle sizes of 4.76, 2.36 and 1.18 mm, respectively, as shown in Figure 2.2. Six densification tests are conducted under uniaxial strain and drained conditions. The six densification tests included four tests on the sample of gradation A with densification times of 2.80, 4.88, 10.21 and 14.81 days, respectively; one test on the sample of gradation B with a densification time of 6.09 days; and one test on the sample of gradation C with a densification time of 6.03 days. Representative test data are shown in Table 2.3. The

results indicated that during densification processes, the elastic modulus, strength, and vertical inelastic strain increase with respect to densification time. With uniform gradations, the densification rate of crushed salt increases when average particle size decreases.

Kelsall et al. (1984) state that the method to improve the performance of a seal or backfill is the initial density or porosity of crushed salt backfill. Greater initial density creates better assurance of attaining an acceptable backfill after emplacement. The compressive strength of intact and crushed salt as a function of porosity is shown in Figure 2.3. The results indicated that in the range of porosity below approximately 0.2 to 0.3, the data generally fit well to a curve obtained from Kingery et al. (1976) which relates porosity to relative strength (strength at zero porosity = 1) for ceramic materials. This relationship provides further evidence that the process of sintering may play a role in the consolidation process, in that the crushed salt appears to behave as a porous solid rather than as a densely compacted granular material.

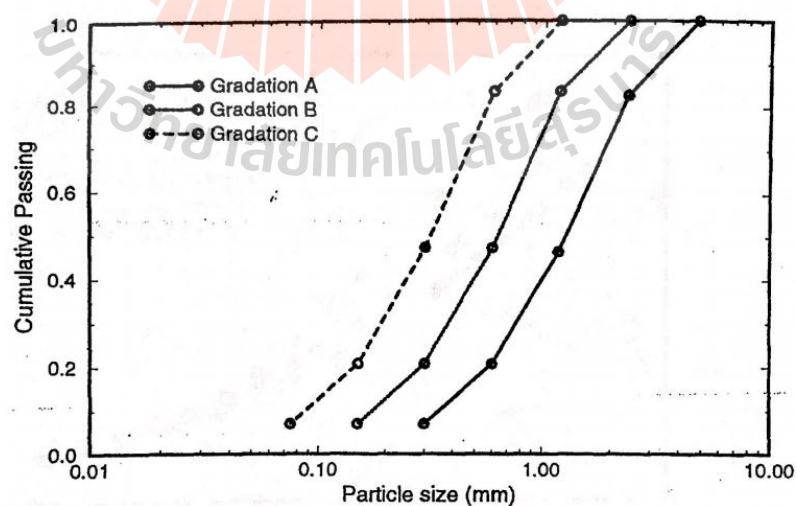
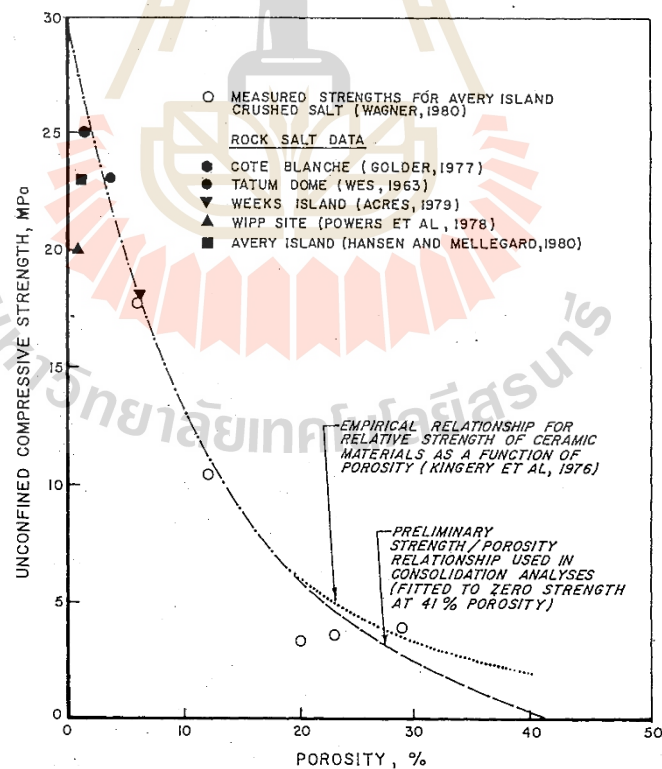


Figure 2.2 Gradations of crushed salt samples (Wang et al., 1994).

Table 2.3 Test data of densification and mechanical properties (Wang et al., 1994).

Specimen	1	2	3	4	5	6
Gradation type	A	A	A	A	B	C
Densification duration (day)	2.80	4.88	10.21	14.81	6.09	6.03
Initial fractional density	0.6449	0.6475	0.6374	0.6552	0.6314	0.6153
Instantaneous fractional density	0.7388	0.7401	0.7395	0.7406	0.7400	0.7370
Final fractional density	0.8770	0.8937	0.9132	0.9237	0.9243	0.9702
Weight of specimen (gram)	344.2	345.6	340.2	337.0	343.8	328.4
Final height of specimen (mm)	88.71	87.07	85.09	83.34	84.96	77.32
Young's modulus (MPa)	3441	4167	4859	5038	4769	4829
Unconfined Strength (MPa)	17.01	23.66	25.46	27.08	29.73	36.00
Vertical Inelastic Strain	0.272	0.291	0.302	0.307	0.323	0.366

**Figure 2.3** Unconfined compressive strength of intact and crushed salt as a function of porosity (Kelsall et al., 1984).

2.5 Constitutive models of crushed salt consolidation

A variety of constitutive models have been developed to predict the behavior of crushed salt consolidation in mine openings. They are derived from test results and can be presented in several forms of mathematical functions. Some that are notably mentioned include viscoelasticity (Munson and DeVries, 1991), elastic viscoplasticity (Van Sambeek, 1992), hot-pressing (Zeuch et al., 1985), pressure solution (Spiers and Brzesowsky, 1993), healing mechanics (Wang et al., 1994; Miao et al., 1995) and empirical models (Sjaardema and Krieg, 1987).

Callahan et al. (1996) examine the mechanical behavior of crushed salt, which is to be used as a long-term seal component for shafts at the WIPP site. Three different equivalent inelastic strain-rate forms are used to describe the consolidation portion of the crushed-salt material model, including:

- Sjaardema and Krieg Empirical Model (Sjaardema and Krieg, 1987).
- Zeuch's Isostatic Hot-Pressing Model (Zeuch, 1990).
- Spiers' Pressure Solution Model (Spiers and Brzesowsky, 1993).

The models are generalized to three-dimensional forms. A database comprised of hydrostatic and shear consolidation tests is created and used to determine the material parameters of the constitutive models. The creep consolidation models have been implemented into the finite element thermo mechanical stress analysis program SPECTROM-32 (Callahan et al., 1989). The results indicated that the lower portion of the crushed-salt seal component attains low permeability after 100 years and fully consolidates for one model (Sjaardema and Krieg Model) reaching the assumed permeability of the host formation (10^{-21} m^2) (Figure 2.4).

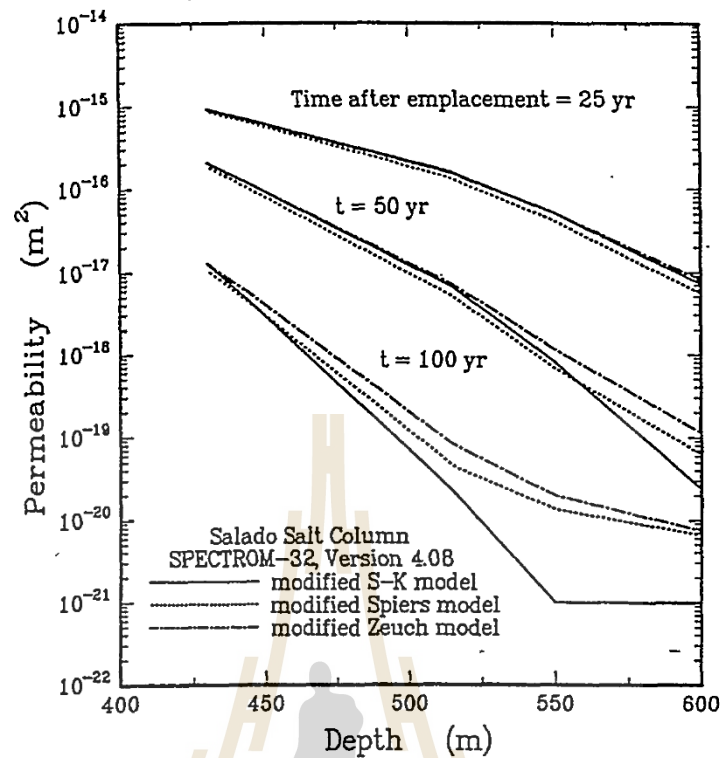


Figure 2.4 Permeability in a crushed-salt shaft seal component (Callahan et al., 1996).

Callahan et al. (1998) develop a constitutive model for crushed salt consolidation. A creep consolidation model is developed to combine dislocation creep and grain boundary diffusional pressure solutioning into a single constitutive model. The dislocation creep model is adapted from the multimechanism deformation constitutive model (e.g., Munson et al., 1989) used to describe creep deformation of intact salt. The pressure solutioning model is adapted from the densification model for wet salt aggregates presented by Spiers and Brzesowsky (1993). In addition, four new laboratory shear consolidation experiments are conducted with fractional densities near the initial fractional density expected in the dynamically compacted, crushed salt seal component (approximately 0.9). These tests expand the database into fractional density ranges previously untested and provide information on the

crushed salt flow behavior as its density increases. These tests are added to the experimental database, which was fit to obtain material parameter values for the crushed-salt constitutive model. The results of the model fitting produced material parameter values representative of the entire database. Two separate fits are performed. The first fit used only the shear consolidation tests in the database, and the second fit used both the shear and hydrostatic consolidation tests. In our previous studies, dramatic changes in the parameter values are observed when the different tests are fit. In the present study, these separate fits produced similar parameter values, which indicates that the constitutive model is more representative of the physics of the creep consolidation of crushed salt than previous models.

Callahan and Hansen (2002) use the finite element program SPECTROM-32 predict the creep deformation of the host rock and the consolidation of the crushed salt seal material in the shafts. The shaft is assumed to be open for 50 years and then instantaneously filled with crushed salt dynamically compacted to a fractional density of 90 percent. Crushed salt is emplaced within the shafts at depths ranging from 430 meters to 600 meters. Figure 2.5 presents the results of six shaft seal analyses using the shear and combined database parameter value sets at three different depths. At depths of 600 m, 515 m and 430 m approximately 60 years, 110 years and 240 years, respectively, are required to attain a crushed salt fractional density of 99 percent. These results show that the responses for either parameter value set at each depth are similar up to a fractional density of about 98 percent. Therefore, the model results diverge slightly. The results also indicated that the shear parameter values set predicts the fastest consolidation rate.

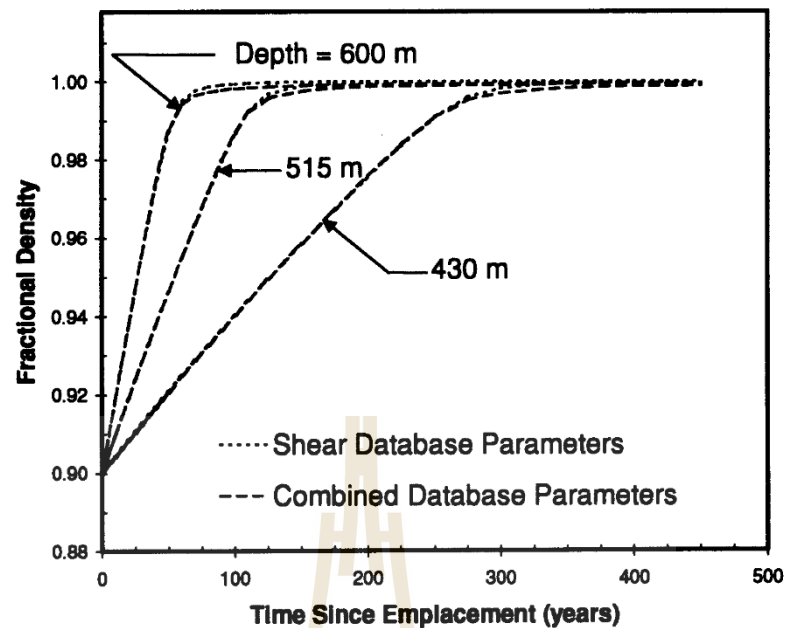


Figure 2.5 Crushed salt fractional density history in a shaft (Callahan and Hansen, 2002).

Van Sambeek (1992) presents the technology developed for calculating the behavior of crushed salt backfill at the Waste Isolation Pilot Plant (WIPP) near Carlsbad, New Mexico. This technology includes laboratory testing results, material constitutive laws, modeling results, and field measurements. Two types of laboratory tests are common: isostatic and odometer consolidation. The consolidation model adopted by the WIPP program for granular halite comprises a total strain rate consisting of three components: nonlinear elastic, creep, and thermal strain. The consolidation data are used to determine the constant parameters in the consolidation model for used in the numerical model. The numerical modeling is used to simulate the crushed salt backfill in potash mine opening with 42 m wide, 4 m room high and 63 m pillars wide under stress field of 20 MPa. The results show that before the

backfill is placed, the closure rates had become nearly constant (a steady-state closure rate) (Figure 2.6). Even after the backfill is placed, the constant closure rate is sustained until 3.6 years (2.2 years after backfill placement). By that time, consolidation of the backfill had caused the density to increase to slightly more than $1,600 \text{ kg/m}^3$ (Figure 2.7) and a 0.5 MPa pressure had developed in the backfill (Figure 2.8). Beyond 3.6 years, the backfill pressure increased (and room closure rate decreased) steadily as additional consolidation occurred. The complete consolidation is achieved by about 10 years and the backfill pressure had reached about 10 MPa.

Kelsall et al. (1984) present the properties of crushed salt and the nature of fracture healing. They compare the consolidation rates obtained from the calculation using the crushed salt properties from Ratigan and Wagner (1978) and Holcomb and Hannum (1982). Using Ratigan and Wagner's data, the consolidations of crushed salt to a low porosity (0.6%) would occur within hundreds of years (Figure 2.9).

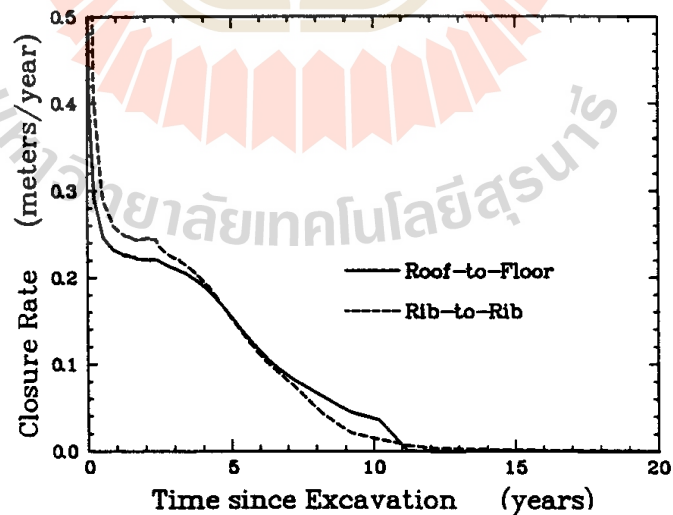


Figure 2.6 Calculated vertical and horizontal closure rates in the test stope (Van Sambeek, 1992).

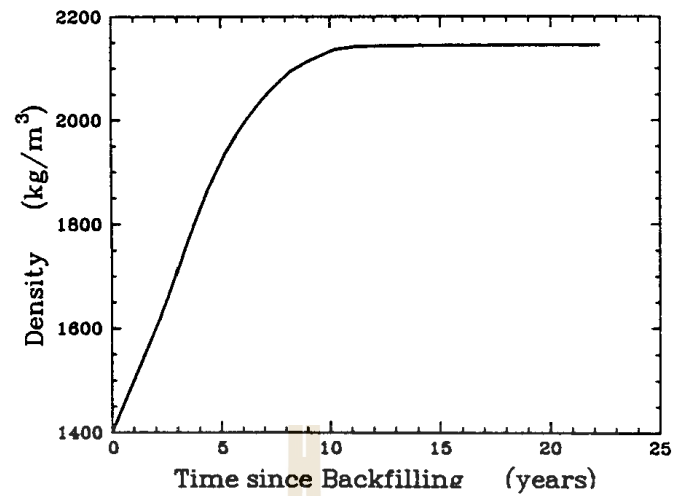


Figure 2.7 Calculated backfill density history for the test stope (Van Sambeek, 1992).

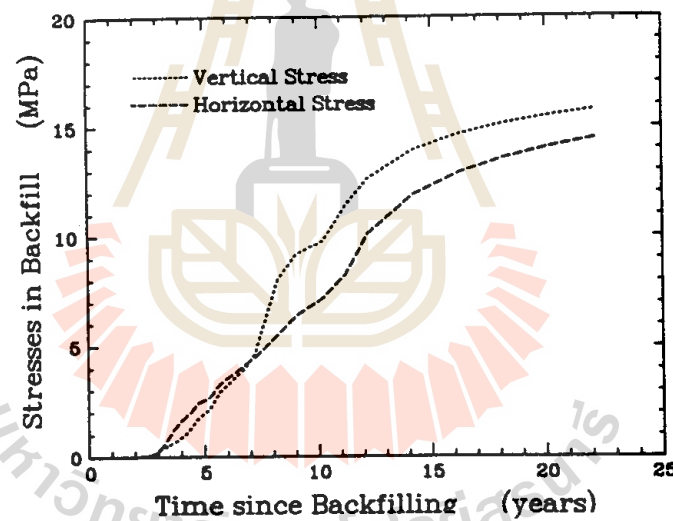


Figure 2.8 Calculated vertical and horizontal backfill stresses in the center of the test stope (Van Sambeek, 1992).

Conversely, with Holcomb and Hannum's data, the effective consolidation would require more than several thousands of years. The different results are depending on the creep rate of the intact rock salt and the creep properties of the

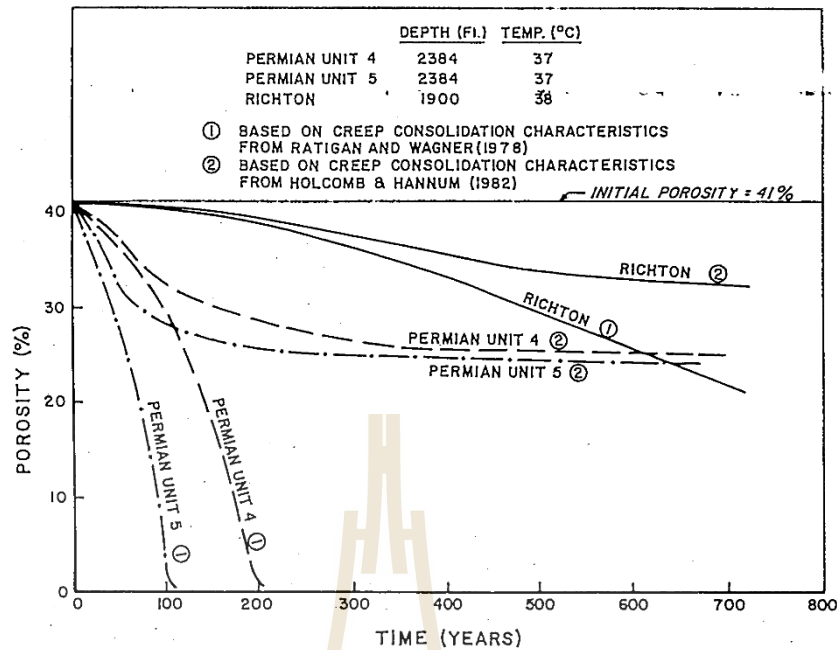


Figure 2.9 Influence of creep consolidation characteristics on consolidation rate (Kelsall et al., 1984).

crushed salt. And the fracture healing should occur relatively rapidly, within tens to hundreds of years.

2.6 Healing mechanisms

Hwang et al. (1993) study the grain boundary healing behavior of crushed rock salt by employing the environmental scanning electron microscope (ESEM) to study the consolidation mechanism of rock salt backfill. Consolidation tests using materials made at different pressures and containing different moisture levels are conducted in order to construct the proposed mechanism. Direct observation of specimens in the ESEM resulted in viewing water trapped on the surface and the formation of a water meniscus between two particles. The concentration of brine at

the grain boundary is observed as contributing to the amount of recrystallization. The amount of water therefore has a great effect on the consolidation of rock salt and is possibly due to the sliding, rotation, or crushing of the contact zone of the granular material. From such a study, tentative healing and consolidation mechanisms can be deduced.

IT Corporation (1987) investigate the consolidation behavior of crushed salt and fracture healing in natural and artificial salt. The fracture healing program included 20 permeability tests conducted on fractured and unfractured samples. The tests are conducted in a Hoek cell at hydrostatic pressures up to 3,000 psi (20.6 MPa) with durations up to 8 days. For the natural rock salt tested, permeability is strongly dependent on confining pressure and time. The effect of confining pressure is much weaker in the artificial salt. In most cases the combined effects of time and pressure are to reduce the permeability of fractured samples to the same order of magnitude (or less) as the permeability measured prior to fracturing.

Miao et al. (1995) state that the healing of rock salt is probably due to the visco-plastic deformation of grains, causing the closure of cracks and pore spaces. The size reduction of the micro-cracks can increase the salt stiffness and strength. The main driving force for fracture healing is a minimization of surface tension and creation of contact areas and covalent bonds between the two surfaces of the fracture.

2.7 Effect of particle size

The rate of consolidation is also dependent on the applied stresses and particle size of crushed salt. The consolidation rate increased with increasing applied stresses and decreased with increasing particle size (Shor et al., 1981). Wang et al. (1994)

study the densification processed of crushed salt consolidation. The sample has been remixed into three gradation types with maximum particle sizes of 4.76, 2.36 and 1.18 mm. The results show the increase of consolidation rate of consolidated crushed salt when average particle size decreases. This is contrary to the findings by Ouyang and Daemen (1989), they found that the sample with larger particle size consolidates more rapidly than the sample of smaller particle size. In addition, particle shape is likely to have an influence on crushed salt consolidation because it influences initial pore space and contacts force between particles (Korthaus, 1998). The effects of particle shape on granular packing are described by Guises et al. (2009), who state that the spherical particles are more packing density than the elliptical shape. The contact friction can be decreased the packing density (Figure 2.10). In general, the friction angle of particle normally increases with increasing angularity of particles (Koener, 1968; Alshibli and Alsaleh, 2004). Cho et al. (2006) confirm the increase of angularity or eccentricity produces an increase in void ratio. The method used to classify the roughness and sphericity of sedimentary particles in two-dimensional are obtained from Powers (1982) and Krumbein and Sloss (1963). They propose a chart to classify roundness and sphericity by using index numbers. This method are quick and easy to estimate particle shape.

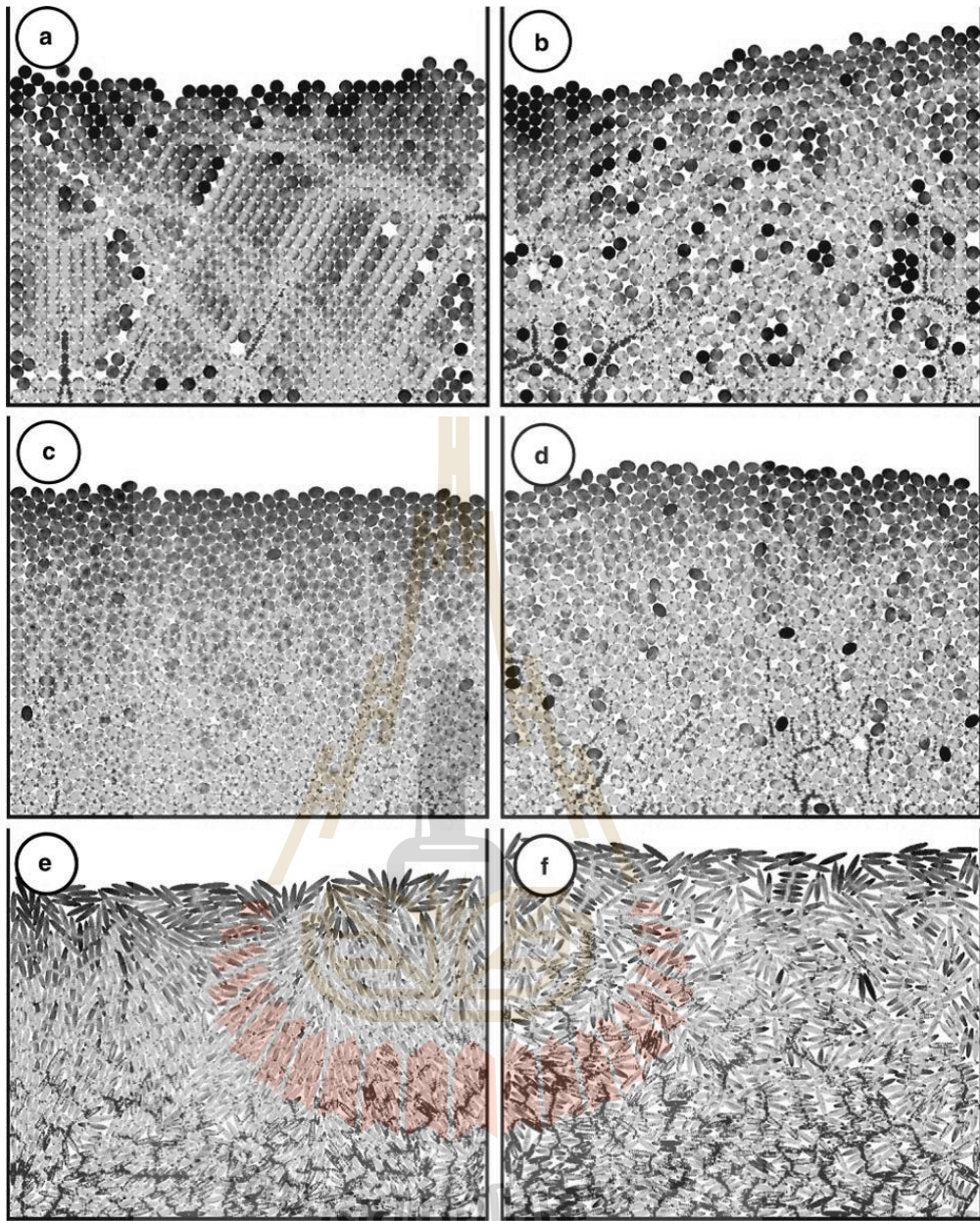


Figure 2.10 Packing of 900 particles where a, c and e are frictionless and b, d and f are frictional ($\mu = 0.5$) (Guises et al., 2009).

2.8 Conclusion of review

Salt and potash mines have used the salt tailing as sealing material due to its availability, low cost and physical, chemical and mechanical compatibility with the host rock. The factors affecting the mechanical performance of consolidated crushed salt are moisture, duration, consolidation stresses, initial density, particle size and temperature. The consolidation is effective only when moisture is available on grain contacts. As a consequence, dry crushed salt shows the lowest consolidation. The permeability of crushed salt can decrease by about two orders of magnitude as fractional density increases from 0.9 to 0.99. The volumetric creep strain rate increases with time and does not reach steady state values even after 1 to 2 months of load application. The uniaxial compressive strength and Young's modulus of crushed rock salt also increase with densification time. A variety of constitutive models have been developed to predict the behavior of crushed salt consolidation in mine openings. They are derived from test results and can be presented in several forms of mathematical functions. Some that are notably mentioned include viscoelasticity, elastic viscoplasticity, hot-pressing, pressure solution, healing mechanics and empirical models.

CHAPTER III

CRUSHED SALT PREPARATION AND INSTRUMENTATION

3.1 Introduction

This chapter describes the crushed salt sample preparation. Crushed salt used in this study is prepared from the Lower member of the Maha Sarakham formation in the Korat basin, northeastern Thailand. The salt cores are donated by Asean Potash Mining Co. Warren (1999) gives detailed origin and geologic description of the Maha Sarakham formation.

3.2 Crushed salt sample

The crushed salt sample belongs to the Lower member of the Maha Sarakham formation. Salt blocks are crushed by hammer mill (2HP-4 POLES, Spec jis c-4004) to produce particle sizes ranging from 0.075 to 4.75 mm (Figure 3.1). This size range is equivalent to those expected to be obtained as waste product from the mines. The specific gravity is 2.160. Table 3.1 gives chemical compositions of the specimens as analyzed by XRF. Five particle size ranges are selected for particle shape classification: 4.75-2.37, 2.36-1.1, 1.0-0.43, 0.42-0.15 and <0.15 mm. Twenty particles of each size range are randomly selected. The sphericity and roughness are determined from individual particles using an optical microscope (Olympus BX51M). Based on the widely used classification systems given by Power (1982) and Krumbein

and Sloss (1963) the crushed salt is classified as angular to sub-angular with high sphericity (Figures 3.2 and 3.3). The average values of roughness and sphericity of particle are shown in Tables 3.2 and 3.3.

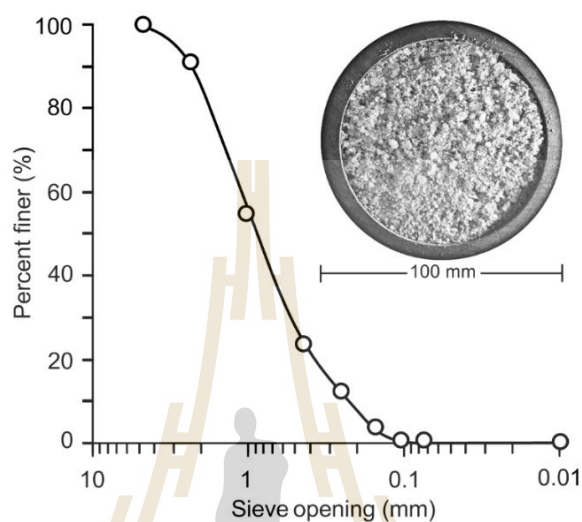


Figure 3.1 Grain size distribution of crushed salt.

Table 3.1 Chemical compositions of crushed salt obtained by XRF analysis.

Oxides	Percentage weight
Na ₂ O	20.70
MgO	4.39
Al ₂ O ₃	N/D
SiO ₂	0.03
SO ₃	0.05
Cl ₂ O	68.03
K ₂ O	6.40
CaO	0.26
Fe ₂ O ₃	N/D
Br ₂ O	0.16
SrO	N/D
Total	100

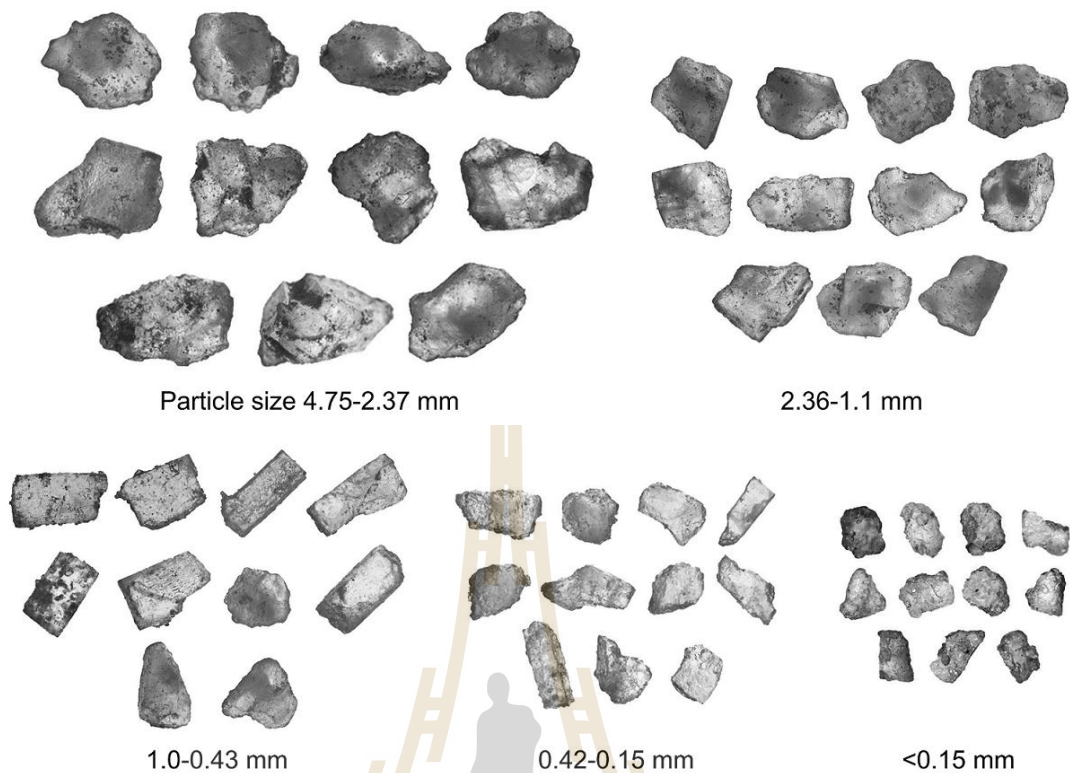


Figure 3.2 Examples of salt grains for different size ranges using Power (1982) method.

Table 3.2 Particle shape classification of crushed salt based on Powers (1982).

Particle size range (mm)	Roundness	Classification	Sphericity	Classification
4.75-2.37	1.5-2.5	Angular – Sub-angular	4.5	Spherical
2.36-1.1	1.5-2.5	Angular – Sub-angular	4.5	Spherical
1.0-0.43	1.5-2.5	Angular – Sub-angular	-2.5	Sub-spherical
0.42-0.15	1.5-2.5	Angular – Sub-angular	-2.5	Sub-spherical
<0.15	1.5-2.5	Angular – Sub-angular	-2.5	Sub-spherical

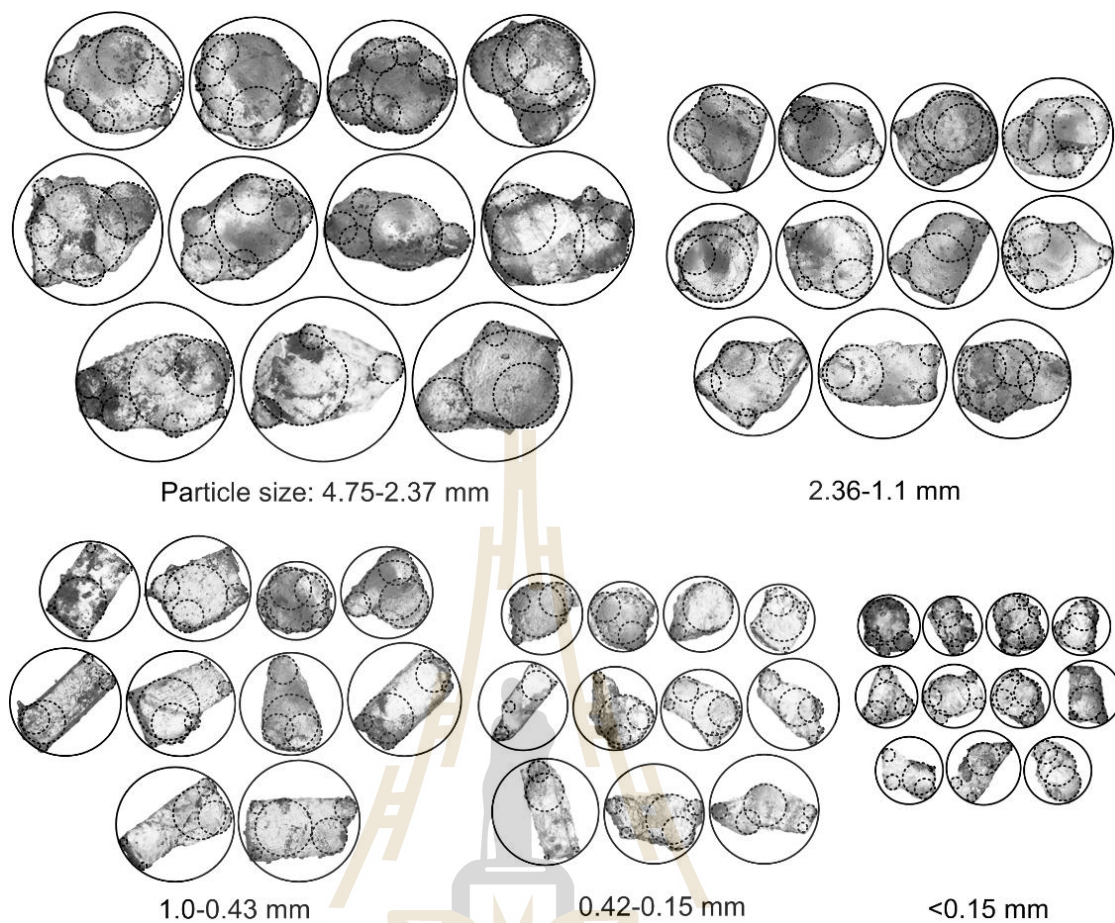


Figure 3.3 Examples of salt grains for different size ranges fitting with circle outline using Krumbein and Sloss (1963) method.

Table 3.3 Particle shape classification of crushed salt based on Krumbein and Sloss (1963).

Particle size range (mm)	Roundness (R)	Sphericity (S)	Regularity [$\rho = (R+S)/2$]
4.75-2.37	0.37	0.62	0.50
2.36-1.1	0.41	0.64	0.52
1.0-0.43	0.36	0.52	0.44
0.42-0.15	0.40	0.53	0.46
<0.15	0.47	0.54	0.51

Particles smaller than 1 mm appear to be more cubic shape than the larger ones. The shape of small particles are probably controlled by the cleavages in the salt crystals. This agrees with the observations obtained by Ouyang and Daemen (1989).

3.3 Saturated brine

Saturated brine is prepared by mixing rock salt with distilled water. The proportion of halite to water is about 39% by weight (Klein et al., 1988). Specific gravity of the saturated brine (S.G.B) is calculated as $S.G.B = \rho_{\text{Brine}}/\rho_{\text{H}_2\text{O}}$, where ρ_{Brine} is density of saturated brine (measured by a hydrometer in kg/m^3) and $\rho_{\text{H}_2\text{O}}$ is density of water. The specific gravity of the saturated brine used here is 1.211 at 21°C.

3.4 Fabrication of test cylinder

The consolidation tests are performed by applying constant axial stresses on the crushed salt mixed with saturated brine installed in a thick-wall stainless steel tube. The inner diameter of the steel tube is 54 mm, the outer diameter is 64 mm and the height is 200 mm (Figure 3.4). Two loading pistons fitted with rubber O-rings are used to apply axial stress on the opposite ends of the specimen. The piston has a drained hole to allow excess fluid to flow out during consolidation.

3.5 Suitable brine content

The suitable brine content is first determined by applying consolidation stresses (σ_{cons}) from 2.5, 5.0, 7.5 to 10 MPa to the crushed salt mixed with saturated brine from 0%, 5% to 10% by weight. The crushed salt and brine are mixed thoroughly in a plastic pan until each salt particle is coated with thin film of brine. This process

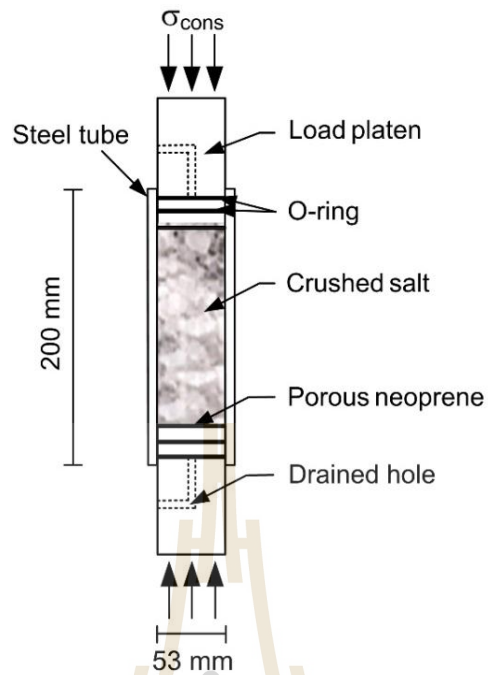


Figure 3.4 Laboratory arrangement for consolidation testing.

takes about 5 minutes. The mixture is then poured into the steel tube and lightly tapped to obtain a flat end. The initial length of specimen is obtained as 140 mm before inserting the loading pistons. This is equivalent to the initial volume of 320.63 cm^3 . This results in the initial densities before loading of 1.184, 1.247 and 1.310 g/cm^3 for the 0%, 5% and 10% brine contents. The results indicate that axial strain (ϵ_{cons}) increases with increasing brine content (Figure 3.5). The dry consolidation has the lowest consolidation. This agrees with results obtained by Shor et al. (1981) and Wang et al. (1992) that a small amount of fluid can significantly enhance the consolidation rate. The axial strains obtained at 5% and 10% brine contents are similar. The saturated brine content used in this study is therefore maintained constant at 5% by weight with the constant initial density of 1.247 g/cm^3 . This initial

density is maintained constant for all test samples by controlling the constant initial sample volume at 320.63 cm^3 (length = 140 mm and diameter = 54 mm).

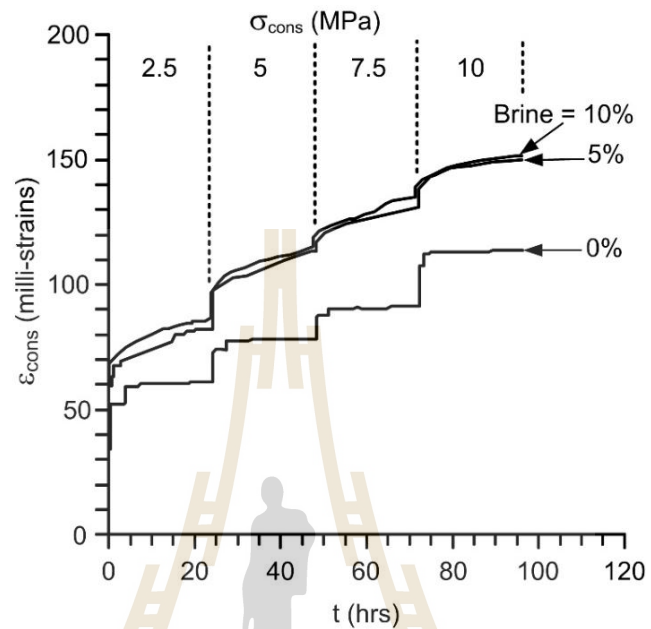


Figure 3.5 Axial strains as a function of time for different axial stresses and brine contents.

CHAPTER IV

LABORATORY TESTING

4.1 Introduction

This chapter describes the method and results of the laboratory experiments. The tests are divided into four groups; consolidation test, permeability test, uniaxial compression test and direct shear test. The results have been used to determine the effects of consolidation stresses and period on physical, hydraulic and mechanical properties of consolidated crushed salt. The results obtained here are also compared with other researches.

4.2 Consolidation test

4.2.1 Test method

The consolidation tests are performed by applying constant axial stresses on the crushed salt mixed with saturated brine installed in a thick-wall stainless steel tube (Figure 4.1). A consolidation load frame applies constant stresses (σ_{cons}) ranging from 2.5, 5, 7.5 to 10 MPa. The axial displacements are monitored by dial gages and are used to calculate the axial (consolidation) strains. The applied load is removed after 30, 90 and 180 days. A total of 12 specimens have been tested.

4.2.2 Consolidation test results

The consolidation test results under σ_{cons} of 2.5, 5, 7.5 and 10 MPa for 3 to 15 days are obtained from Somtong et al. (2014). Figure 4.2 and Table 4.1 show the axial strains (ϵ_{cons}) and density (ρ_{cons}) as a function of consolidation period (t) up

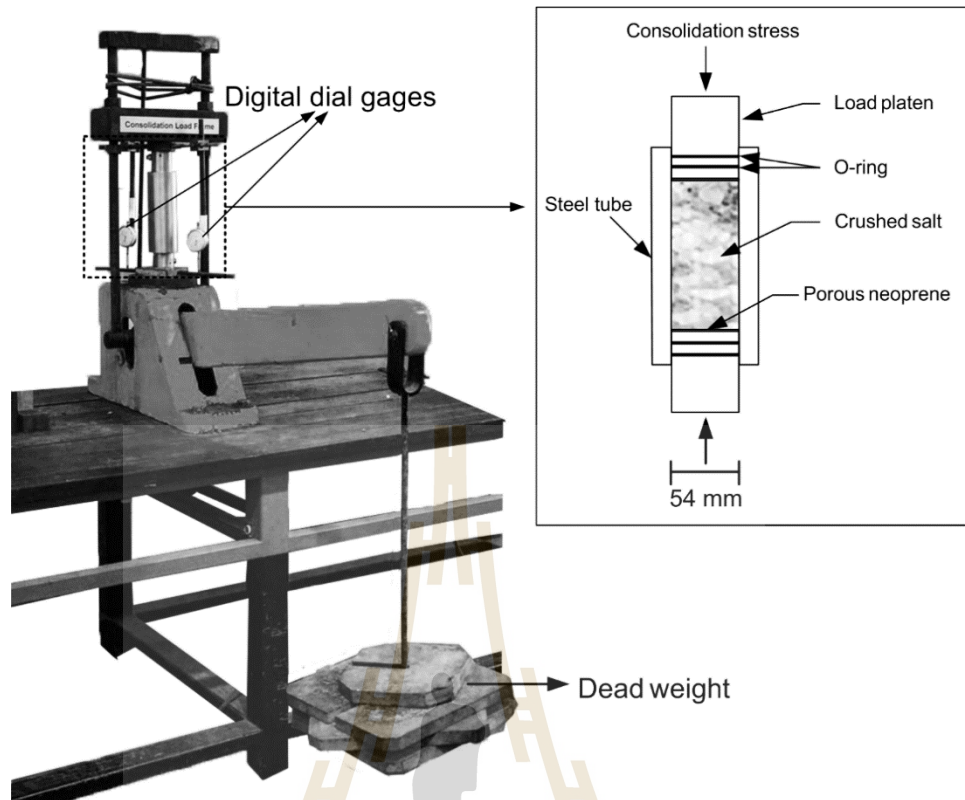


Figure 4.1 Laboratory arrangement for consolidation testing.

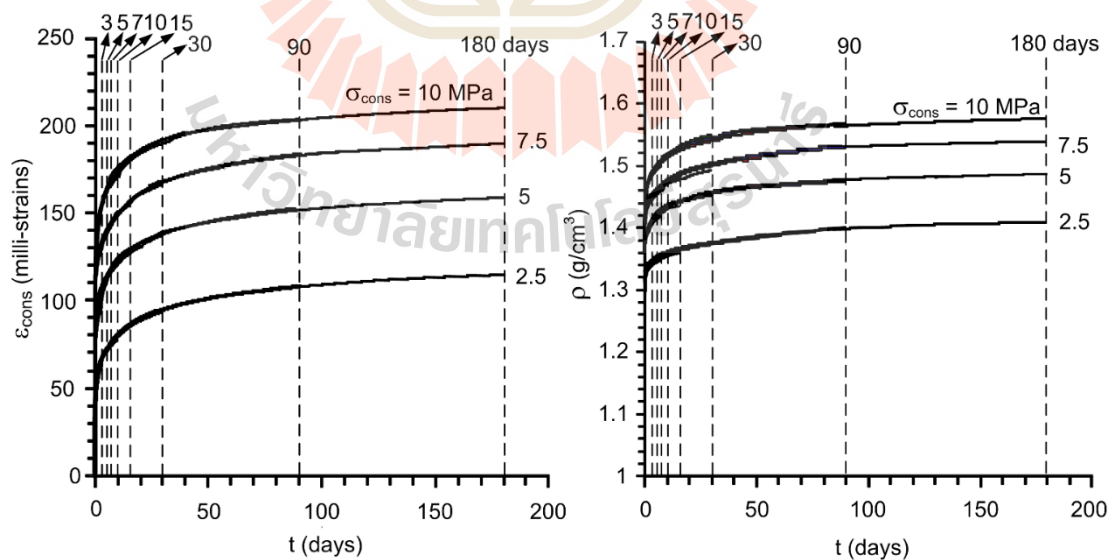


Figure 4.2 Axial strain (ϵ_{cons}) and density (ρ_{cons}) as a function of consolidation period (t) for different consolidation stresses (σ_{cons}).

Table 4.1 Physical properties of crushed salt after consolidation.

σ_{cons} (MPa)	Parameters	t (days)							
		3	5	7	10	15	30	90	180
2.5	ϵ_{cons} (milli-strains)	62.10	69.00	69.03	75.90	82.69	95.99	108.90	115.22
	ρ_{cons} (g/cm ³)	1.33	1.34	1.34	1.35	1.36	1.38	1.40	1.41
5	ϵ_{cons} (milli-strains)	108.90	115.22	115.22	121.45	127.59	139.63	151.33	162.72
	ρ_{cons} (g/cm ³)	1.40	1.41	1.41	1.42	1.43	1.45	1.47	1.49
7.5	ϵ_{cons} (milli-strains)	133.65	139.63	145.52	151.33	157.07	164.30	184.61	189.91
	ρ_{cons} (g/cm ³)	1.44	1.45	1.46	1.47	1.48	1.49	1.53	1.54
10	ϵ_{cons} (milli-strains)	157.07	162.72	168.31	173.81	184.61	195.14	205.39	210.42
	ρ_{cons} (g/cm ³)	1.48	1.49	1.50	1.51	1.53	1.55	1.57	1.58

to 180 days. A higher applied consolidation stress (σ_{cons}) leads to a higher strain and density. The strains increase immediately after the axial stress is applied. The strain rates decrease with time, and tend to remain relatively unchanged after 30 days. The samples under the same applied stress show the same trend of the $\epsilon_{\text{cons}}-t$ curves, suggesting that the test results are repeatable and the consolidation procedure is reliable. The observations agree reasonably with those obtained by Case et al. (1987) who found that the volumetric creep strain rate decreases with time and does not reach steady state values even after 1 to 2 months of load application.

4.2.3 Deformation mechanisms

The deformation mechanisms such as grain re-orientation, grain breakage (crushing), plastic deformation (intragranular gliding and dislocation), possibly dissolution-precipitation are involved in the natural consolidation of

sediments (De Boer, 1977). The consolidation of a soil sample usually involves the following three mechanical: 1) deformation of grains, 2) compression of air and fluids in the voids, and 3) squeezing out of air and fluids from the voids (Holtz and Kovacs, 1981). However, the concept of deformation mechanism of crushed salt consolidation is not the same with the consolidation of soil sample due to the crushed salt is the viscous material. The deformation of the crushed salt may be divided into two phases: instantaneous and transient deformations (Figure 4.3). The mechanism governing the instantaneous deformation is the rearrangement of the salt particles which occurs immediately after load application (Hwang et al., 1993; Callahan et al., 1996). The main factor in this phase is the brine content, which supports the results shown in Figure 3.5 that axial strain of consolidation test increases with increasing brine content. The reasons agree with the conclusion drawn by Shor et al. (1981) who suggest that the consolidation of crushed salt may be greatly enhanced by the presence of brine, and by Hwang et al. (1993) who conclude that the water has a great effect on the consolidation of crushed salt, possibly due to the sliding, rotation, or crushing of the contact zone of the granular material. The transient phase involves cracking and sliding between salt particles and creep deformation of the salt particles. This leads to the deceleration of the deformation. The deformation mechanism in transient phase is supported by Hansen (1997) who discusses the optical photomicrographs of thin sections of crushed salt from the consolidation tests.

4.2.4 Strain energy density principle

The strain energy density principle is applied here to determine the energy required to consolidate the crushed salt under different stresses and periods. It is postulated that the crushed salt can be consolidated by applying the mean strain energy

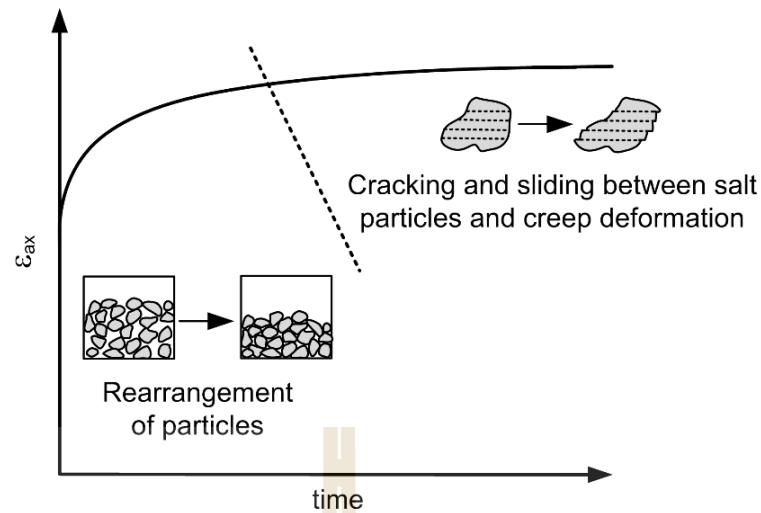


Figure 4.3 Conceptual mechanism of crushed salt deformation.

(W_m). This energy can be calculated from mean stresses (σ_m) and strains (ϵ_m) (Jaeger et al., 2007):

$$W_m = (3/2) \cdot \sigma_m \cdot \epsilon_m \quad (4.1)$$

$$\sigma_m = (\sigma_1 + \sigma_2 + \sigma_3) / 3 \quad (4.2)$$

$$\epsilon_m = (\epsilon_1 + \epsilon_2 + \epsilon_3) / 3 \quad (4.3)$$

The lateral stresses (σ_2 and σ_3) on the specimen can be calculated as a function of time based on the uniaxial strain condition, i.e. assuming that no lateral strain occurs in the steel tube during consolidation. The axial strains from the measurement results therefore represent the volumetric strain.

$$\sigma_2 = \sigma_3 = [v / (1-v)] \sigma_1 \quad (4.4)$$

where ν is Poisson's ratio, and σ_1 is consolidation stress (σ_{cons}). The calculated mean stress, strain and strain energy density are given in Table 4.2. The specimens under higher consolidation stress and period lead to higher mean strain energy densities (Figure 4.4).

4.3 Permeability test

The nitrogen gas flow testing is performed to determine intrinsic permeability of crushed salt consolidation that changes over time. The flow rates under constant head are continuously monitored every 6 hours for 30, 90 and 180 days of each test conditions. Nitrogen gas is injected under 10 psi into the tube test to measure

Table 4.2 Mean stresses and strains and mean strain energy densities applied to crushed salt during consolidation.

σ_{cons} (MPa)	Parameters	t (days)							
		3	5	7	10	15	30	90	180
2.5	σ_m (MPa)	N/A	1.85	1.81	1.81	1.81	1.77	1.73	1.69
	ϵ_m (10^{-3})	N/A	23.33	25.00	26.67	29.33	31.67	35.00	38.33
	W_m (MPa)	N/A	0.058	0.062	0.066	0.073	0.079	0.067	0.095
5	σ_m (MPa)	3.54	3.46	3.46	3.46	3.38	3.31	3.24	3.16
	ϵ_m (10^{-3})	33.33	38.00	39.33	40.33	42.67	46.00	50.00	56.67
	W_m (MPa)	0.165	0.188	0.195	0.200	0.212	0.228	0.248	0.281
7.5	σ_m (MPa)	5.03	4.97	4.96	4.90	4.85	4.75	4.64	4.63
	ϵ_m (10^{-3})	41.67	47.33	49.00	50.33	53.33	56.00	61.33	66.67
	W_m (MPa)	0.310	0.352	0.365	0.374	0.397	0.417	0.456	0.496
10	σ_m (MPa)	6.33	6.33	6.19	6.19	6.19	6.12	6.06	5.99
	ϵ_m (10^{-3})	53.33	55.67	57.33	58.33	61.33	63.33	67.67	70.00
	W_m (MPa)	0.530	0.553	0.569	0.579	0.609	0.629	0.672	0.695

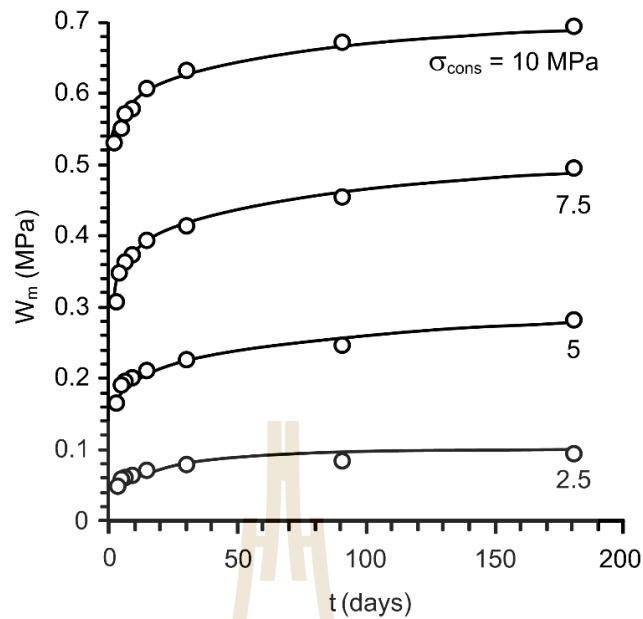


Figure 4.4 Mean strain energy densities (W_m) as a function of consolidation period (t) for different consolidation stresses (σ_{cons}).

permeability of crushed salt sample. The test arrangement (Figure 4.5) comprises a nitrogen gas tank pressure, regulating valve, high pressure tubing and air flow meter.

The permeability coefficient (K') can be calculated by ASTM (D2434-68): $\Delta h = (\Delta P / \gamma_f)$ where Δh is head difference (m); ΔP is difference pressure at the initial point and end point (kPa); and γ_f is unit weight of fluid (kN/m^3), the flow in longitudinal direction of a tested system is described by Darcy's law. The coefficient of permeability can be calculated from the equation (Indrarata and Ranjith, 2001).

$$Q = K'A (\Delta h/L) \quad (4.5)$$

where K' is hydraulic conductivity (m/s); Q is flow rate (m^3/s); A is a cross-section area of flow (m^2); $\Delta h/L$ is hydraulic head gradient. The hydraulic conductivity used to

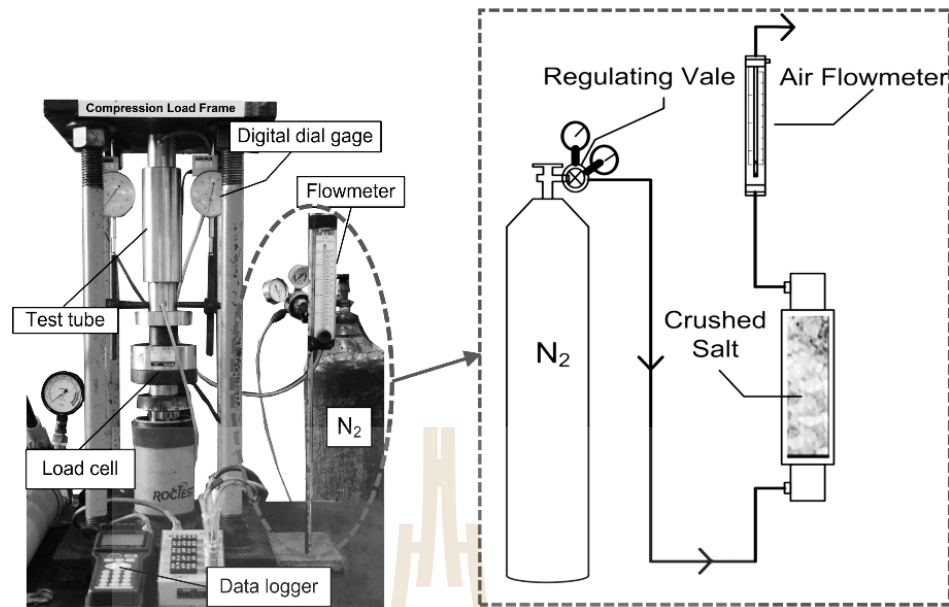


Figure 4.5 Laboratory arrangement for permeability testing.

$$k = (K'\mu/\gamma_f) \quad (4.6)$$

calculate the intrinsic permeability (k) from equation: where k is intrinsic permeability (m^2 ; and μ is dynamic viscosity of nitrogen gas ($Pa \cdot s$). The results indicate that when the consolidation increases the intrinsic permeability of crushed salt decreases (Loken et al., 1997), as shown in Figure 4.6.

4.4 Uniaxial compression tests

4.4.1 Test method

To assess the mechanical properties of the consolidated crushed salt the specimens are removed from the steel tube after 30, 90 and 180 days. They appear solidified, particularly under long consolidation period and high stress. The specimen ends are dried-cut to obtain flat and parallel surfaces. The length-to-

diameter ratios are about 2.0-2.2. The specimen compressive strengths are determined by axially loading under constant rate of 0.5-1 MPa/second until failure (Figure 4.7).

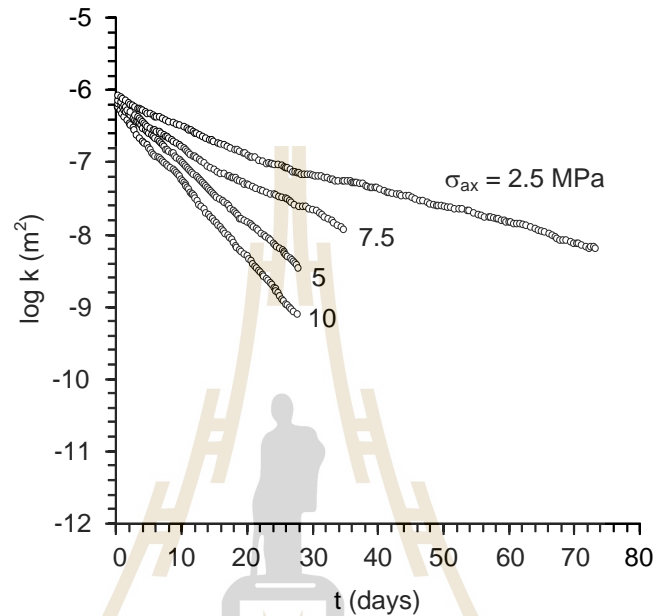


Figure 4.6 Intrinsic permeability (k) as a function of consolidation period (t) and for different consolidation stresses (σ_{cons}).

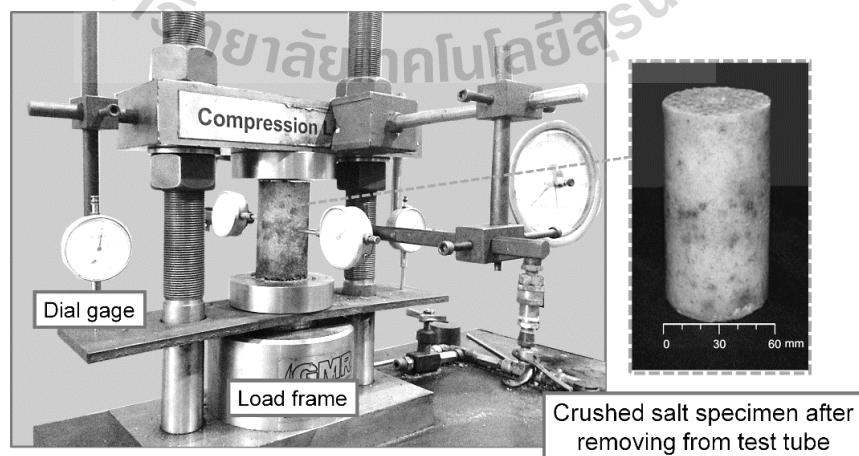


Figure 4.7 Uniaxial compression test.

Neoprene sheets are used to minimize the friction at the interfaces between the loading platen and the sample surface. The axial and lateral displacements are monitored. The compressive strength, elastic modulus and Poisson's ratio are determined in accordance with the ASTM (D2938-95) standard practice. The post-failure characteristics are observed and recorded. Tables 4.3 shows the dimensions and weigh of the specimen for uniaxial compression tests.

4.4.2 Uniaxial compression test results

The uniaxial compression test results under σ_{cons} of 2.5, 5, 7.5 and 10 MPa for 3 to 15 days are obtained from Somtong et al. (2014). The specimen density after removed from the steel tube is measured. A higher applied consolidation stress leads to a higher density (Table 4.3). The density increases rapidly from 1.247 g/cm³ within 3 days after load application. The increasing rate reduces after 15 days of consolidation. There are more sensitive to the consolidation stresses than to the consolidation period. The increase of density can be represented by an empirical equation, as shown in Figure 4.8.

Figure 4.9 shows the stress-strain curves obtained from different consolidation stresses and periods. High consolidation period shows a higher strength. This effect becomes larger under higher σ_{cons} . The uniaxial compressive strength is reached to 20 MPa under consolidation stress of 10 MPa for 180 days, which was 74% of the average strength of intact rock salt obtained by Sriapai et al. (2012). Some post-test specimens of consolidated crushed salt after uniaxial compression test are shown in Figure 4.10. Bulging failure is observed for low applied consolidation stress and period while the extension and shear failure modes are found under the high applied consolidation stress and period.

Table 4.3 Crushed salt consolidation specimens prepared for uniaxial compression tests.

σ_{cons} (MPa)	t (days)	Diameter (cm)	Length (cm)	Weight (g)	Density (g/cm ³)
2.5	3	5.4	12.95	398.1	1.34
	5	5.4	12.90	398.1	1.35
	7	5.4	12.86	398.8	1.35
	10	5.4	12.83	399.4	1.36
	15	5.4	12.71	399.4	1.37
	30	5.4	12.59	398.7	1.38
	90	5.4	12.38	399.2	1.41
	180	5.4	12.26	399.7	1.42
5	3	5.4	12.41	399.6	1.41
	5	5.4	12.27	398.5	1.42
	7	5.4	12.28	399.2	1.42
	10	5.4	12.20	399.9	1.43
	15	5.4	12.12	399.4	1.44
	30	5.4	11.95	399.5	1.46
	90	5.4	11.74	398.5	1.48
	180	5.4	11.68	399.2	1.49
7.5	3	5.4	12.00	398.7	1.45
	5	5.4	11.89	398.9	1.46
	7	5.4	11.89	399.7	1.47
	10	5.4	11.79	398.5	1.48
	15	5.4	11.73	399.6	1.49
	30	5.4	11.58	399.8	1.51
	90	5.4	11.35	399.9	1.54
	180	5.4	11.27	399.8	1.55
10	3	5.4	11.65	399.5	1.50
	5	5.4	11.60	399.5	1.50
	7	5.4	11.53	399.4	1.51
	10	5.4	11.43	399.9	1.53
	15	5.4	11.34	399.3	1.54
	30	5.4	11.21	399.9	1.56
	90	5.4	11.05	400.0	1.58
	180	5.4	11.02	400.0	1.58

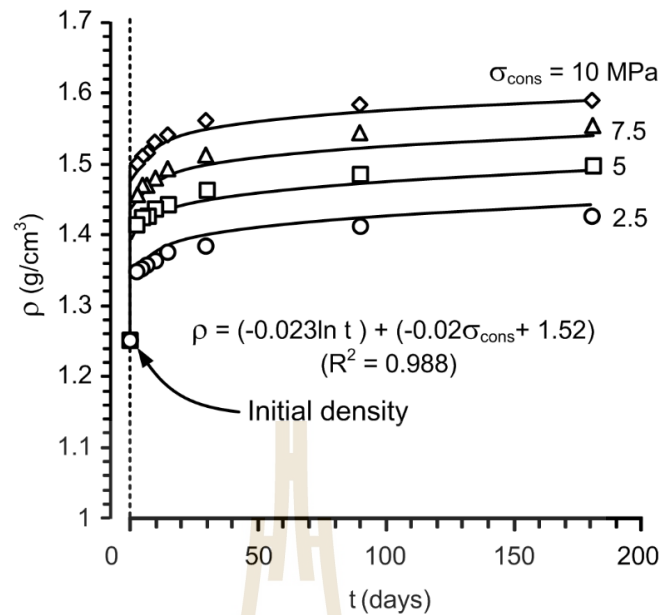


Figure 4.8 Density of crushed salt specimens after consolidation.

Table 4.4 summarizes the mechanical properties of the consolidated crushed salt specimens. Longer consolidation period and higher consolidation stress lead to higher strength and elasticity of the specimens. The Poisson's ratios however decrease slightly with increasing consolidation period. This generally agrees with the results obtained from Wang et al. (1994) and Miao et al. (1995) who performed uniaxial compression test on compacted crushed salt specimens. They report that under 15 MPa consolidation stresses the strength and elastic modulus increase up to 28.4 MPa and 9.46 GPa after being consolidated for 97 days. Figure 4.11 shows the variation of the specimen compressive strength (σ_c) and elastic parameters (E and ν) with time under different consolidation stresses. The results indicate that the crushed salt becomes denser, stiffer, stronger and less compressible with time and applied stress. This may involve the recrystallization of brine, and rearrangement and deformation of salt particles.

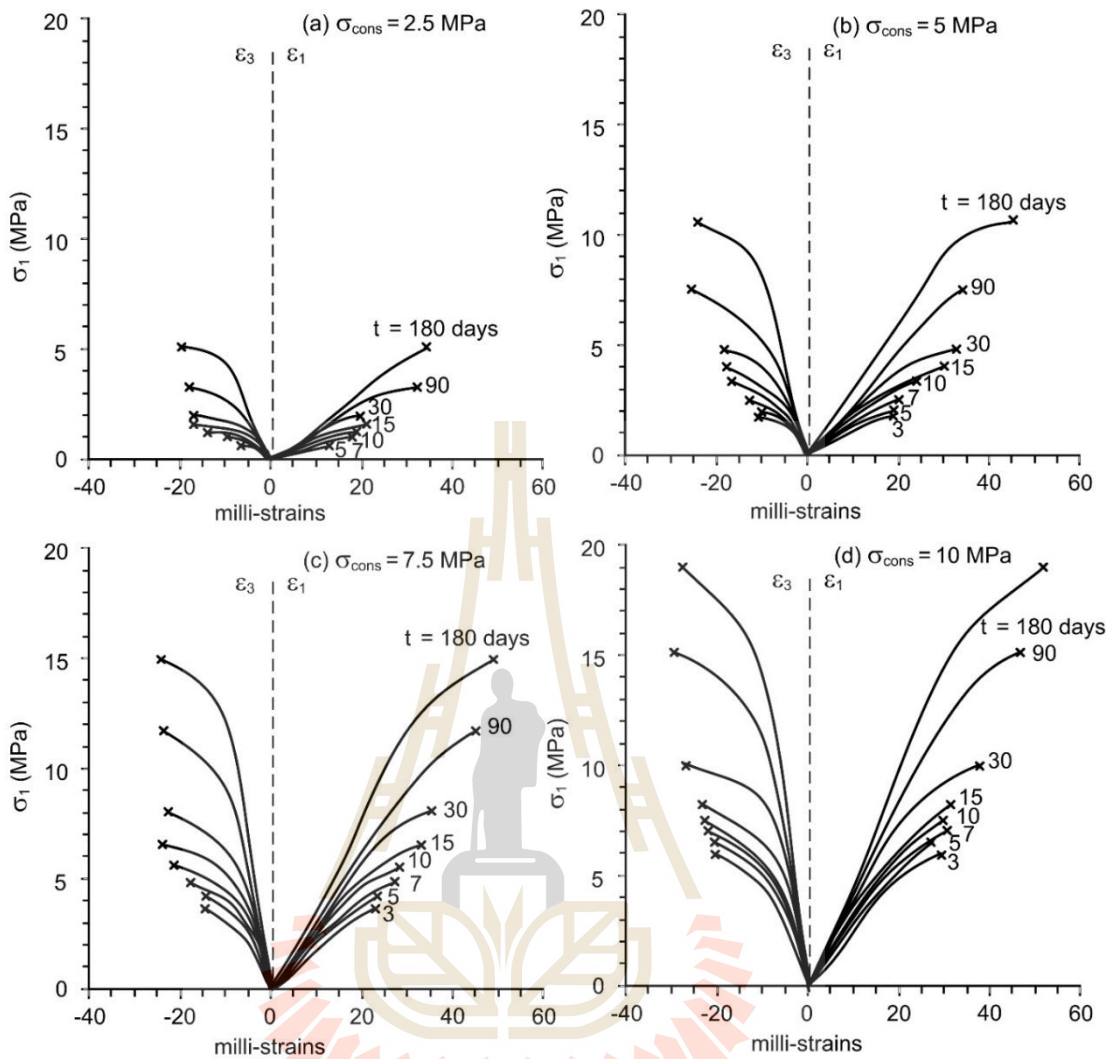


Figure 4.9 Stress-strain curves obtained from uniaxial compression testing of crushed salt specimens after consolidation.

4.4.3 Empirical equations

The mechanical results are used to develop a set of empirical equations. The empirical equations are presented as a function of consolidation period and consolidation stress. The regression analysis on the test data using IBM SPSS Statistics 19 (Wendai, 2000) determines the relevant parameters in the empirical equation. The coefficient of correlation (R^2) is used to indicate the accuracy and

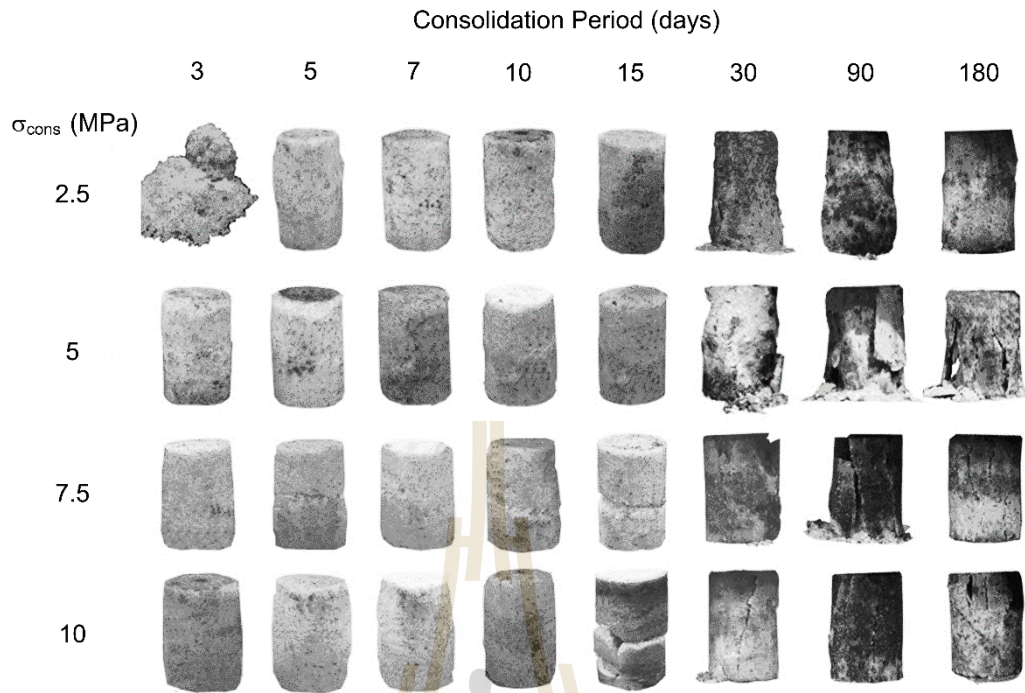


Figure 4.10 Post-test specimens of uniaxial compression testing.

Table 4.4 Mechanical properties of crushed salt after consolidation.

σ_{cons} (MPa)	Parameters	t (days)							
		3	5	7	10	15	30	90	180
2.5	σ_c (MPa)	N/A	0.52	1.03	1.22	1.62	1.98	3.23	5.10
	E (MPa)	N/A	62.0	74.1	82.0	100.3	110.9	139.9	160.0
	ν	N/A	0.38	0.37	0.37	0.37	0.36	0.35	0.34
5	σ_c (MPa)	2.01	2.03	2.60	3.34	4.14	4.82	7.38	10.51
	E (MPa)	121.0	142.2	160.2	172.2	180.1	199.9	230.2	280.1
	ν	0.36	0.35	0.35	0.35	0.34	0.33	0.32	0.31
7.5	σ_c (MPa)	3.78	4.15	4.82	5.50	6.48	7.28	11.71	15.06
	E (MPa)	189.3	213.2	229.4	250.0	260.0	291.0	331.9	400.1
	ν	0.34	0.34	0.33	0.33	0.32	0.31	0.30	0.30
10	σ_c (MPa)	6.20	6.52	7.10	7.51	8.21	10.00	15.07	19.02
	E (MPa)	271.0	299.9	321.0	340.9	361.2	370.1	438.9	500.0
	ν	0.31	0.31	0.30	0.30	0.30	0.29	0.29	0.28

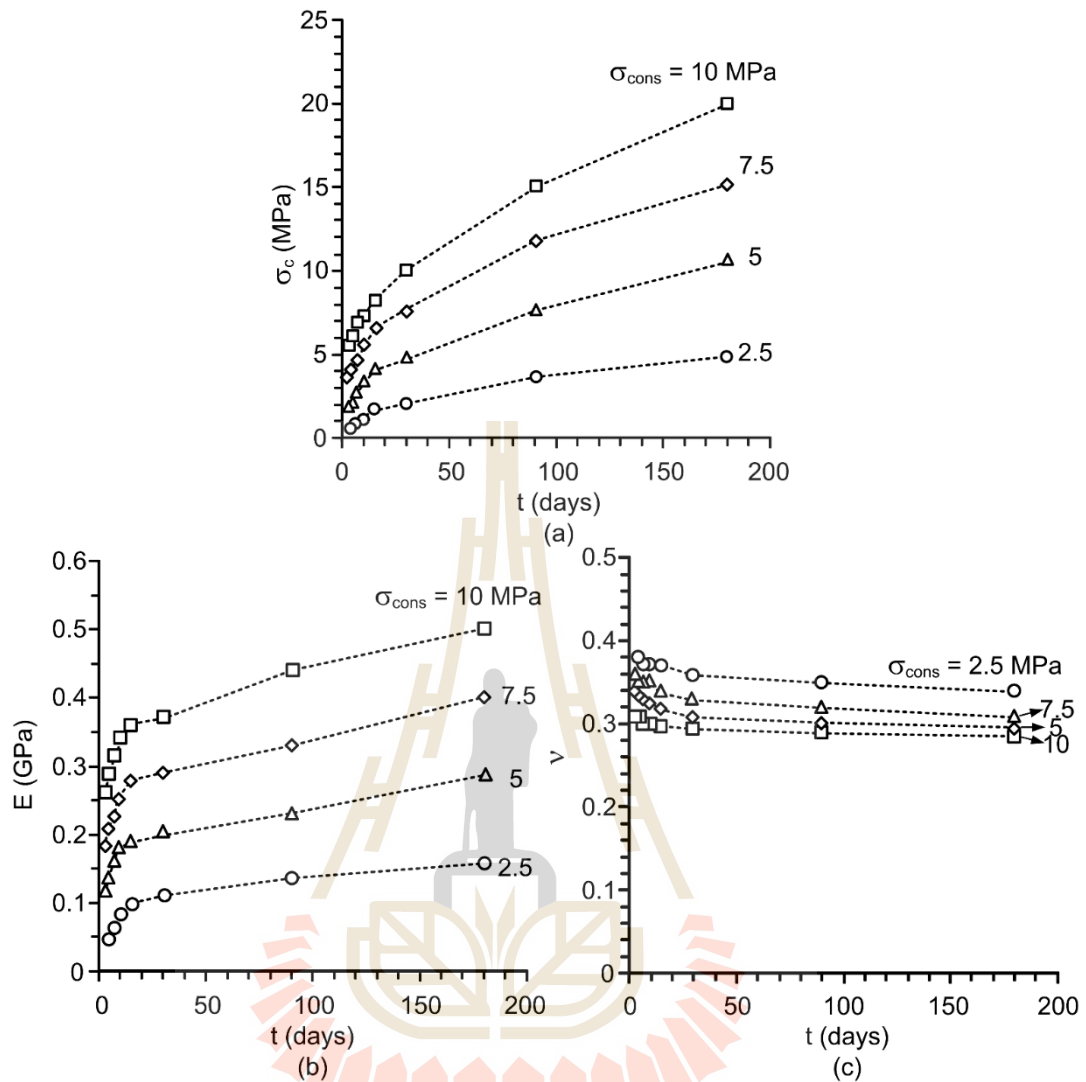


Figure 4.11 Uniaxial compressive strength (a), elastic modulus (b) and Poisson's ratio (c) as a function of consolidation period (t) for different consolidation stresses (σ_{cons}).

reliability of the proposed empirical equation. The relationships between compressive strength, elastic modulus and Poisson' ratio as a function of consolidation stress and consolidation period which can be represented by an exponential equation:

$$\sigma_c = (\alpha\sigma_{\text{cons}}) / (1 - \exp(\beta t)^{\lambda}) \quad (4.7)$$

$$E = (\delta\sigma_{\text{cons}}) / (1 - \exp(\eta t)^\phi) \quad (4.8)$$

$$\nu = (\kappa \ln t) + (\lambda\sigma_{\text{cons}} + \iota) \quad (4.9)$$

where σ_c is uniaxial compressive strength of crushed salt specimen, E is elastic modulus, ν is Poisson's ratio, t is time for consolidation, and $\alpha, \beta, \chi, \delta, \eta, \phi, \kappa, \lambda,$ and ι are empirical constants, as shown in Figure 4.12. All empirical equation can provide good correlation with the test data, with R^2 greater than 0.9. These equations can link the mechanical properties of the consolidated crushed salt with the consolidation stress and period.

4.4.4 Octahedral shear stresses and shear strains

The octahedral shear stresses and shear strains at failure are also determined using the following relations (Jaeger et al., 2007):

$$\tau_{\text{oct}} = (1/3) [2 (\sigma_1 - \sigma_3)^2]^{1/2} \quad (4.10)$$

$$\gamma_{\text{oct}} = (1/3) [(\varepsilon_1 - \varepsilon_2)^2 + (\varepsilon_1 - \varepsilon_3)^2 + (\varepsilon_2 - \varepsilon_3)^2]^{1/2} \quad (4.11)$$

where σ_1, σ_2 and σ_3 are the major, intermediate and minor principal stress, $\varepsilon_1, \varepsilon_2$ and ε_3 are the major, intermediate and minor principal strains.

The applied octahedral shear stresses are plotted as a function of octahedral shear strain in Figures 4.13. The shear stress-strain relations are nonlinear, particularly under high consolidation period. Higher consolidation period result in higher octahedral shear stresses and lower octahedral shear strains at failure.

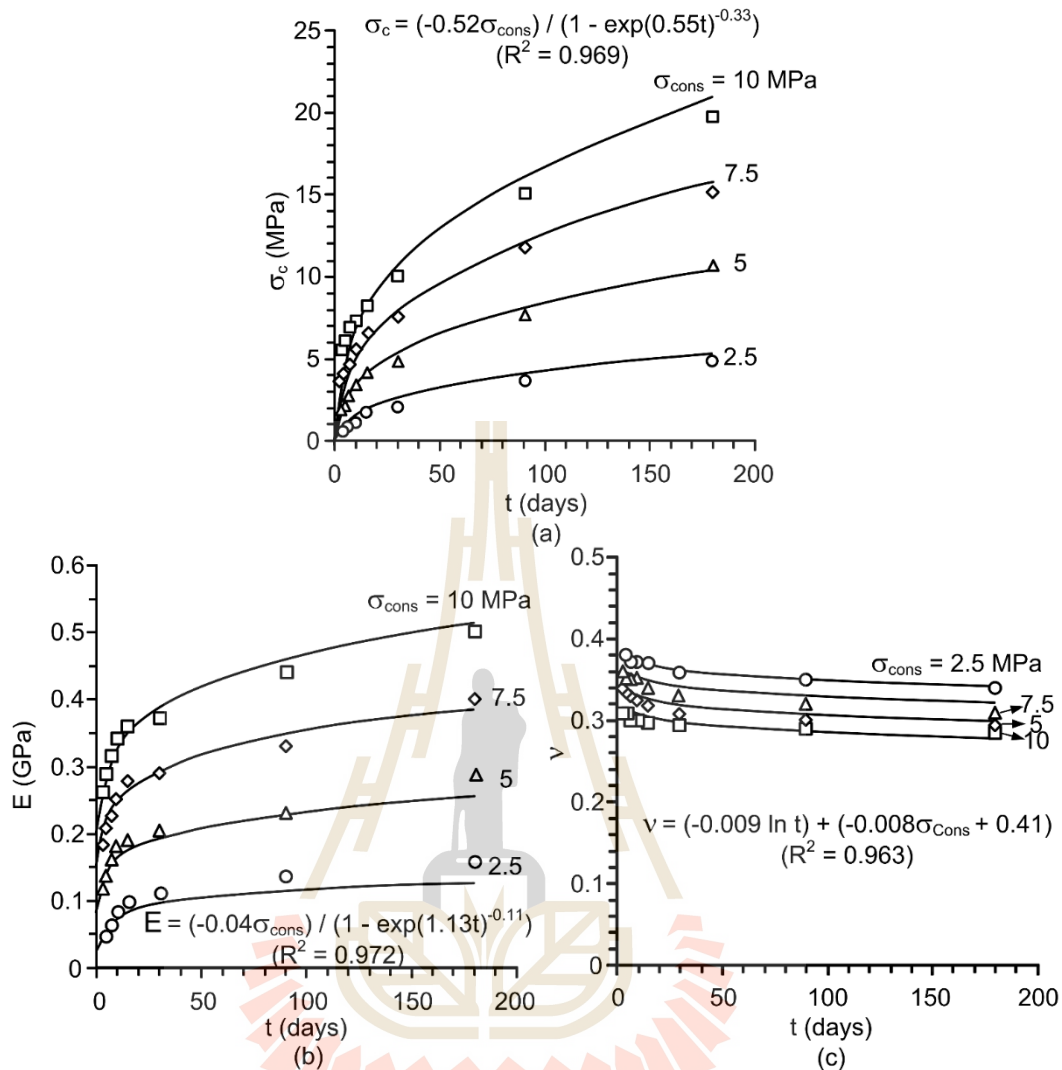


Figure 4.12 Predicted uniaxial compressive strength (a), elastic modulus (b) and Poisson's ratio (c) as a function of consolidation period (t) for different consolidation stresses (σ_{cons}).

4.5 Direct shear test

4.5.1 Test method

The direct shear tests are performed to determine the maximum shear stress of rock salt and crushed salts. The test method and calculation follow the ASTM (D5607-08) standard practice. The normal force is applied by the vertical hydraulic

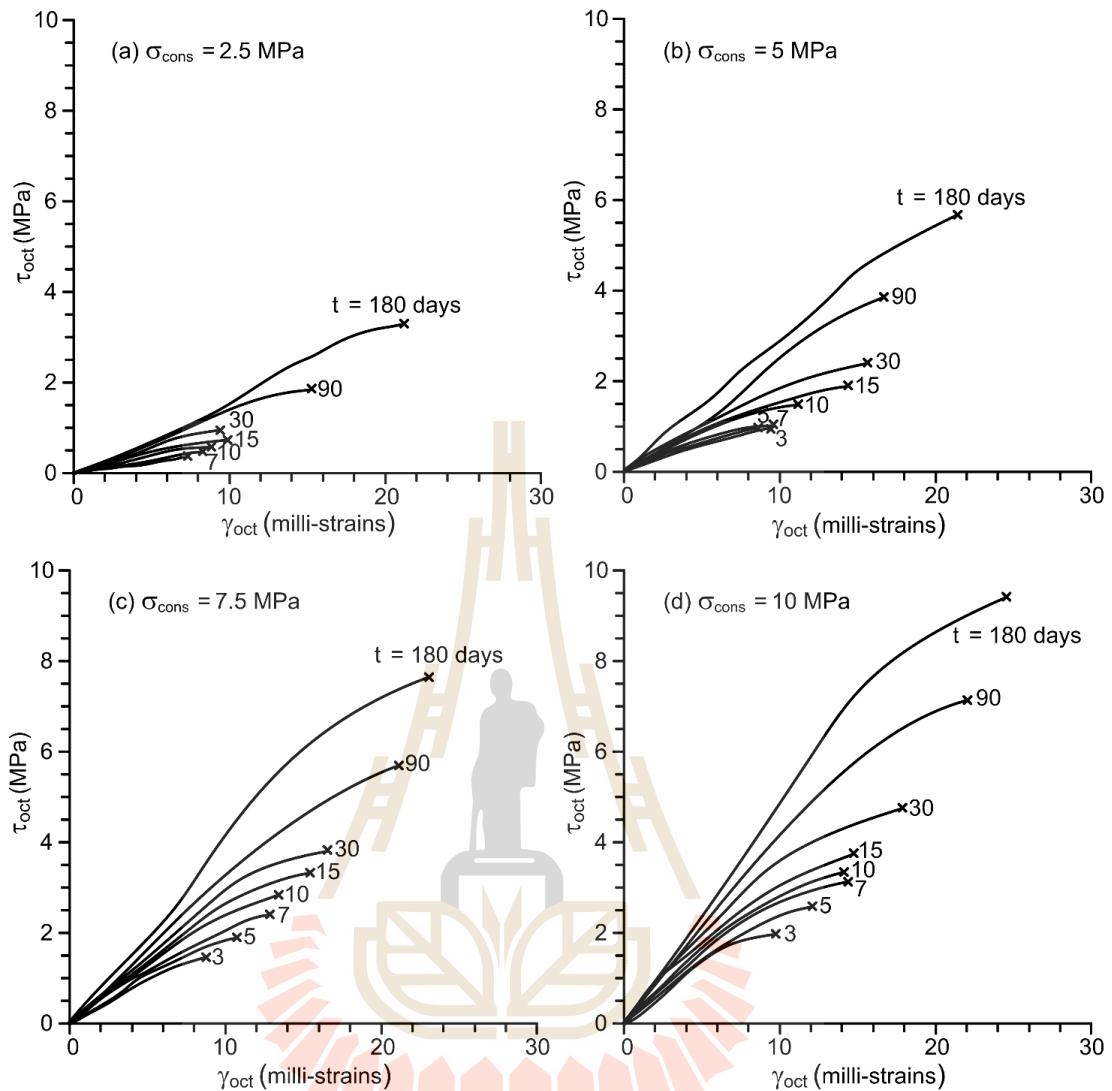


Figure 4.13 Octahedral shear stress-strain curves of crushed salt after consolidation under different consolidation stresses and periods.

load cell are 0.5, 1, 1.5 and 2 MPa for rock salt and 0.04, 0.08, 0.1 and 0.15 MPa for crushed salt. Shear force is applied by a horizontal hydraulic load cell. The peak shear strength is used to calculate the cohesion and friction angle. Each specimen is sheared once under the predefined constant normal stress using a direct shear device. The shear force is continuously applied until a total shear displacement of 5 mm is

reached. The applied normal and shear forces and the corresponding normal and shear displacements are monitored and recorded.

4.5.2 Direct shear test results

The shear stresses as a function of shear displacement and peak shear stresses as a function of normal stresses from the direct shear test are shown in Figures 4.14 for rock salt and Figure 4.15 for crushed salt. The shear strength (τ) is calculated based on the Coulomb's criterion (Jaeger et al., 2007) as follows:

$$\tau_p = c_p + \sigma_n \tan \phi_p \quad \text{for peak shear strength} \quad (4.12)$$

where σ_n is the normal stress, c_p is the peak cohesion and ϕ_p is the peak friction angle.

The results indicate that the shear stresses increase with shearing displacement, particularly under high normal stresses. The cohesion of rock salt and crushed salt are 0.033 MPa and 0.055 MPa and friction angle are 19° and 29°, respectively. The cohesion and friction angle will be used in the numerical analysis to assess the effectiveness of the pre-consolidated crushed salt for subsidence reduction in salt and potash mines.

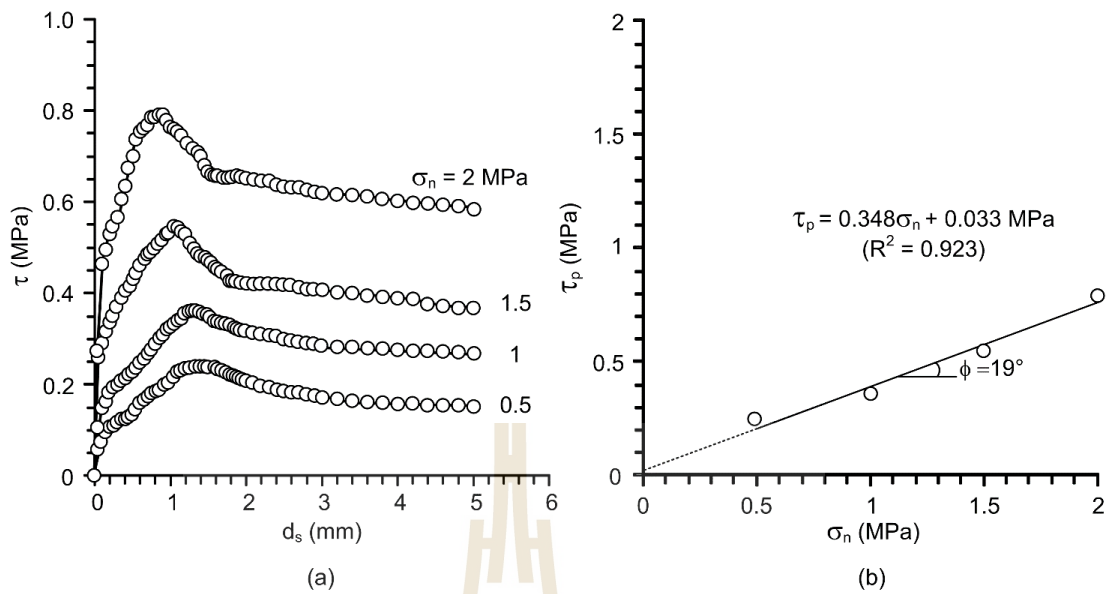


Figure 4.14 Direct shear test results of rock salt; (a) shear stress (τ) as a function of shear displacement (d_s); (b) shear strength (τ_p) as a function of normal stress (σ_n).

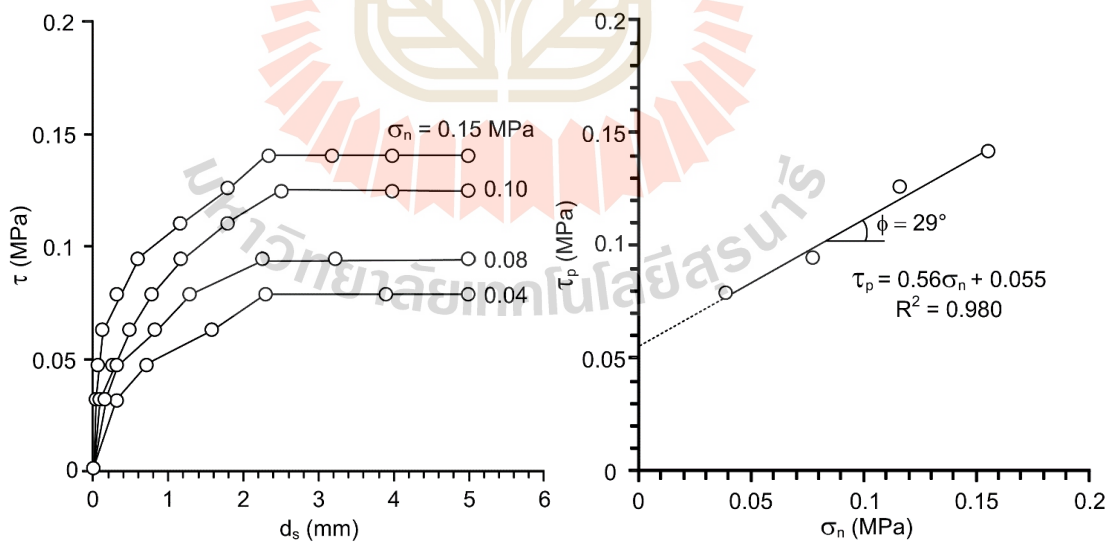


Figure 4.15 Direct shear test results of crushed salt; (a) shear stress (τ) as a function of shear displacement (d_s); (b) shear strength (τ_p) as a function of normal stress (σ_n).

CHAPTER V

MODELLING OF SUBSIDENCE REDUCTION

BY CRUSHED SALT BACKFILL IN MINE OPENINGS

5.1 Introduction

Series of numerical analyses are performed to assess the effectiveness of the pre-consolidated crushed salt for subsidence reduction in salt and potash mines. A finite difference code (FLAC) is used to calculate the creep deformation of room and pillar before and after the crushed salt backfill has been installed. The subsidence magnitudes under a variety of crushed salt properties and emplacement periods are used as an indicator of the subsidence reduction effectiveness.

5.2 Boundary conditions

The finite difference code FLAC (Itasca, 1992) is used in the simulations of the room and pillar mining under plane strain. The rock sequences at Kham Thale So district, Nakhon Ratchasima province are used in the simulations (Figures 5.1 and 5.2). To cover the entire range of the mine opening dimensions, over 3,000 meshes have been constructed to obtain accurate simulation results. The left and right boundaries are fixed in the x-axis, and the bottom boundary is fixed in the y-axis. The top boundary can move freely in both directions. The smallest mesh used around the opening is $0.35 \times 0.35 \text{ m}^2$ because the stress and strain gradients are high at this zone. The mesh far from the opening is gradually larger.

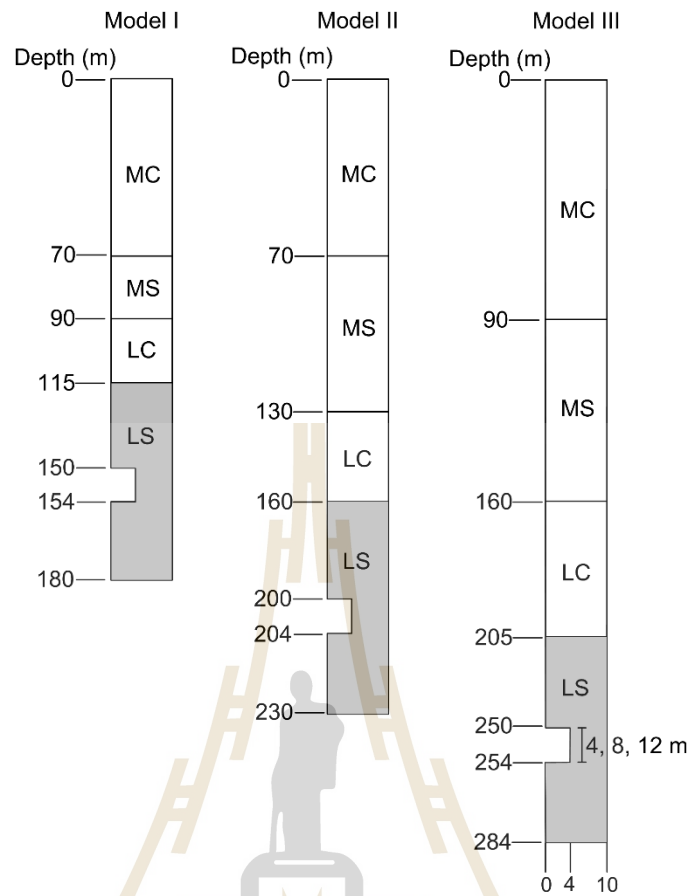


Figure 5.1 Geologic sequences used in simulations for salt mine.

5.3 Mechanical properties

Table 5.1 gives material properties from the Lower Salt member: rock salt with pure halite and potash with carnallite (carnallite content, $C\% = 40$). The $C\%$ of 40 is commonly found at the APMC mine. The overburden formations are assumed to be elastic. The Lower Salt member is assumed to behave as the Burgers material. The Burgers constitutive equation is a built-in subroutine in FLAC. Findley et al. (1989) and Jaeger et al. (2007) provide a governing equation for the Burgers model as:

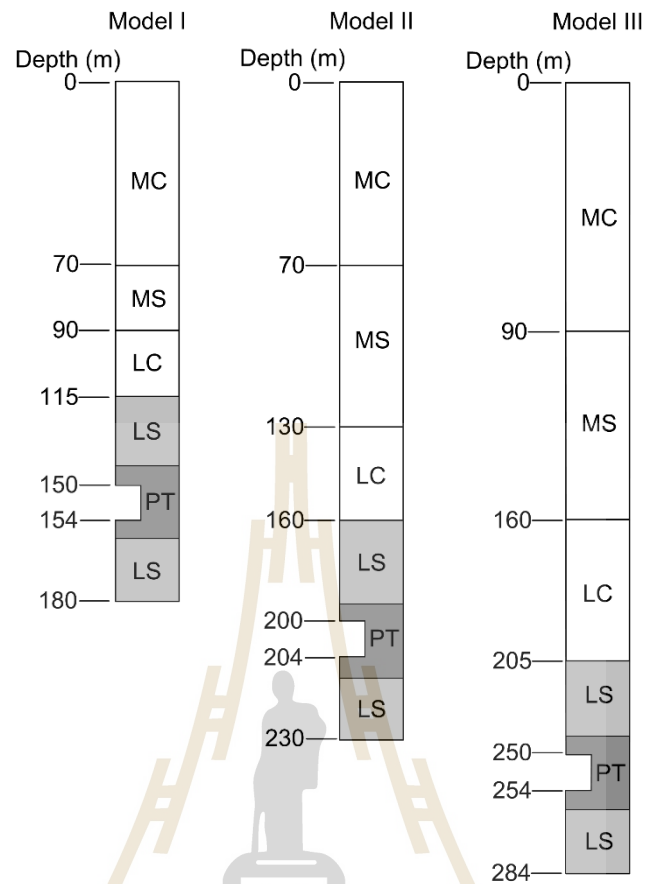


Figure 5.2 Geologic sequences used in simulations for potash mine.

Table 5.1 Parameters used in numerical simulations (Sriapai et al., 2012; Crosby, 2007; Luangthip et al., 2016).

Properties	Rock types				
	Middle clastic	Middle salt	Lower clastic	Lower salt	
				Halite	Carnallite (C% = 40)
Density, ρ (kg/m ³)	2,490	2,140	2,180	2,160	1,824
Bulk modulus, K (GPa)	3.52	2.22	0.54	19.89	11.36
Shear modulus, G (GPa)	1.44	1.67	0.25	6.66	2.65
Cohesion, c (MPa)	3.5	0.5	0.88	4.82	2.86
Internal friction angle, ϕ (Degrees)	25	50	15	45	45
Tension, σ_t (MPa)	0.83	1.00	0.83	1.88	0.81

$$\gamma_{\text{oct}} = \tau_{\text{oct}} \left[\left(\frac{t}{\eta_1} + \frac{1}{E_1} + \frac{\eta_1}{\eta_2 E_2} \right) - \left(\frac{\eta_1}{\eta_2 E_2} \exp \left(\frac{-E_2 t}{\eta_2} \right) \right) \right] \quad (5.1)$$

where τ_{oct} is octahedral shear stresses (MPa), t is time (day), E_1 is elastic modulus (GPa), E_2 is spring constant in visco-elastic phase (GPa), η_1 is visco-plastic coefficient in steady-state phase (GPa-day) and η_2 is visco-elastic coefficient in transient phase (GPa-day). These parameters can be calibrated from creep testing where the applied differential stresses are constant. Since no creep testing is performed in this study, the Burgers parameters for the rock salt and potash are obtained from the calibration results of Wilalak and Fuenkajorn (2016) who perform creep testing of the same rock salt. These parameters are given in Table 5.2. The mechanical properties of the crushed salt used as backfill material in the simulations are obtained after consolidating for 15, 60 and 180 days under σ_{cons} of 2.5, 5, 7.5 and 10 MPa (Tables 4.1 and 4.4). In practice the installation of the crushed salt may be accomplished by consolidating the crushed salt as rectangular blocks. These blocks can then be arranged in the openings.

Table 5.2 Creep properties of pure salt and potash used in FLAC simulations (Wilalak and Fuenkajorn, 2016; Luangthip et al., 2016).

Properties	Rock types	
	Halite	Potash (C% = 40)
Elastic modulus, E_1 (GPa)	2.48	0.95
Spring constant in visco-elastic phase, E_2 (GPa)	2.22	1.12
Visco-plastic coefficient in steady-state phase, η_1 (GPa.day)	45.16	9.88
Visco-elastic coefficient in transient phase, η_2 (GPa.day)	1.29	0.42

5.4 Boundary conditions

The room and pillar widths are maintained constant at 8 and 12 m for all cases. The pillar heights vary from 4, 8 to 12 m. The opening depths (D) are 150, 200 and 250 m. The times at which the crushed salt is emplaced are 6, 12 and 24 months. In the simulation the crushed salt emplacement leaves about 30 cm gap between the roof and the top of the backfill. The subsidence predictions are made up to 10 years after excavations. Figures 5.3 and 5.4 show the mesh models representing the salt and

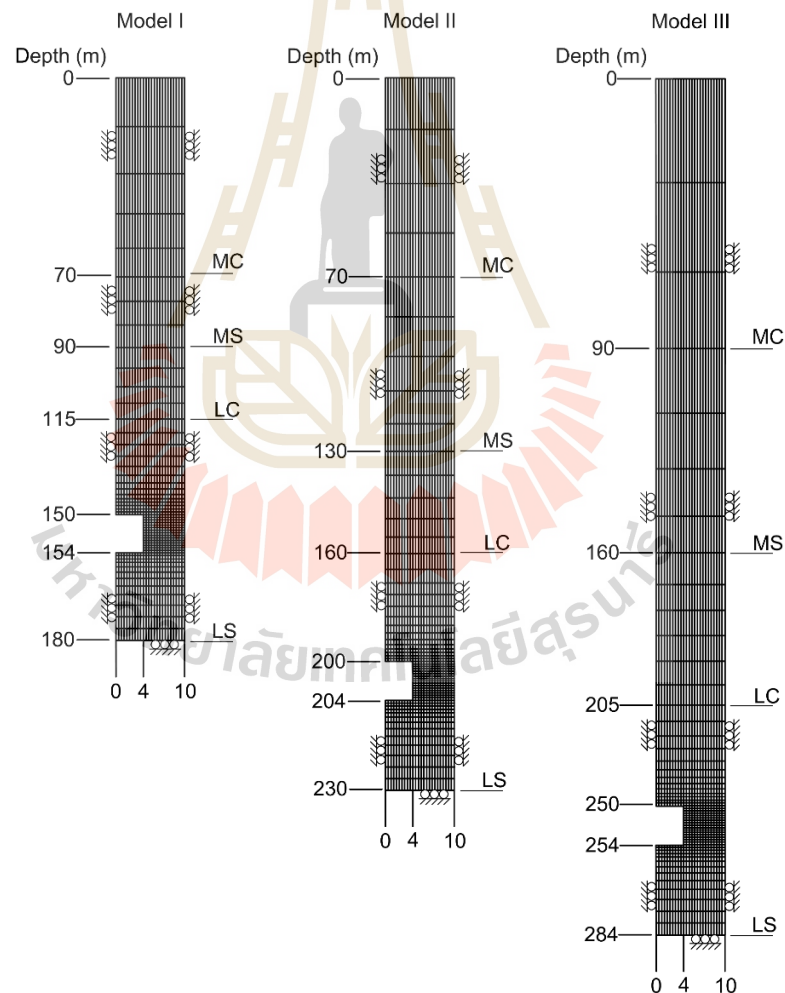


Figure 5.3 Example of finite difference mesh developed for FLAC simulation of salt mine opening.

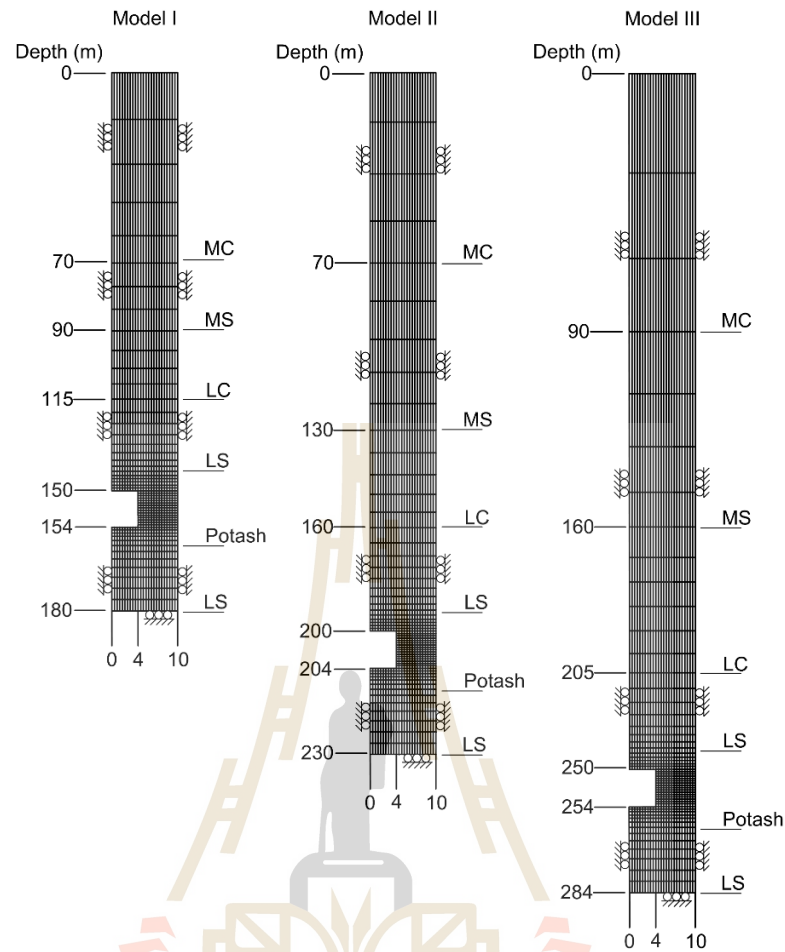


Figure 5.4 Example of finite difference mesh developed for FLAC simulation of potash mine opening.

potash mine openings from the ground surface to the depth of 150, 200 and 250 m at Kham Thale So District.

5.5 Numerical results

5.5.1 Surface subsidence

Figure 5.5 shows example of surface subsidence magnitude as affected by mining excavation at 250 m depth and 12 m pillar height. The results indicate that the surface subsidence reaches 10 cm for salt mine and 100 cm for potash mine after

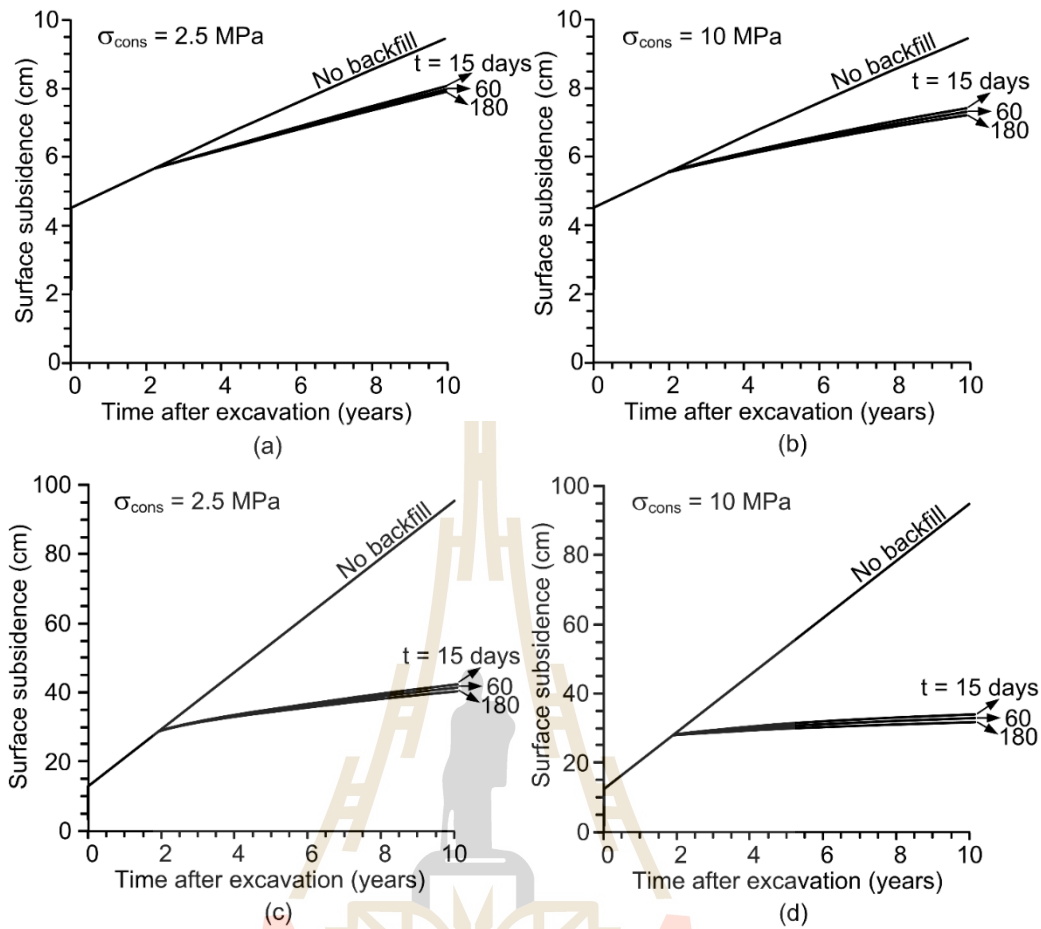


Figure 5.5 Example of comparison surface subsidence between mine opening with and without backfilled after 2 years excavation under various backfill properties in salt (a, b) and potash (c, d) mines.

10 years (for the case without backfill material). The backfilling after excavation can reduce the surface subsidence in the potash mine more effective than in salt mine. The pre-consolidated crushed salt under consolidation stress of 10 MPa can reduce the surface subsidence slightly more than under lower consolidation stress. The times at which the backfill is installed between 15 and 180 days show insignificant differences. Figure 5.6 shows the reduction of surface subsidence after backfilling, where crushed salt is pre-compressed under various consolidation stresses (2.5, 5, 7.5

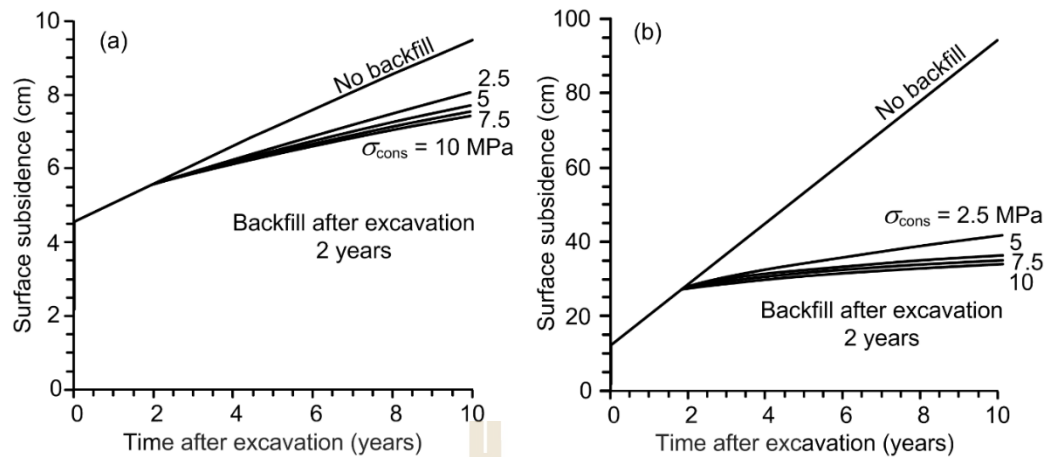


Figure 5.6 Surface subsidence under various consolidation stresses (σ_{cons}) of backfill material after consolidation for 15 days in salt (a) and potash (b) openings.

and 10 MPa). The mine opening filled with 5, 7.5 and 10 MPa consolidation stresses of backfill shows comparable subsidence magnitude. The pre-consolidation at 2.5 MPa has higher subsidence than other consolidation stresses. The consolidation under stresses between 5 MPa and 10 MPa shows insignificant differences. The simulations of backfilling in mine opening under various periods after excavation are shown in Figure 5.7. The effects of backfilling duration in the potash mine are clearly demonstrated. The subsidence magnitudes for the case of backfilling between 0.5 and 2 years are similar.

Figure 5.8 shows the maximum surface subsidence after 10 years under various mining depths and room heights. The material properties are selected for 5 MPa applied stress under 15 days of consolidated, and placed in opening after 2 years. The results show that the subsidence magnitudes increase with the mining depth and room height. The performance of backfill material tends to increase with

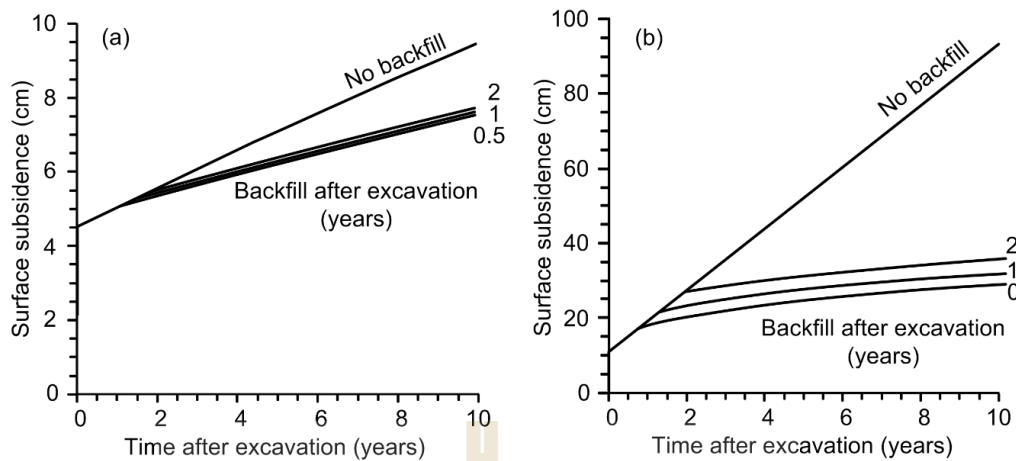


Figure 5.7 Surface subsidence as a function of time for salt (a) and potash (b) openings with different time of crushed salt backfill.

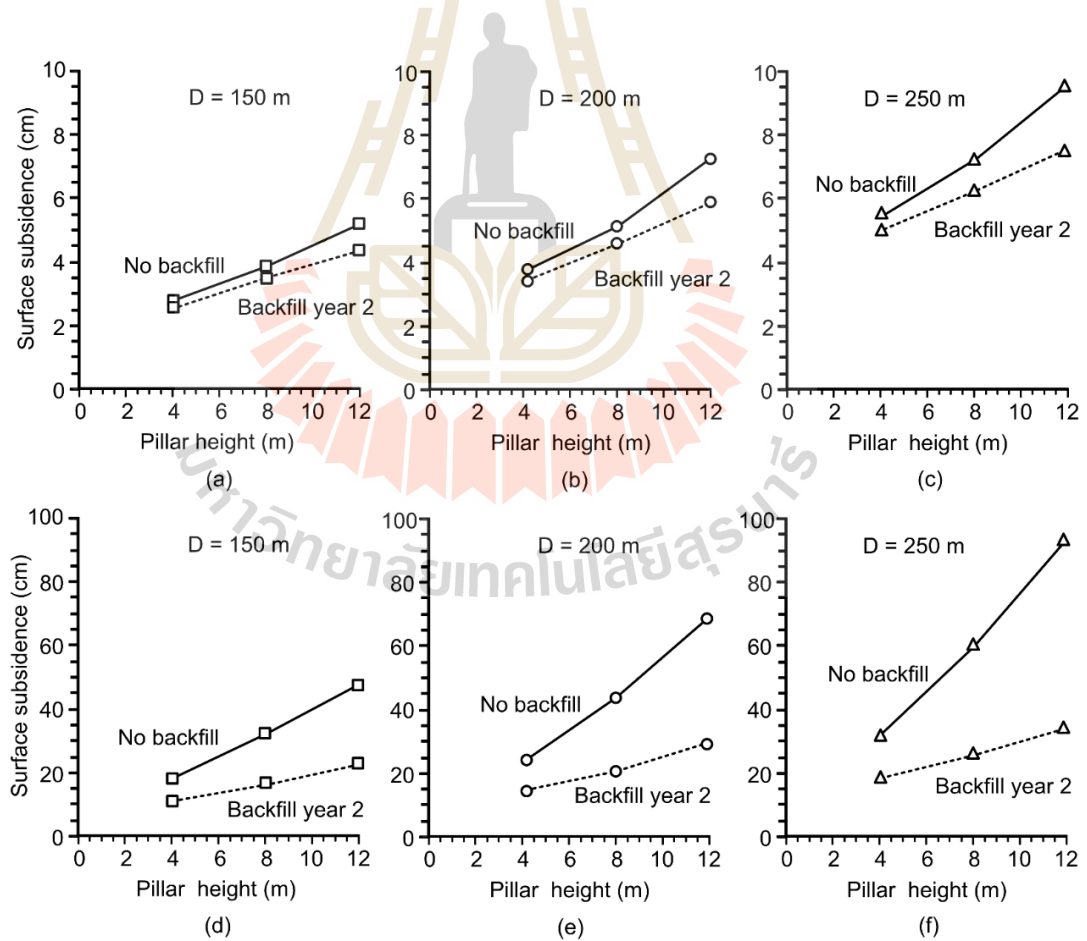


Figure 5.8 Surface subsidence after 10 years in salt (a, b, c) and potash (d, e, f) openings with different pillar heights and depths.

increasing of room height. For example, the percentages of reduction of subsidence magnitude increase from 9.1, 12.9 to 21.1% for salt mine and from 44.4, 54.7 to 60.9% for potash mine for the mining depth of 250 m and room heights of 4, 8 and 12 m, respectively. Figure 5.9 shows the surface subsidence rate as a function of time after excavation for both with and without backfilling cases. The subsidence rate in salt mine without backfilling in the mine opening tend to decrease slightly while the subsidence rates in potash mine are constant after excavation. After opening is backfilled with the crushed salt pre-consolidated at 5 MPa for 15 days, the subsidence rates decrease with time, particularly for the potash mine. The subsidence rate in the

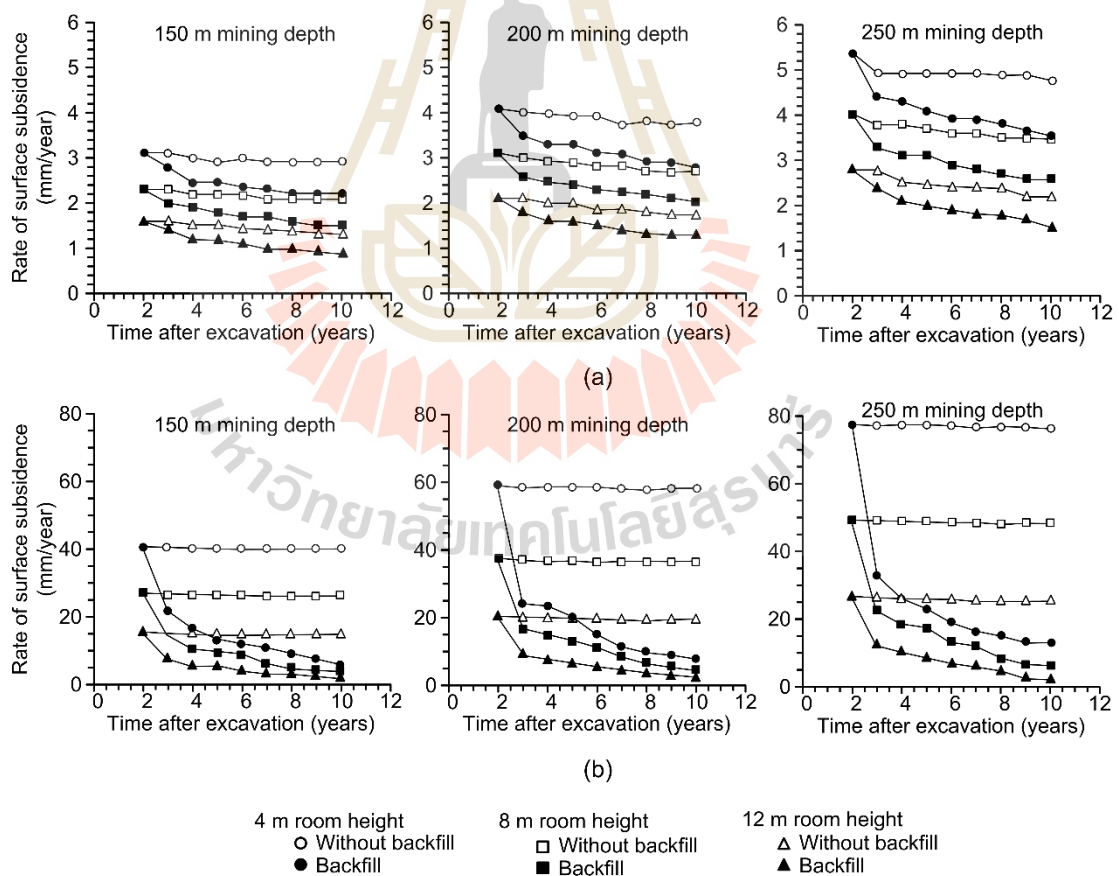


Figure 5.9 Surface subsidence rate in salt (a) and potash (b) openings with different pillar heights and depths.

potash mine model approaches a constant value after 10 years. The crushed salt is installed in the higher and deeper rooms show the higher rate of subsidence reduction.

5.5.2 Roof and pillar deformations

The roof, floor and pillar deformations, room closure, and pillar yielding after 10 years of excavation are determined from the simulations. For this demonstration, the properties of the crushed salt are taken for the constant stress of 5 MPa for 15 days. It is installed in the mine opening after 2 years of excavation. The results indicate that the roof deformations increase with increasing room heights and mining depths (Figure 5.10). After the crushed salt is installed in the salt opening, the

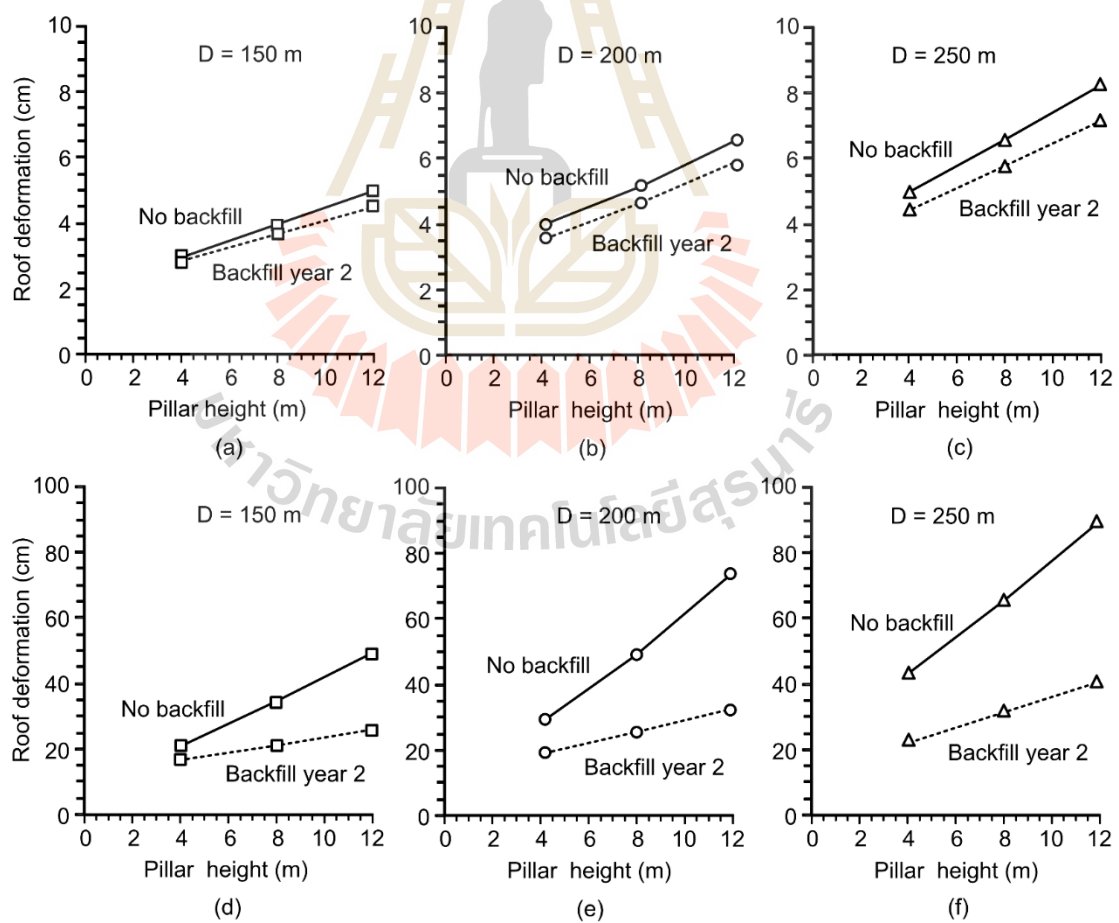


Figure 5.10 Roof deformation in salt (a, b, c) and potash (d, e, f) opening.

roof deformation slightly decreases for all cases, compared those obtained from the potash mine. Figure 5.11 shows the floor deformation in salt and potash openings. The crushed salt backfill can reduce the floor heave by up to 40% for the salt mine, and 70% for the potash mine. The relationships between the vertical room closure and mining depth and opening height are shown in Figure 5.12. Figures 5.13 and 5.14 show the pillar deformation. The results indicate that the performance of crushed salt backfill in the potash mine is better than those of the salt mine. Greater opening depths and room heights show larger reduction of the pillar deformation. This suggests that the properties of the surrounding rock is an important factor to indicate

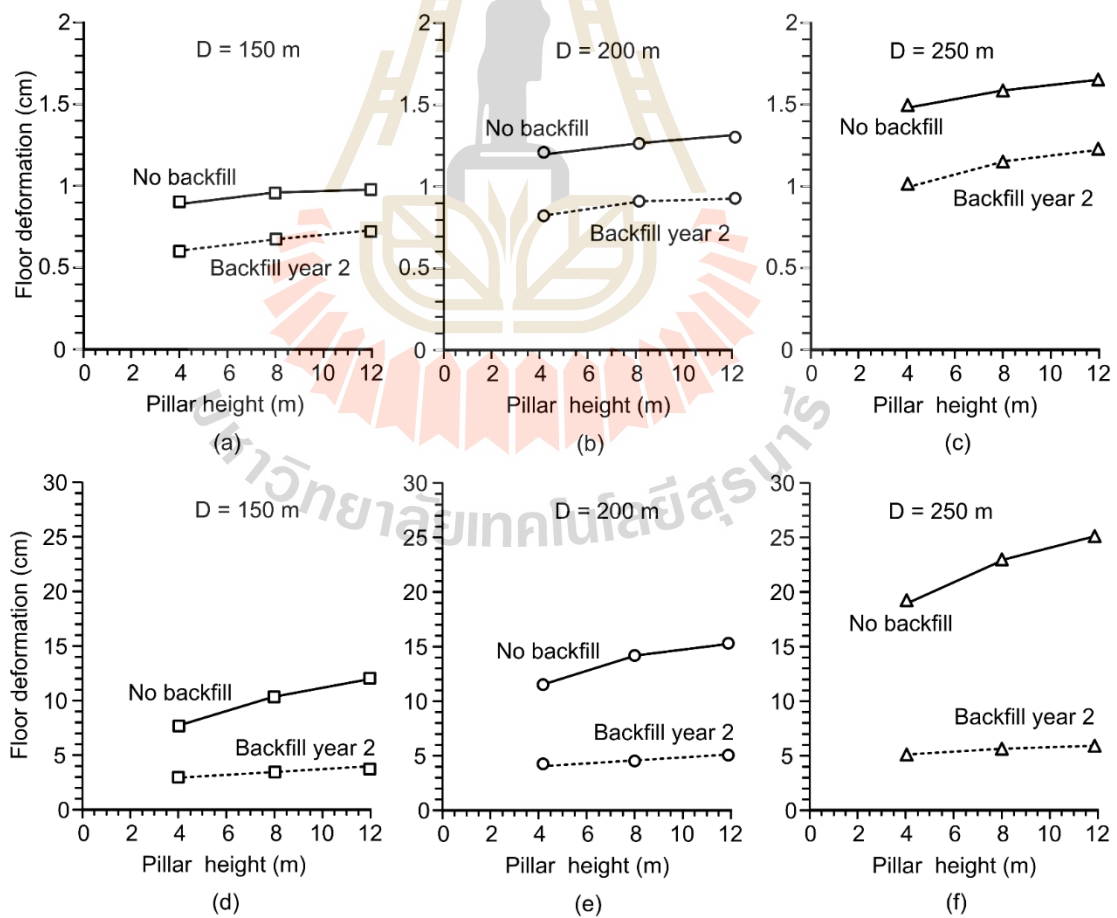


Figure 5.11 Floor deformation in salt (a, b, c) and potash (d, e, f) opening.

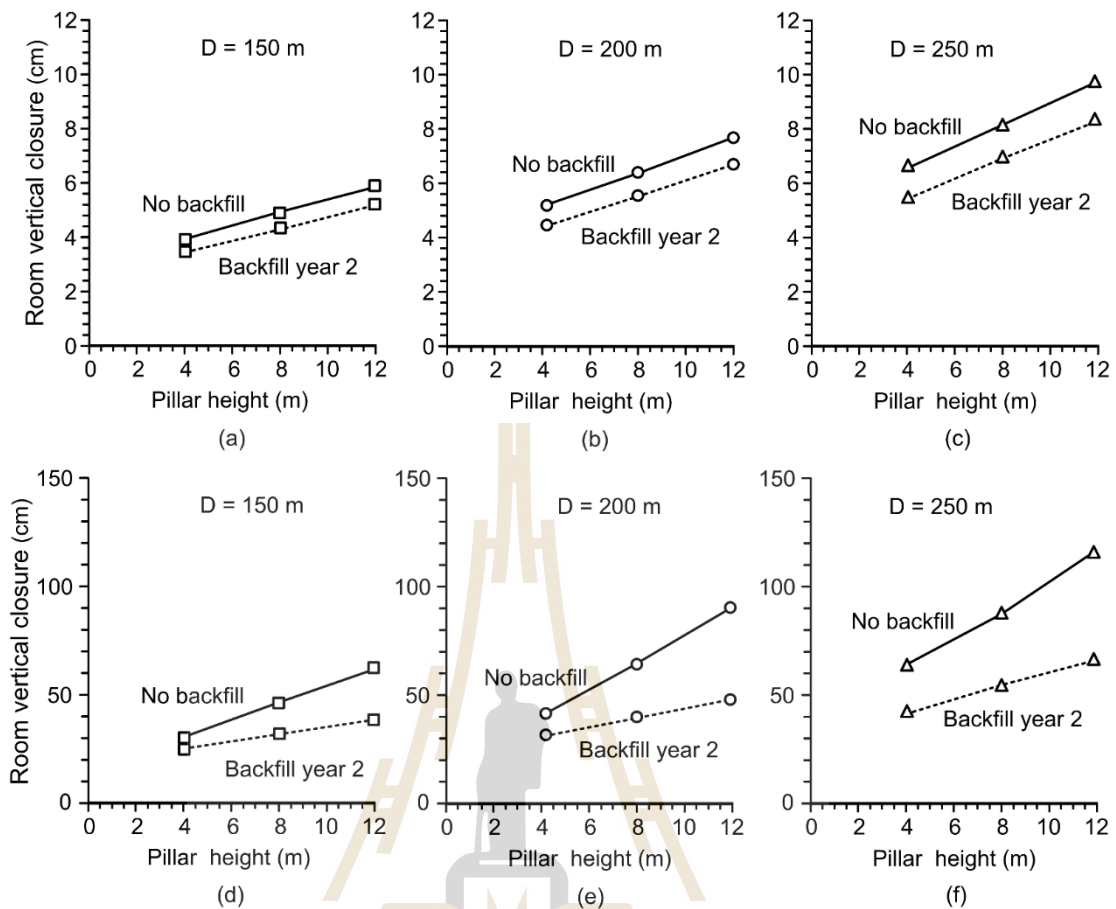


Figure 5.12 Vertical room closure in salt (a, b, c) and potash (d, e, f) opening.

the performance of the backfill. If the surrounding rock has the low creep deformation, the crushed salt backfill may be unnecessary.

5.5.3 Factor of safety of pre-consolidated crushed salt

The octahedral shear stresses obtained from the laboratory test (Chapter IV) are used here to calculate the factor of safety (FS) of the pre-consolidated crushed salt in the mine opening. The finite difference program - FLAC (Itasca, 1992) is used to simulate the mine opening under plane strain. For this demonstration the openings are excavated at 250 m depth with 12 m height. From the previous section the suitable consolidation period of pre-consolidated crushed salt is

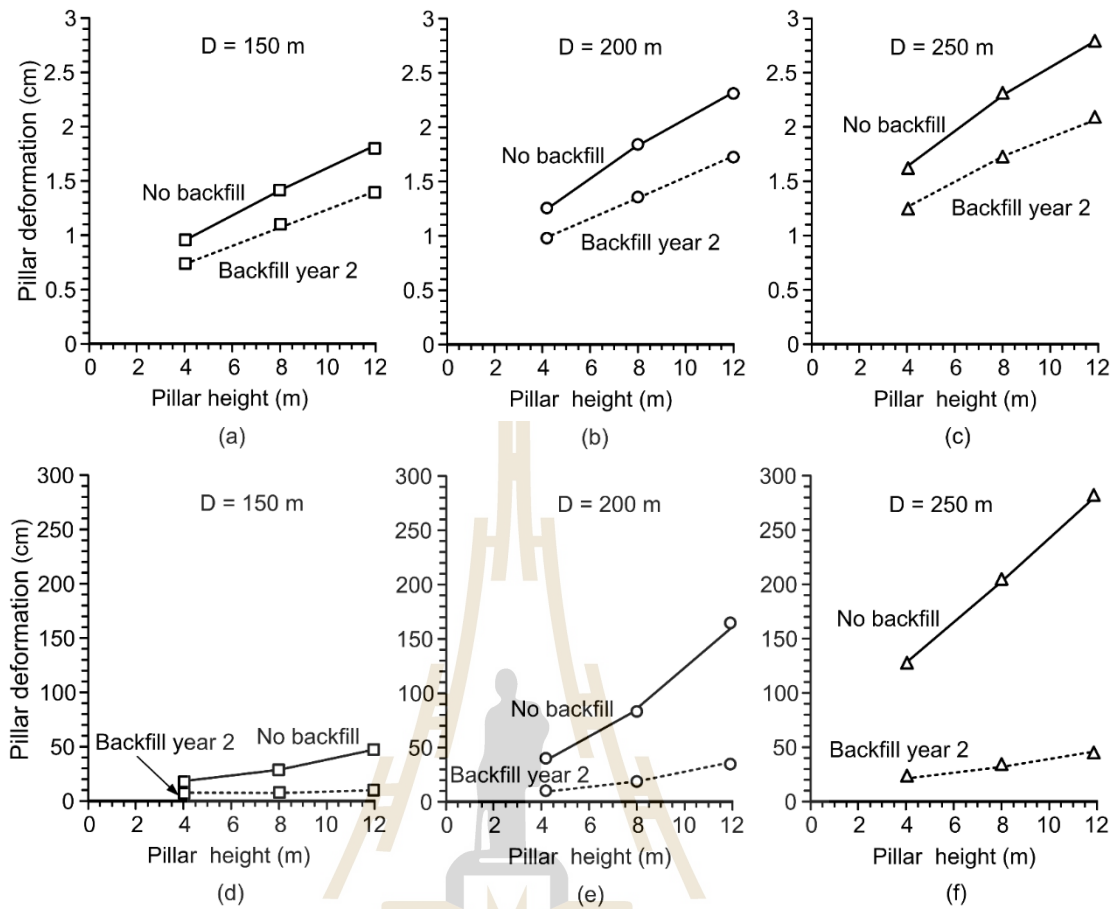


Figure 5.13 Pillar deformation in salt (a, b, c) and potash (d, e, f) opening.

15 days which is used in this simulation. The σ_{cons} of pre-consolidated crushed salt is varied from 2.5, 5, 7.5 and 10 MPa. The principal stresses induced in the pre-consolidated crushed salt are used to calculate the octahedral shear stresses. The factor of safety (FS) of crushed salt backfill can be calculated as:

$$\text{FS} = \tau_{\text{oct}} / \tau_{\text{oct,backfill}} \quad (5.2)$$

where τ_{oct} is the octahedral shear stress at failure obtained from uniaxial compression tests, and $\tau_{\text{oct,backfill}}$ is the induced octahedral shear stress obtained from numerical model.

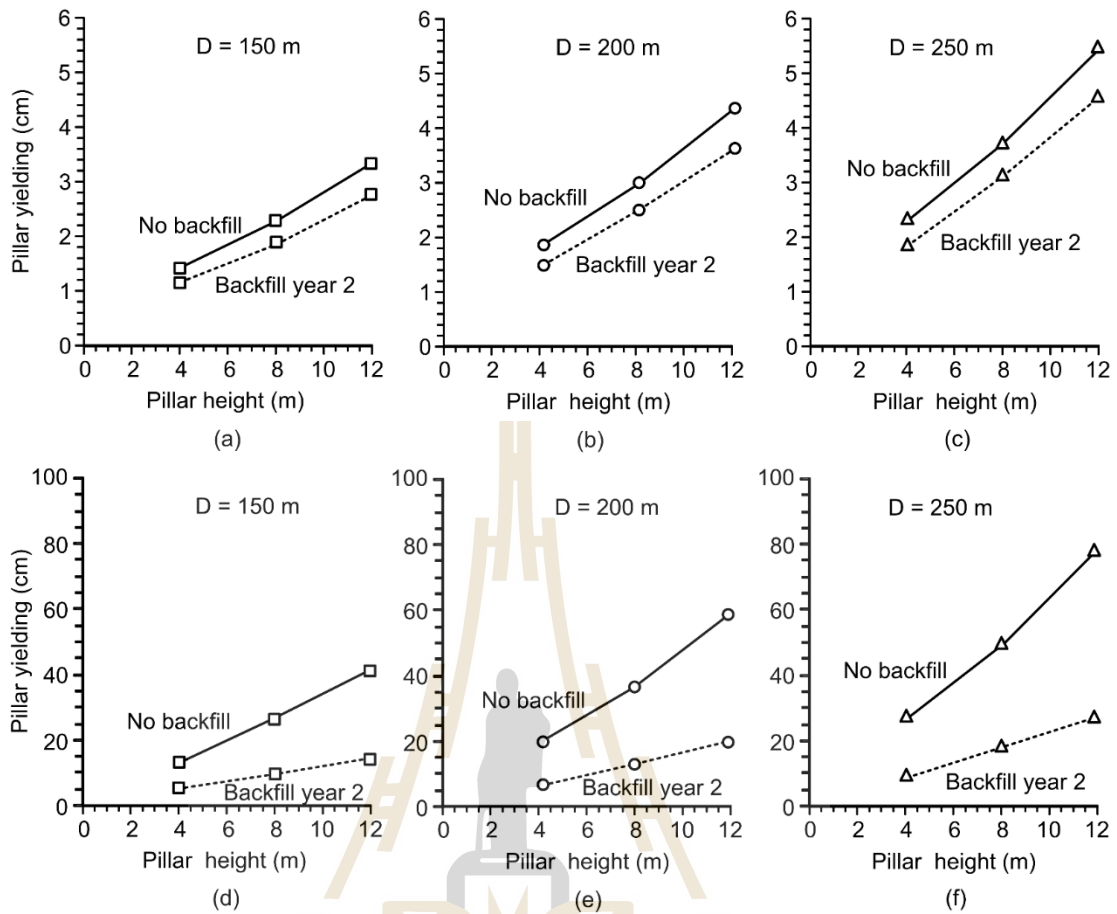


Figure 5.14 Pillar yielding in salt (a, b, c) and potash (d, e, f) opening.

The localized shear stresses induced in the backfill with different crushed salt properties are shown in Figure 5.15. They are concentrated around the corner of the roof and floor. The higher concentration of the shear stresses is found in the pre-consolidated crushed salt under higher consolidation stresses. Table 5.3 summarizes the results of FS of pre-consolidated crushed salt in the salt and potash mine openings. The crushed salt under higher consolidation stress gives the largest FS value. Crushed salt in the potash mine shows the FS values lower than those in the salt mine.

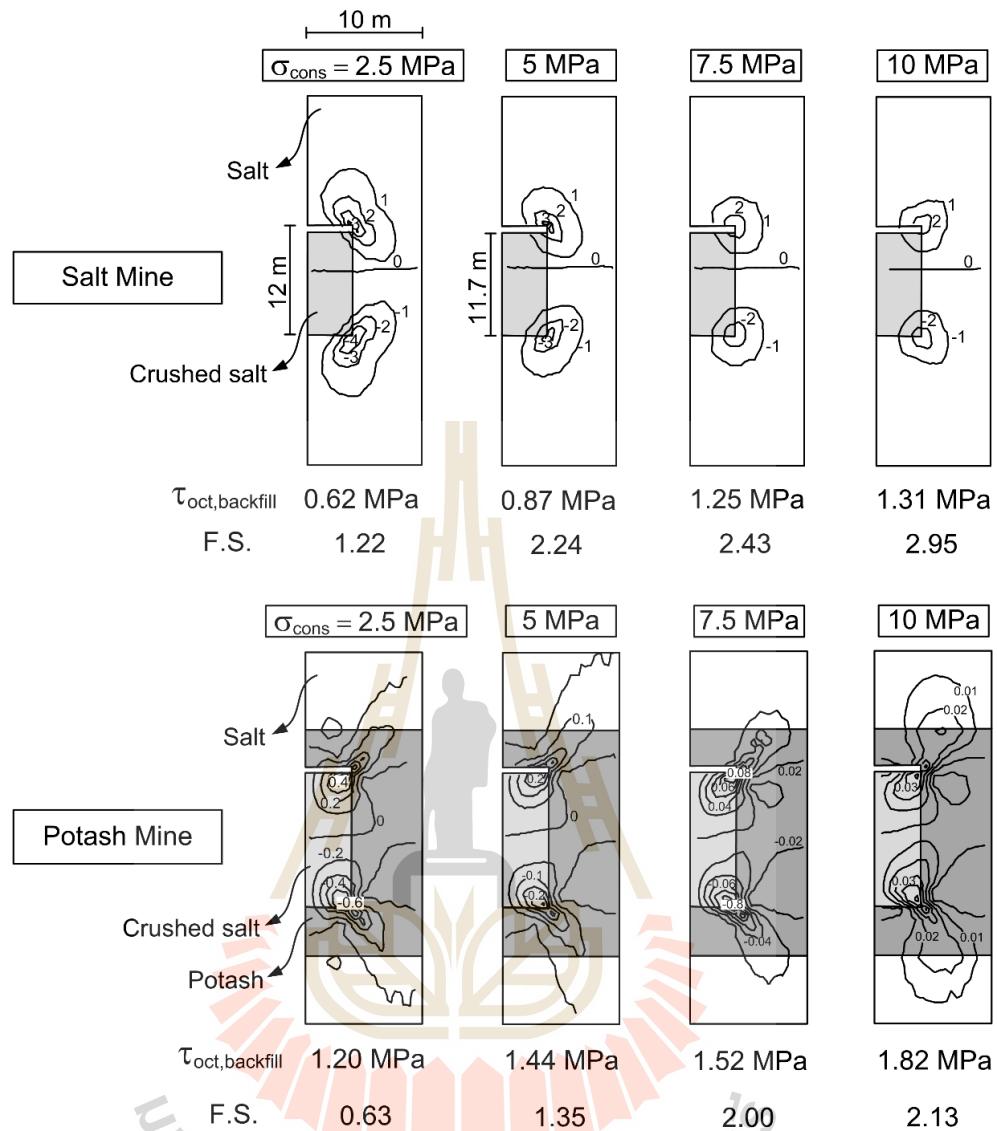


Figure 5.15 Shear stresses induced in salt and potash openings.

The FS of pre-consolidated crushed salt in salt mine are higher than 1.0 for all cases. For the potash mine the crushed salt under 2.5 MPa σ_{cons} shows FS values lower than 1.0. This suggests that the crushed salt backfill in the potash mine should be consolidated under stresses greater than 5 MPa for the minimum consolidation period of 15 days.

Table 5.3 Stresses, strains, octahedral shear stresses and factors of safety of crushed salt backfill.

Rock type	σ_{cons}	Numerical simulations				τ_{oct} (MPa)	FS
		$\sigma_{1,\text{backfill}}$ (MPa)	$\sigma_{2,\text{backfill}}$ (MPa)	$\sigma_{3,\text{backfill}}$ (MPa)	$\tau_{\text{oct,backfill}}$ (MPa)		
Salt	2.5	4.40	3.90	2.90	0.62	0.76	1.22
	5	5.70	5.00	3.60	0.87	1.95	2.24
	7.5	6.50	5.60	3.50	1.26	3.05	2.43
	10	7.16	6.28	4.04	1.31	3.87	2.95
Potash	2.5	9.85	9.40	7.10	1.20	0.76	0.63
	5	9.80	9.50	6.60	1.44	1.95	1.35
	7.5	9.75	9.50	6.40	1.52	3.05	2.00
	10	9.74	9.57	5.80	1.82	3.87	2.13

CHAPTER VI

DERIVATION OF EMPIRICAL EQUATIONS

6.1 Introduction

The crushed salt properties are used to develop a set of empirical equations as a function of mean strain energy and consolidation period by SPSS statistical software. The relations are used to predict the crushed salt properties installed in shafts and boreholes.

6.2 Crushed salt properties as a function of mean strain energy density

An attempt is made to correlate the crushed salt properties with the applied mean strain energy density during consolidation. It is first postulated that two main mechanisms govern the changes of the properties of crushed salt: consolidation and recrystallization (Callahan et al., 1998). The first mechanism involves the volumetric reduction of the crushed salt mass by particle rearrangement, creep, cracking and sliding between grain boundaries. It is reflected by instantaneous and transient deformations which are mainly controlled by the applied energy. The second mechanism involves the recrystallization and healing between salt particles (Hwang et al., 1993; Hansen, 1997). This mechanism does not decrease the crushed salt volume. It can however strengthen and stiffen the specimen as the consolidation period increases.

6.2.1 Crushed salt density

Based on the concept above the change of the crushed salt density (ρ) can be represented by:

$$\rho = \rho_{\text{initial}} + \Delta\rho_{\text{cons}} \quad (6.1)$$

where ρ_{initial} is the initial density before applying the mean strain energy (equal to 1.247 g/cm³) and $\Delta\rho_{\text{cons}}$ is the reduction of bulk density due to the strain energy and consolidation period. Regression analysis of the test data (Figure 4.8 and 4.11) by SPSS software (Wendai, 2000) can determine $\Delta\rho_{\text{cons}}$ as a function of W_m and t :

$$\Delta\rho_{\text{cons}} = 0.044 \cdot W_m^{0.391} \cdot t^{0.059} \quad (\text{g/cm}^3) \quad (6.2)$$

Good correlation is obtained ($R^2 > 0.9$). Figure 6.1 compares the curve fits with the test results. It should be noted that the crushed salt density is independent of the recrystallization and healing because these processes do not reduce the bulk volume of specimens.

6.2.2 Crushed salt porosity

Similar to the density prediction above the reduction of crushed salt porosity (n) during consolidation can be determined by the regression analysis of the test data:

$$n = n_{\text{initial}} - \Delta n_{\text{cons}} \quad (6.3)$$

where n_{initial} is the initial crushed salt porosity (42%) and Δn_{cons} is the porosity reduction which can be represented by a power equation:

$$\Delta n_{\text{cons}} = 480.203 \cdot W_m^{0.411} \cdot t^{0.070} \quad (\%) \quad (6.4)$$

The diagrams in Figure 6.2 suggest that the applied mean strain energy affects the porosity reduction and the density increase more than does the consolidation period.

6.2.3 Crushed salt strength

The crushed salt strength (σ_c) is controlled by both consolidation and recrystallization. The effects from the two mechanisms can be superimposed as:

$$\sigma_c = \Delta\sigma_{c,\text{cons}} + \Delta\sigma_{c,\text{rec}} \quad (6.5)$$

where $\Delta\sigma_{c,\text{cons}}$ is the strength increase due to consolidation and $\Delta\sigma_{c,\text{rec}}$ is the strength increase by recrystallization. They can be represented by the following empirical equations:

$$\Delta\sigma_{c,\text{cons}} = 6.873 \cdot W_m^{0.799} \cdot t^{0.220} \quad (\text{MPa}) \quad (6.6)$$

$$\Delta\sigma_{c,\text{rec}} = 0.009 \cdot t \cdot \exp(W_m) \quad (\text{MPa}) \quad (6.7)$$

The empirical constants are obtained from the regression analysis of the test data using equation (6.5). Figure 6.3 compares the predictions with the test results. Note that under $W_m = 0$ the specimen strength can increase with time due to the recrystallization and healing.

6.2.4 Crushed salt elastic modulus

The crushed salt elastic modulus (E) is also controlled by both consolidation and recrystallization mechanisms:

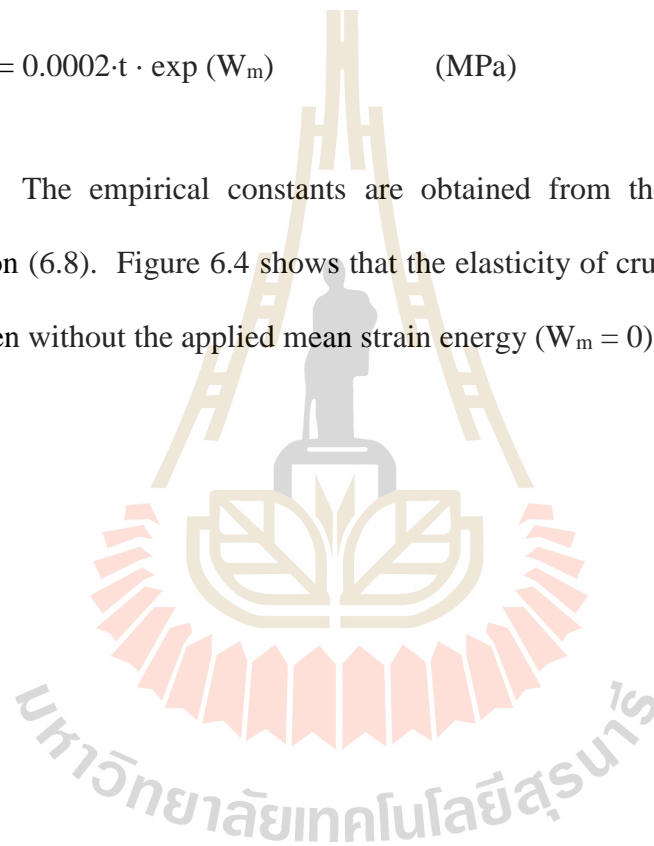
$$E = \Delta E_{\text{cons}} + \Delta E_{\text{rec}} \quad (6.8)$$

where ΔE_{cons} is the increase of elastic modulus due to consolidation and ΔE_{rec} is the increase of elastic modulus by recrystallization. They can be represented by:

$$\Delta E_{\text{cons}} = 0.399 \cdot W_m^{0.658} \cdot t^{0.061} \quad (\text{MPa}) \quad (6.9)$$

$$\Delta E_{\text{rec}} = 0.0002 \cdot t \cdot \exp(W_m) \quad (\text{MPa}) \quad (6.10)$$

The empirical constants are obtained from the regression analysis using equation (6.8). Figure 6.4 shows that the elasticity of crushed salt can increase with time even without the applied mean strain energy ($W_m = 0$).



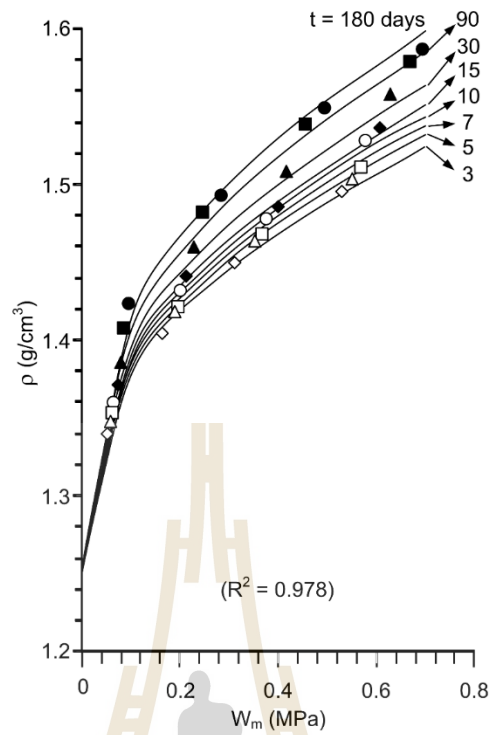


Figure 6.1 Density as a function of mean strain energy density.

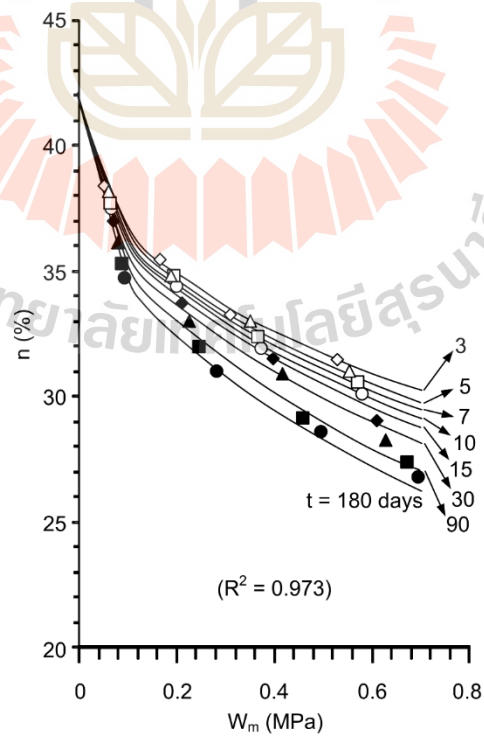


Figure 6.2 Porosity as a function of mean strain energy density.

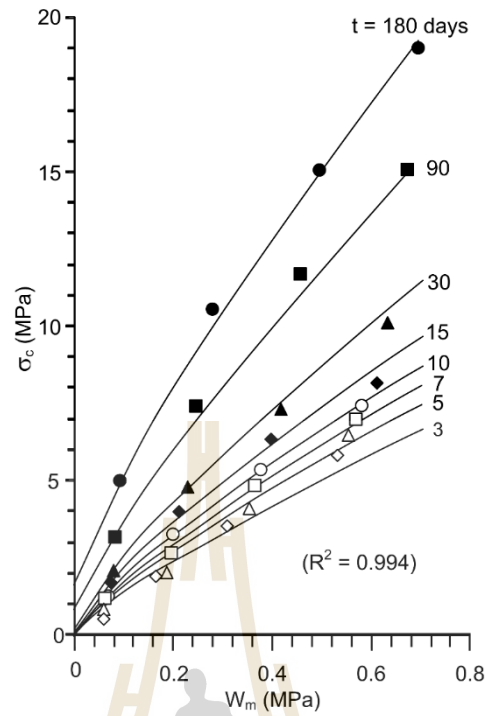


Figure 6.3 Uniaxial compressive strength as a function of mean strain energy density.

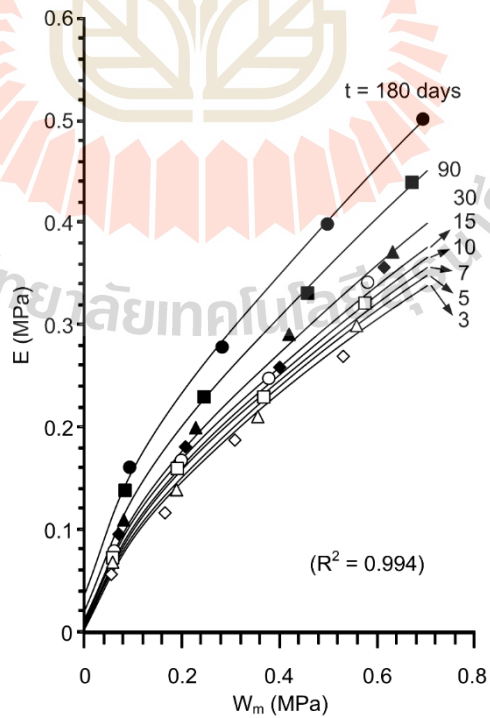


Figure 6.4 Elastic modulus (d) as a function of mean strain energy density.

CHAPTER VII

ANALYTICAL SOLUTION OF CRUSHED SALT

PROPERTIES AFTER EMPLACEMENT IN BOREHOLE

7.1 Introduction

The objective of this chapter is to predict the mechanical properties of crushed salt backfill emplaced in boreholes and shafts. The time-dependent closure of borehole and shaft is calculated in terms of the released mean strain energy density. The crushed salt properties are predicted for different opening depths and installation periods.

7.2 Circular opening in salt mass subjected to uniform external pressure

The mean strain energy released by creep closure of circular openings (shaft or borehole) in infinite salt mass subjected to uniform external pressure (in-situ stress) is determined and used to predict the changes of the crushed salt properties after emplacement. The released energy ($W_{m,s}$) can be calculated from the stresses and strains at the opening wall as:

$$W_{m,s} = (3/2) \cdot [(\sigma_r + \sigma_\theta + \sigma_z) / 3] \cdot [(\varepsilon_r + \varepsilon_\theta + \varepsilon_z) / 3] \quad (7.1)$$

where σ_r , σ_θ and σ_z are radial, tangential and axial stresses and ε_r , ε_θ and ε_z are radial,

tangential and axial strains.

Under plane strain condition the radial and tangential stresses obtained from the Kirsch's solution can be presented as (Jaeger et al., 2007):

$$\sigma_r = [1 - (a^2/r^2)] \cdot P_o \quad (7.2)$$

$$\sigma_\theta = [1 + (a^2/r^2)] \cdot P_o \quad (7.3)$$

where P_o is external pressure, a is opening radius and r is radial distance from the center. The axial stress (σ_z) can be determined by:

$$\sigma_z = \nu (\sigma_r + \sigma_\theta) \quad (7.4)$$

At the opening boundary the strains are defined as:

$$\varepsilon_r = \varepsilon_r^e + \varepsilon_r^c \quad (7.5)$$

$$\varepsilon_z = \varepsilon_\theta = 0 \quad (7.6)$$

where ε_r^e is the elastic radial strain and ε_r^c is the time-dependent radial strain controlling the creep closure of the opening.

The elastic radial strain can be obtained by (Jaeger et al., 2007):

$$\varepsilon_r^e = \frac{1}{E} \left\{ (1 - \nu^2) \sigma_r - \nu(1 + \nu) \sigma_\theta \right\} \quad (7.7)$$

Nair and Borezi (1970) and Fuenkajorn and Daemen (1988) have derived the radial creep strain around circular hole based on the potential creep law and the associated flow rule as:

$$\varepsilon_r^c = \frac{3}{2} \kappa' (\sigma^*)^{(\beta'-1)} \cdot S_r (t_1^{\gamma'} - t_0^{\gamma'}) \quad (7.8)$$

where κ' , β' and γ' are material constants of the potential creep law, S_r is the radial stress deviation, and σ^* is the equivalent (effective) stress. The stress deviation can be obtained from:

$$S_r = \sigma_r - (\sigma_r + \sigma_\theta + \sigma_z)/3 \quad (7.9)$$

Based on the von Mises flow rule σ^* is defined as:

$$\sigma^* = \frac{1}{\sqrt{2}} \left\{ (\sigma_r - \sigma_\theta)^2 + (\sigma_\theta - \sigma_z)^2 + (\sigma_z - \sigma_r)^2 \right\}^{\frac{1}{2}} \quad (7.10)$$

Substituting equations (7.2) to (7.10) into equation (7.1) the released mean strain energy (by closure) at the opening boundary can be calculated.

To demonstrate the application of the strain energy concept used here, the mechanical and rheological parameters of the rock salt and potash (40% carnallite, and 60% halite) obtained from Wilalak and Fuenkajorn (2016) are assigned to the equations above (Table 7.1). The elastic parameters are obtained from Luangthip et al. (2016) who report the elastic modulus and Poisson's ratio for the Lower Salt Member of the Maha Sarakham formation (Table 7.1). The released energy at the

Table 7.1 Mechanical and rheological parameters of the rock salt and potash (Wilalak and Fuenkajorn, 2016; Luangthip et al., 2016).

Parameters	Rock salt	Potash (C% = 40)
E (GPa)	16.89	7.30
ν	0.27	0.32
κ' (1/MPa ·day)	0.0003	0.001
β'	1.43	1.459
γ'	0.218	0.213

opening boundary is calculated for the external pressures of 5, 10 and 15 MPa for rock salt (equivalent to the depths approximately of 200, 370 and 550 m) and 4.5, 5.5 and 6.5 MPa for potash (equivalent to the depths approximately of 160, 200 and 240 m). Figures 7.1 and 7.2 plot the released strain energy density ($W_{m,s}$) as a function of time after excavation in salt and potash opening. The $W_{m,s}$ increases rapidly after excavation particularly during the first year. The rate of releasing energy reduces with time. The greater external pressures (deeper opening) lead to the larger released energy. The diagrams suggest that the time at which the crushed salt backfill is installed (t_B) is a significant factor dictating the amount of released energy remaining for consolidating the crushed salt backfill.

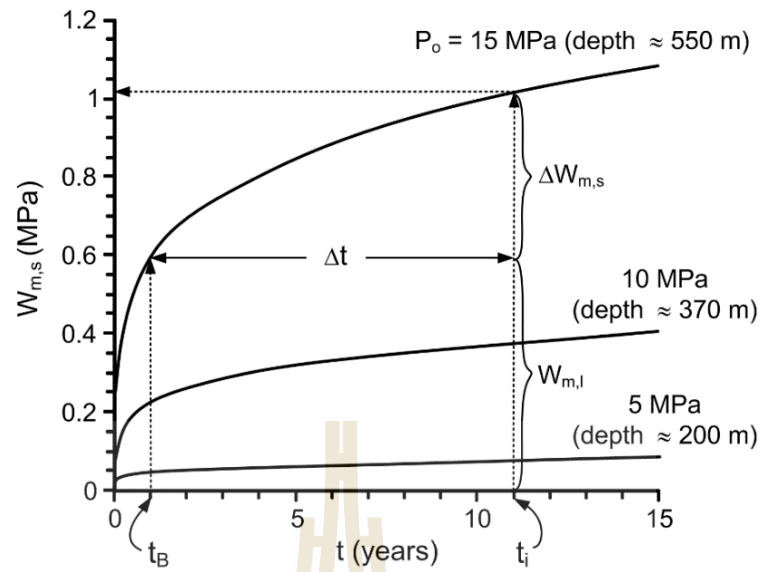


Figure 7.1 Mean strain energy density (W_m) released from closure of circular openings excavated in rock salt under different uniform external pressure (P_o).

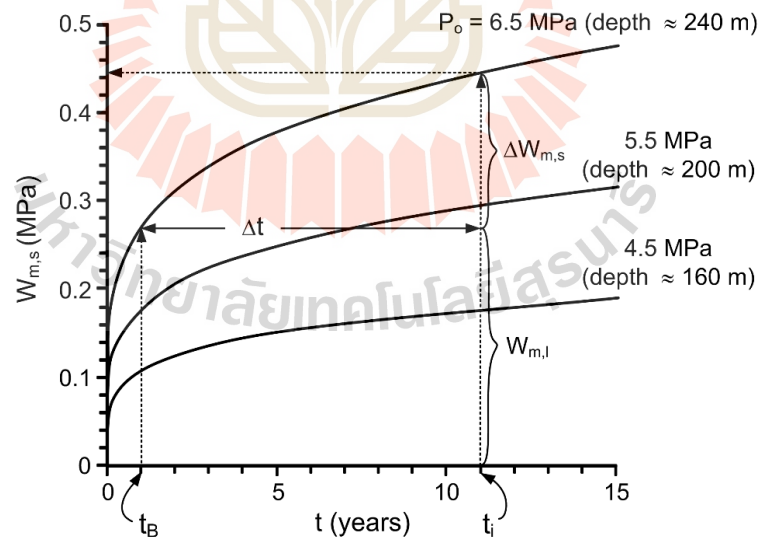


Figure 7.2 Mean strain energy density (W_m) released from closure of circular openings excavated in potash under different uniform external pressure (P_o).

7.3 Prediction of crushed salt properties after emplacement

To predict the crushed salt properties after emplacement, the strain energy left for the consolidation is needed. It can be obtained from:

$$\Delta W_{m,s} = W_{m,s} - W_{m,l} \quad (7.11)$$

where $W_{m,s}$ is the total released energy from excavation to any selected period (t_i) determined as if no backfill is installed, and $W_{m,l}$ is the energy lost due to creep closure before backfill is installed. The time at which the backfill is installed is designated as t_B in Figures 7.1 and 7.2. The duration for consolidation (Δt) can be obtained from:

$$\Delta t = t_i - t_B \quad (7.12)$$

For salt mine, the $\Delta W_{m,s}$ at depths of 200, 370 and 550 m are calculated for $t_B = 1, 3$ and 5 years. The $\Delta W_{m,s}$ at depths of 160, 200 and 240 m are calculated for $t_B = 1, 2$ and 3 years in potash mine. The prediction period (Δt) is up to 10 years after emplacement. From equation (7.11) $\Delta W_{m,s}$ can be calculated as a function of Δt as shown in Figure 7.3 and 7.4 for salt and potash mines. The results indicate that the $\Delta W_{m,s}$ values increase with time (Δt). This is due to the fact that the released energy by creep closure of the opening after backfill emplacement is contributed by the increase of the radial stresses and the decrease of the radial strain rate at the opening boundary. This is caused by the mechanical interaction between the opening wall and the installed crushed salt. The effect of t_B is more pronounced under high P_0 than

under low P_o . This implies that the time at which the crushed salt backfill is installed is more critical for deep openings than for the shallow ones.

Substituting $\Delta W_{m,s}$ and Δt values from Figures 7.3 and 7.4 into W_m and t values in equations (6.1) through (6.10) the density, porosity, compressive strength and elastic modulus can be predicted, as shown in Figures 7.5 to 7.8. For this demonstration the predictions are made up to 10 years. The results suggest that the crushed salt density increases with time (Δt) from its initial value of 1.247 g/cm^3 (Figure 7.5). Subsequently the corresponding porosity decreases with Δt (Figure 7.6). Without applying W_m the density and porosity of the crushed salt backfill remain unchanged. Both σ_c and E increase with P_o and Δt (Figures 7.7 and 7.8). Under no W_m application they can also increase with time due to the recrystallization and healing. The effects of t_B on the strength and elasticity is more pronounced for the crushed salt backfill installed in deep openings than in shallow ones.

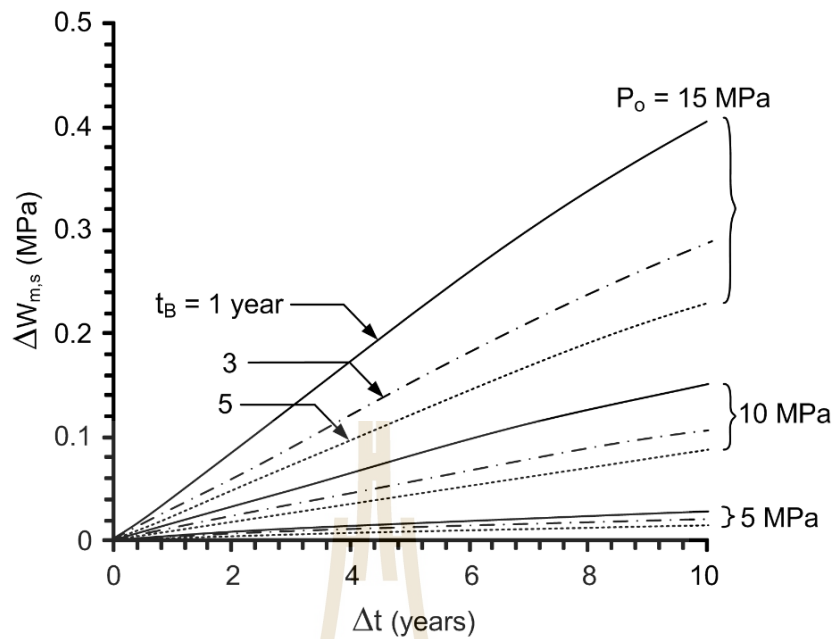


Figure 7.3 Remaining mean strain energy density (ΔW_m) as a function of time after backfill emplacement in salt circular hole.

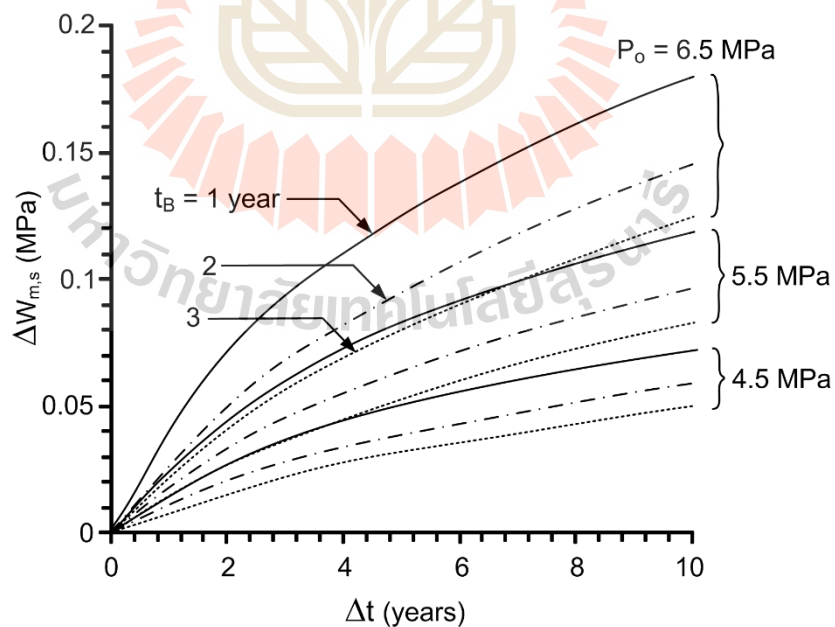


Figure 7.4 Remaining mean strain energy density (ΔW_m) as a function of time after backfill emplacement in potash circular hole.

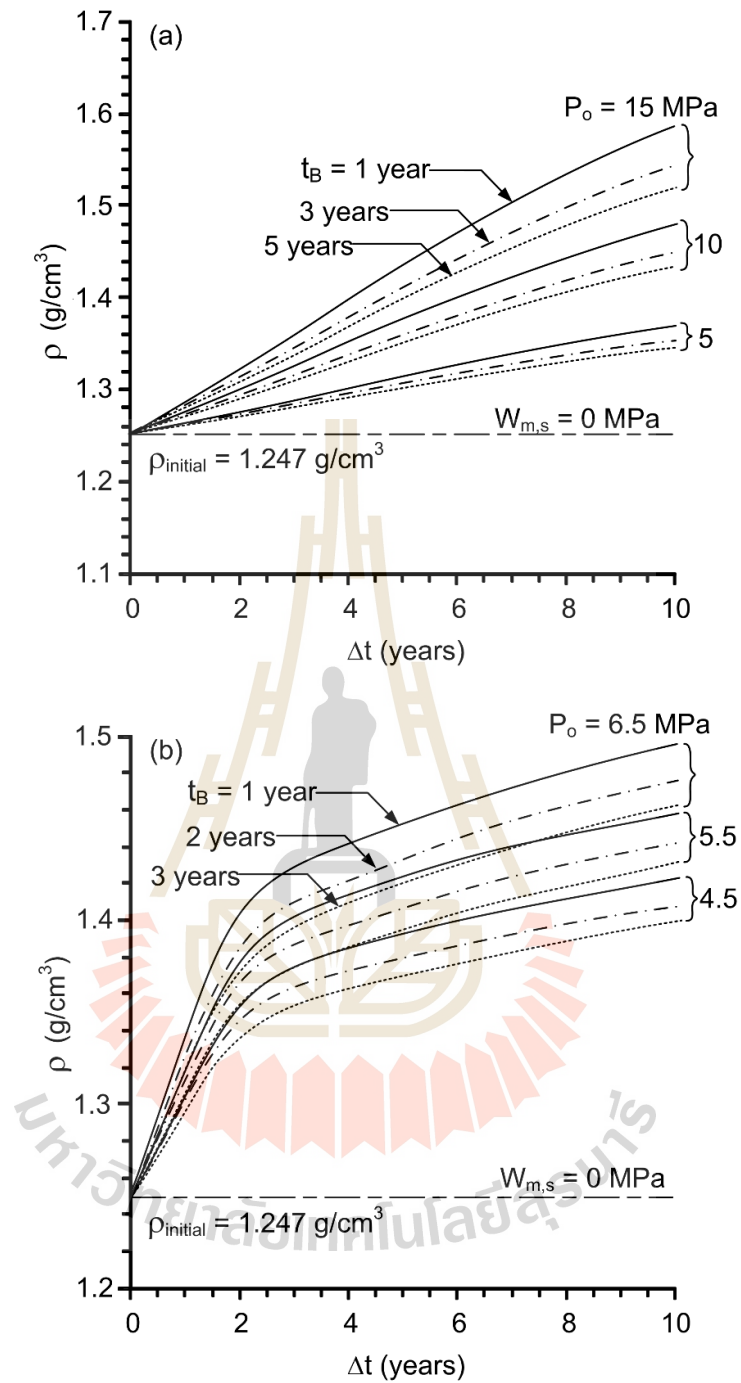


Figure 7.5 Density of crushed salt as a function of time after emplacement in salt (a) and potash (b) circular openings.

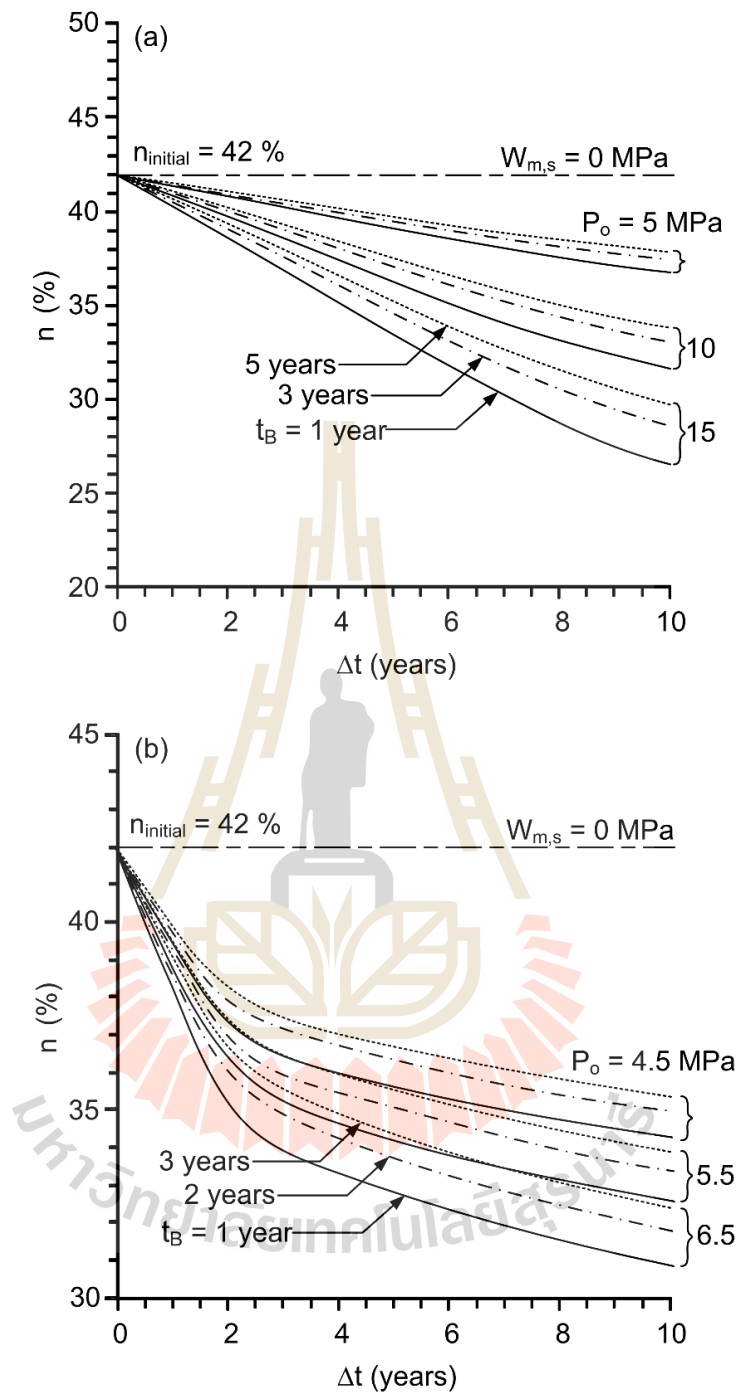


Figure 7.6 Porosity of crushed salt as a function of time after emplacement in salt (a) and potash (b) circular openings.

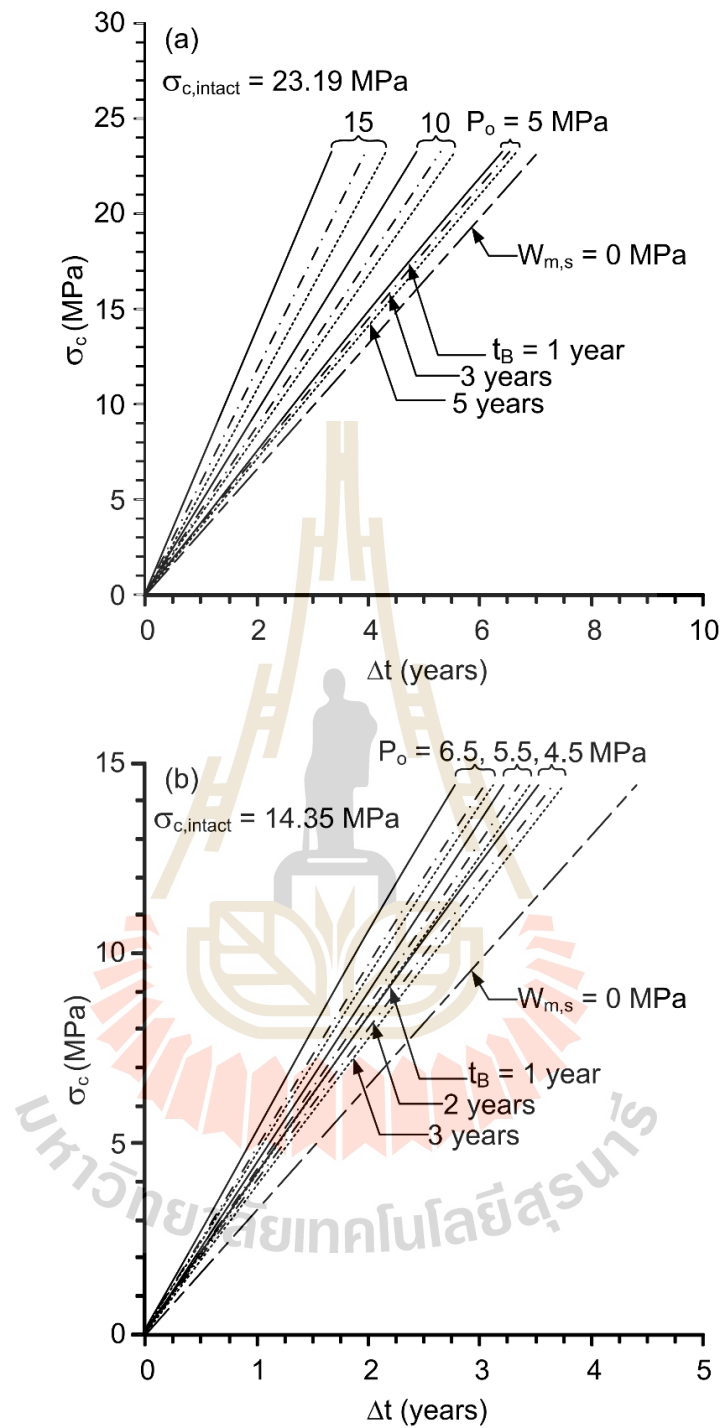


Figure 7.7 Uniaxial compressive strength of crushed salt as a function of time after emplacement in salt (a) and potash (b) circular openings.

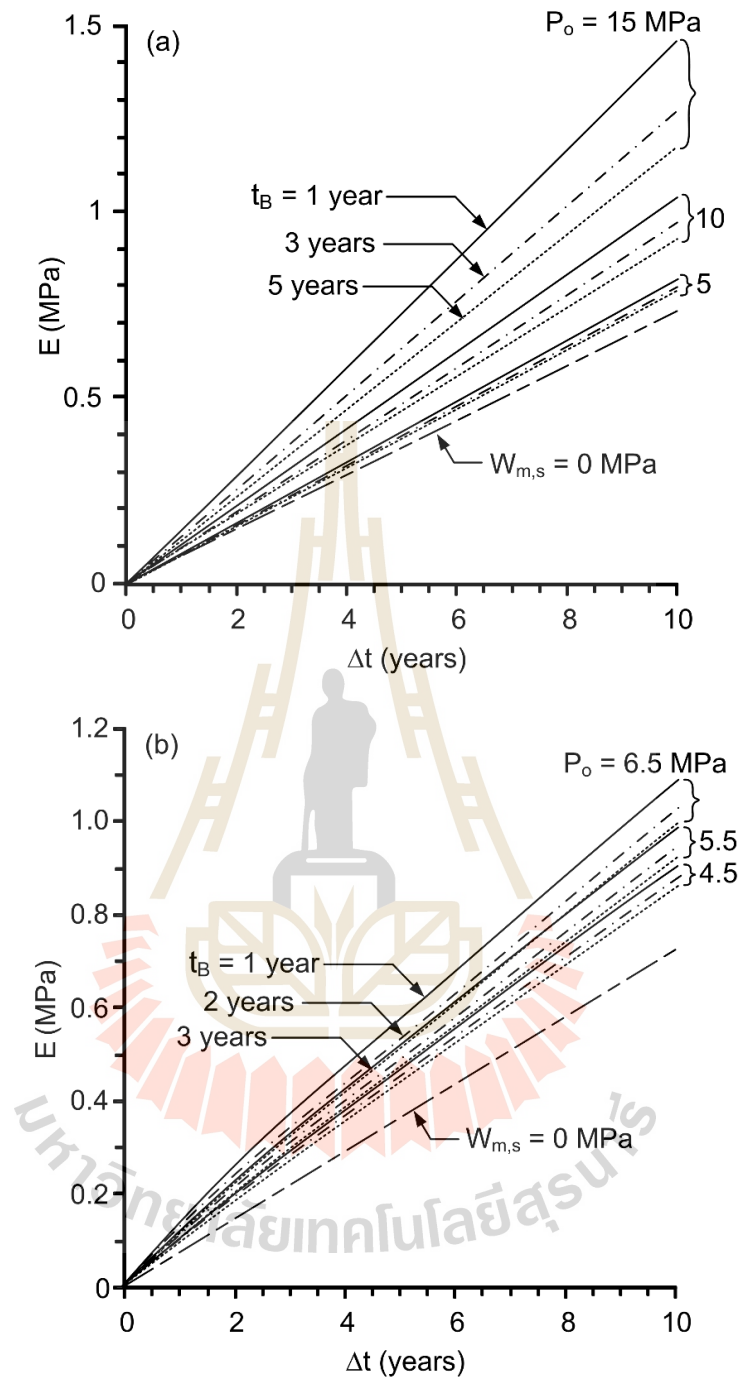


Figure 7.8 Elastic modulus of crushed salt as a function of time after emplacement in salt (a) and potash (b) circular openings.

CHAPTER VIII

DISCUSSIONS AND CONCLUSIONS

8.1 Discussions

1) A total of 32 crushed salt specimens have been consolidated under periods of 3 to 180 days. These are the longest consolidation periods as compared to the experimental work performed on crushed salt elsewhere (Case et al., 1987; Miao et al., 1995; Pfeifle, 1991). The results are believed to be reliable as evidenced by the overlapping (repeating) of the measured axial strains under different periods with the same σ_{cons} .

2) The crushed salt consolidation have been performed on a range of consolidation periods and consolidation stresses, which supports the results shown in Figure 4.2 that the axial strain rates decrease with time, and tend to remain relatively unchanged after 30 days.

3) The specimens are prepared for the uniaxial compression tests may be disturbed during removing from the steel tube due to the friction between steel tube and crushed salt is relatively high. As a result, the grain contact of crushed salt may be loosed, and hence the discrepancy of mechanical properties is obtained, particularly under low consolidation stresses with a short consolidation periods.

4) As evidenced by the good correlation coefficients ($R^2 > 0.9$) obtained from the proposed empirical equation, the test results are believed to be reasonably reliable. This is true for all testing: consolidation, permeability and uniaxial compression test

results. It is however not intention here to claim that the proposed empirical form of the physical, hydraulic and mechanical empirical is universally applicable to all grain size distributions and all particle shape characteristics. The proposed equation, however, obvious advantage that it can represent the consolidation behavior of crushed salt which has size range is equivalent to those expected to be obtained as waste product from the potash mines.

5) The proposed empirical equations in this study may be limited for predicting the crushed salt properties with an initial density 1.247 g/cm^3 . The higher or lower initial density may be provided the slowly or rapidly consolidation more than the results obtained from this study and hence the different physical, hydraulic and mechanical properties is likely obtained.

6) The prediction of the crushed salt properties after emplacement in exploratory boreholes presented here may be conservative because the axial load imposed by the seal gravity is excluded from the calculation. Depending on the emplacement depth the weight of the crushed salt seal can contribute to the mean strain energy applied to the crushed salt.

7) The diagrams in Figures 7.5 to 7.8 can be used as a guideline for the seal planning and for the performance assessment of the crushed salt backfill properties. Care should be taken to apply the results obtained here to other salt formations and locations. The mechanical properties predictions are also sensitive to the creep parameters calibrated from the laboratory test results. Application of different constitutive creep models for the surrounding salt mass may also result in different predictions of the crushed salt properties.

8.2 Conclusions

1) The consolidation of crushed salt increases with increasing brine content until the optimum brine content is reached, which is 5% by weight. The volumetric strain and density increase with consolidation stresses and periods. These findings agree well with those from other researchers (Holcomb and Hannum, 1982; Holcomb and Shields, 1987; Hansen et al., 1993).

2) Two main mechanisms simultaneously occur in the crushed salt: (1) consolidation by volumetric change due to particle rearrangement, cracking and creep of the salt crystals, and (2) recrystallization and healing processes. Both can strengthen and stiffen the crushed salt mass. The water has a great effect on the consolidation of crushed salt, possibly due to the sliding, rotation, or crushing of the contact zone of the granular material.

3) The crushed salt can be compacted and its initial void ratio and permeability are decreased with increasing of the density. Uniaxial compressive strength and elastic modulus of the crushed salt specimens increases with the applied consolidation stresses and periods. These results generally agree with the results obtained by Wang et al. (1994) and Miao et al. (1995). The Poisson's ratios however tend to decrease with consolidation period. The relationships between compressive strength, elastic modulus and Poisson' ratio as a function of consolidation stress and consolidation period which can be represented by an exponential equation.

4) From the direct shear tests, the results indicate that the shear stresses increase with shearing displacement, particularly under high normal stresses. The cohesion of rock salt prepared for smooth surface and crushed salt are 0.033 MPa and 0.055 MPa and friction angle are 19° and 29° , respectively.

5) The results obtained from the modelling of subsidence reduction by crushed salt backfill in mine openings indicate that the subsidence magnitudes increase with the mining depth and room height. The performance of backfill material tends to increase with increasing of room height. For example, the percentages of reduction of subsidence magnitude increase from 9.1, 12.9 to 21.1% for salt mine and from 44.4, 54.7 to 60.9% for potash mine for the mining depth of 250 m and room heights of 4, 8 and 12 m, respectively.

6) The pre-consolidated crushed salt under stress of 5 MPa for 15 days is probably the most suitable for backfilling in mine openings because the effectiveness of backfill remains unchanged even if the consolidated stress and period are higher.

7) The test results lead to the development of the empirical formulae relating the crushed salt properties with the applied mean strain energy density. The application of the strain energy principle allows considering both stress and strain to which the crushed salt specimens are subjected. This approach is considered more fundamental and simpler than those of the complex creep and healing constitutive equations proposed elsewhere for the sealing of nuclear waste repository. The prediction indicated that the density, uniaxial compressive strength and elastic modulus of consolidated crushed salt increase and porosity decrease with increasing of time and external pressure. Two main mechanisms govern the changes of the properties of crushed salt is consolidation and recrystallization. The crushed salt density and porosity are independent of the recrystallization and healing because these processes do not reduce the bulk volume of specimens. The strength and elasticity of crushed salt can increase with time even without the applied mean strain energy ($W_m = 0$) due to the recrystallization and healing.

8) The results from the analytical solution of crushed salt properties after emplacement in borehole indicate that the energy transfer from rock formation to the sealing material increases with increasing installation depth. The crushed salt density increases and porosity decreases with time (Δt) and applied mean strain energy. Without applying W_m the density and porosity of the crushed salt backfill remain unchanged. Both σ_c and E increase with P_o and Δt . Under no W_m application they can also increase with time due to the recrystallization and healing.

9) The time at which the backfill is installed (t_B) in borehole is an important factor to increase the mechanical performance of the crushed salt, particularly under great depth. Under shallow depth the crushed salt density and porosity can not be effectively increased because the available mean strain energy at the borehole boundary is low. The strength and elastic parameters can nevertheless be improved even under shallow depth (low mean strain energy). This is because these mechanical properties are governed by both consolidation and recrystallization.

8.3 Recommendations for future studies

The uncertainties of the investigation and results discussed above lead to the recommendations for further studies. To confirm the conclusions drawn in this research, more testing is required as follows:

1. Similar tests should be performed on varied of backfill material such as the bentonite-crushed salt and sludge-crushed salt.
2. The variation of the initial porosity and density of crushed salt should be investigated and established the relation with the physical, hydraulic and mechanical properties of crushed salt.
3. More testing is required on a variety of grain size distributions.
4. The crushed salt consolidation under hydrostatic stresses should be performed.
5. A relationship between the temperature and mechanical and hydraulic properties of crushed salt during consolidation is desirable.

REFERENCES

- Alshibli, K.A. and Alsaleh, M.I. (2004). Characterizing surface roughness and shape of sands using digital microscopy. **Journal of Computing in Civil Engineering**. 18(1): 36-45.
- ASTM D2434-68 (2006). **Standard test method for permeability of granular soils (constant head)**. Annual Book of ASTM Standards, American Society for Testing and Materials, West Conshohocken, PA.
- ASTM D2938-95 (2002). **Standard test method for unconfined compressive strength of intact rock core specimens**. Annual book of ASTM standards, American Society for Testing and Materials, West Conshohocken, PA.
- ASTM Standard D5607-08 (2008). **Standard test method for performing laboratory direct shear strength tests of rock specimens under constant normal force**. Annual Book of ASTM Standards, American Society for Testing and Materials, West Conshohocken, PA.
- Brodsky, S., Zeuch, H. and Holcomb, J. (1995). Consolidation and permeability of crushed WIPP salt in hydrostatic and triaxial compression. In **Proceedings of the 35th US Symposium on Rock Mechanics** (pp. 497-502).
- Butcher, B.M. (1991). **The advantages of a salt/bentonite backfill for waste isolation pilot plant disposal rooms**. Technical Report No.SAND90-3074, Sandia National Laboratories, Albuquerque, NM.
- Callahan, G.D. and Hansen, F.D. (2002). Crushed salt constitutive model. In **Proceedings of the Basic and Applied Salt Mechanics** (pp. 239-252).

- Callahan, G.D., Fossum, A.F. and Svalstad, D.K. (1989). **Documentation of SPECTROM-32: A finite element thermomechanical stress analysis program.** Rep. No. DOE/CH10378-2, Prepared by RE/SPEC Inc., Rapid City, SD.
- Callahan, G.D., Loken, M.C., Hurtads, L.D. and Hansen, F.D. (1996). Evaluation of constitutive models for crushed salt. In **Proceedings of the 5th Mechanical Behavior of Salt** (pp. 317-330). Clausthal-Zellerfeld, Germany.
- Callahan, G.D., Mellegard, K.D. and Hansen, F.D. (1998). **Constitutive behavior of reconsolidating crushed salt.** Rep. No. SAND98-0179, Sandia National Laboratories, Albuquerque, NM.
- Case, J.B. and Kelsall, P. (1987). Laboratory investigation of crushed salt consolidation. **International Journal of Rock Mechanics and Mining Sciences and Geomechanics Abstracts.** 25(5): 216-223.
- Case, J.B., Kelsall, P.C. and Withiam, J.L. (1987). Laboratory investigation of crushed salt consolidation. In **Proceedings of the 28th U.S. Symposium on Rock Mechanics (USRMS).** Tucson, Arizona.
- Cho, G.C., Dodds, J. and Santamarina, J.C. (2006). Particle shape effects on packing density, stiffness, and strength: natural and crushed sands. **Journal of Geotechnical and Geoenvironmental Engineering.** 132(5): 591-602.
- Crosby, K.S. (2005). Overview of the geology and resources of the Udon Potash (sylvinitic) deposits, Udon Thani province, Thailand. In **Proceedings of the International Conference on Geology, Geotechnology and Mineral Resources of Indochina** (pp. 283-299). Khon Kaen, Thailand.

- Crosby, K.S. (2007). Integration of rock mechanics and geology when designing the Udon South sylvinitic mine. In **Proceedings of the 1st Thailand Symposium on Rock Mechanics** (pp. 3-22).
- Daemen, J.J.K. and Fuenkajorn, K. (1996). Design of borehole seals: process, criteria and considerations. In **Proceedings of the Sealing of Boreholes and Underground Excavations in Rock** (pp. 267-279).
- De Boer, R.B. (1977). On the thermodynamics of pressure solution-interaction between chemical and mechanical forces. **Geochimica et Cosmochimica Acta**. 41(2): 249-256.
- Findley, W.N., Lai, S.J. and Onaran, K. (1989). **Creep and Relaxation of Nonlinear Viscoelastic Materials: with an Introduction to Linear Viscoelasticity**. Courier Dover, New York.
- Fuenkajorn, K. and Daemen, J.J.K. (1988). Borehole closure in salt. **PhD. Thesis, University of Arizona, U.S.A.**
- Guises, R., Xiang, J., Latham, J.P. and Munjiza, A. (2009). Granular packing: numerical simulation and the characterization of the effect of particle shape. **Granular Matter**. 11(5): 281-292.
- Hansen, F.D. (1997). Reconsolidating salt: compaction, constitutive modeling, and physical processes. **International Journal of Rock Mechanics and Mining Sciences**. 34(3-4): 119.e1–119.e12.
- Hansen, F.D. and Mellegard, K.D. (2002). Mechanical and permeability properties of dynamically compacted crushed salt. In **Proceedings of the Basic and Applied Salt Mechanics** (pp. 253-256).

- Hansen, F.D., Callahan, G.D. and Van Sambeek, L.L. (1993). Reconsolidation of salt as applied to permanent seals for the waste isolation pilot plant. In **Proceedings of the 3rd on the Mechanical Behavior of Salt** (pp. 323-335). Transtech Publications, Palaiseau, France.
- Holcomb, D.J. and Hannum, D.W. (1982). **Consolidation of crushed-salt backfill under conditions appropriate to the WIPP facility**. Rep. No. SAND82-0630, Sandia National Laboratories, Albuquerque, NM.
- Holcomb, D.J. and Shields, M. (1987). **Hydrostatic creep consolidation of crushed salt with added water**. Rep. No. SAND87-1990, Sandia National Laboratories, Albuquerque, NM.
- Holtz, R.D. and Kovacs, W.D. (1981). **An Introduction to Geotechnical Engineering**. Prentice-hall, Inc., Englewood cliffs, NJ.
- Hwang, C.L., Wang, M.L. and Miao, S. (1993). Proposed healing and consolidation mechanisms of rock salt revealed by ESEM. **Microscopy Research and Technique**. 25(5-6): 456-464.
- Indraratna, B. and Ranjith, P. (2001). **Hydromechanical Aspects and Unsaturated Flow in Joints Rock**. Lisse: A.A. Balkema.
- IT Corporation (1987). **Laboratory investigation of crushed salt consolidation and fracture healing**. Rep. No. BMI/ONWI-631, Columbus, OH.
- Itasca (1992). **User Manual for FLAC-Fast Lagrangian Analysis of Continua**. Version 4.0, Minneapolis, Minnesota.
- Jaeger, J.C., Cook, N.G.W. and Zimmerman, R.W. (2007). **Fundamentals of Rock Mechanics**. 4th ed. Blackwell, Australia.

- Kelsall, P.C., Case, J.B., Nelson, J.W. and Franzone, J.G. (1984). **Assessment of crushed salt consolidation and fracture healing in a nuclear waste repository in salt.** D'Appolonia Waste Mangement Services.
- Kingery, W.D., Bowen, H.K. and Uhlmann, D.R. (1976). **Introduction to Ceramics.** 4th ed. Jorn Wiley, NY.
- Klein, C., Hurlbut, C.S. and Dana, J.D. (1988). **Manual of Mineralogy.** John Wiley and Sons Inc.
- Koener, R.M. (1968). The behavior of cohesionless soils formed from various minerals. **PhD. dissertation, Duke University, Raleigh, NC.**
- Korthaus, E. (1998). **Experiments on crushed salt consolidation with true triaxial testing device as a contribution to an EC benchmark exercise.** Rep. No. FI4W-CT95-0009.
- Krumbein, W.C. and Sloss, L.L. (1963). **Stratigraphy and Sedimentation.** 2nd ed. Freeman and Company, San Francisco.
- Loken, M.C. and Statham, W. (1997). Calculation of density and permeability of compacted crushed salt within an engineered shaft sealing system. **Computing in Civil Engineering.** 485-492.
- Luangthip, A., Khamrat, S. and Fuenkajorn, K. (2016). Effects of carnallite contents on stability and extraction ratio of potash mine. In **Proceedings of the 9th Asian Rock Mechanics Symposium.** Bali, Indonesia.
- Miao, S., Wang, M.L. and Schreyer, H.L. (1995). Constitutive models for healing of materials with application to compaction of crushed rock salt. **Journal of Engineering Mechanics.** 121(10): 1122-1129.

- Munson, D. and Devries, K. (1991). Development and validation of a predictive technology for creep closure of underground rooms in salt. In **Proceedings of the 7th ISRM Congress**. Aachen, Germany.
- Munson, D.E., Fossum, A.F. and Senseny, P.E. (1989). **Advances in resolution of discrepancies between predicted and measured in situ WIPP room closures**. Rep. No. SAND88-2948, Sandia National Laboratories, Albuquerque, NM.
- Nair, K. and Boreasi, A.P. (1970). Stress analysis for time dependent problems in rock mechanics. In **Proceedings of the 2nd Congress of the International Society for Rock Mechanics** (pp. 531-536). Belgrade.
- Olivella, S. and Gens, A. (2002). A constitutive model for crushed salt. **International Journal for Numerical and Analytical Methods in Geomechanics**. 26: 719-746.
- Ouyang, S. and Daemen, J.J.K. (1989). **Crushed salt consolidation**. Rep. No. NUREG/CR-5402, Prepared by Department of Mining and Geological Engineering, University of Arizona.
- Pfeifle, T.W. (1991). **Consolidation, permeability, and strength of crushed salt/bentonite mixtures with application to the WIPP**. Rep. No. SAND90-7009, Sandia National Laboratories, Albuquerque, NM.
- Pfeifle, T.W., Senseny, P.E. and Mellegard, K.D. (1987). **Influence of variables on the consolidation and unconfined compressive strength of crushed salt**. Technical Report BMI/ONWI-627, Prepared by RE/SPEC, Inc., Rapid city, SD.

- Power, M.C. (1982). **Comparison charts for estimating roughness and shericity.**
AGI Data Sheets, American Geological Institute, Alexandria, VA.
- Ratigan, J.L. and Wangner, R.A. (1978). Thermomechanical analysis of crushed-salt backfilled disposal rooms in a conceptual radioactive waste repository in dome salt. In **Conceptual Design Report, National Waste Terminal Storage Repository for Storing Reprocessing Wastes in Dome Salt Formation** (No. 2, Vol. 18). Stearns-Roger Service, Denver, CO.
- Salzer, K., Popp, T. and Böhnel, H. (2007). Mechanical and permeability properties of highly pre-compacted granular salt bricks. In **Proceedings of the 6th Conference on the Mechanical Behavior of Salt** (pp. 239-248). Hannover, Germany.
- Shor, A.J., Baes, C.F. and Canonico, C.M. (1981). **Consolidation and permeability of salt in brine.** Rep. No. ORNL-5774, Oak Ridge National Laboratory, Oak Ridge, TN.
- Sjaardema, G.D. and Krieg, R.D. (1987). **A constitutive model for the consolidation of WIPP crushed salt and its use in analyses of backfilled shaft and drift configurations.** Rep. No. SAND87-1977, Sandia National Laboratories, Albuquerque, NM.
- Somtong, S., Khamrat, S. and Fuenkajorn, K. (2014). Laboratory performance assessment of consolidated crushed salt for backfill material in potash mine openings. **Research and Development Journal of the Engineering Institute of Thailand.** 26(1): 15-22.

- Spiers, C.J. and Brzezowski, R.H. (1993). Densification behavior of wet granular salt: theory versus experimental. In **Proceedings of the 7th Symposium on Salt** (pp. 83-92). Amsterdam.
- Sriapai, T., Walsri, C. and Fuenkajorn, K. (2012). Effects of temperature on compressive and tensile strengths of salt. **ScienceAsia**. 38: 166-174.
- Van Sambeek, L.L. (1992). Testing and modelling of backfill used in salt and potash mines. In **Proceedings of the Rock Support in Mining and Underground Construction** (pp. 583-589). Balkema, Rotterdam.
- Wang, M.L., Maji, A.K. and Miao, S. (1994). **Deformation mechanisms of WIPP backfill**. Technical Completion Report, U.S. Department of Energy.
- Wang, M.L., Miao, S.K., Maji, A.K. and Hwang, C.L. (1992). Effect of water on the consolidation of crushed rock salt. In **Proceedings of the Engineering Mechanics** (pp. 531-534). ASCE.
- Warren, J. (1999). **Evaporites: Their Evolution and Economics**. Blackwell science, Oxford, UK.
- Wendai, L. (2000). **Regression Analysis, Linear Regression and Profit Regression, In 13 Chapters; SPSS for Windows: Statistical Analysis**. Publishing House of Electronics Industry, Beijing.
- Wilalak, N. and Fuenkajorn, K. (2016). Constitutive equation for creep closure of shaft and borehole in potash layers with varying carnallite contents. In **Proceedings of the 9th Asian Rock Mechanics Symposium**. Bali, Indonesia.
- Zeuch, D.H. (1990). Isostatic hot-pressing mechanism maps for pure and natural sodium chloride-applications to nuclear waste isolation in bedded and domal

salt formations. **International Journal of Rock Mechanics and Mining Sciences and Geomechanics Abstracts.** 27(6): 505-524.

Zeuch, D.H., Holcomb, D.J. and Lauson, H.S. (1985). **Analysis of consolidation of granulated rock salt using a plastic flow model of isostatic hot-pressing.** Rep. No. SAND84-1106, Sandia National Laboratories, Albuquerque, NM.



BIOGRAPHY

Miss Supattra Khamrat was born on December 21, 1989 in Chaiyaphum Province, Thailand. She received her Bachelor's Degree in Engineering (Geotechnology) from Suranaree University of Technology in 2011 and received her Master's Degree in Engineering (Geotechnology) from Suranaree University of Technology in 2014. For her post-graduate, she continued to study with a Doctor of Philosophy Program in the Geological Engineering Program, Institute of Engineering, Suranaree university of Technology. During graduation, 2012-2016, she was a part time worker in position of research associate at the Geomechanics Research Unit, Institute of Engineering, Suranaree University of Technology.

